71-4079

SEBASTIAN, Richard Lee, 1942-
ULTRASONIC INVESTIGATION OF STRONG-COUPLING SUPERCONDUCTIVITY IN LEAD.

University of Maryland, Ph.D., 1970
Physics, solid state

University Microfilms, Inc., Ann Arbor, Michigan

THIS DISSERTATION HAS BEEN MICROFILMED EXACTLY AS RECEIVED

ULTRASONIC INVESTIGATION OF STRONG-COUPLING SUPERCONDUCTIVITY IN LEAD

by

Richard Lee Sebastian

Dissertation submitted to the Faculty of the Graduate School
of the University of Maryland in partial fulfillment
of the requirements for the degree of
Doctor of Philosophy
1970

Cop 1

APPROVAL SHEET

Title of Thesis: Ultrasonic Investigation of Strong-Coupling Superconductivity in Lead

Name of Candidate: Richard L. Sebastian
Doctor of Philosophy, 1970

Thesis and Abstract Approved: J. R. Leibowitz

J. R. Leibowitz
Associate Professor
Department of Physics
Catholic University of America

Date Approved: May 4, 1970

ABSTRACT

Title of Thesis: Ultrasonic Investigation of Strong-Coupling Superconductivity in Lead

Richard L. Sebastian, Ph.D., 1970

Thesis directed by: Dr. Jack R. Leibowitz

An investigation of the strong-coupling properties of lead is made with longitudinal ultrasound for a frequency range up to 510 MHz. The results of this study are compared with computed theoretical values of the superconducting and normal state longitudinal ultrasonic attenuation α_s and α_n. These computations are based upon a strong-coupling calculation by Nam and a numerical calculation for the energy-dependent renormalization and gap parameters for lead by Swihart, Scalapino, and Wada. The temperature and frequency dependences of the attenuation ratio α_s/α_n are explained in terms of the energy dependence of the electron mean free path.

A "shelf" feature of the $\alpha_s(T)$ curve is observed at several ultrasonic frequencies. It is explained in terms of a Granato-Lücke model for amplitude-independent dislocation attenuation adapted to the superconducting state. Values are obtained for the damping force per unit length of the electron system on a dislocation loop and for the resonant frequency of the dislocation loops.

At the highest frequencies another contribution of dislocation attenuation is identified. This attenuation is temperature-dependent, amplitude independent, and appears to be linear in frequency. It represents a serious obstacle to the study of strong-coupling properties in lead for $q\ell >> 1$.

An intermediate state amplitude dependent magnetoacoustic effect is observed. This effect correlates strongly with features of the onset of the intermediate state observed directly in lead by Traüble and Essman.

ACKNOWLEDGEMENTS

I am grateful to Professor Jack R. Leibowitz for his constant enthusiasm and valuable assistance throughout this work.

I would like to thank Dr. Uve Essmann for his detailed communications which added helpful insight to our intermediate state observations. I would like to thank Dr. R. E. Reed who, in supplying high-purity niobium samples, has made possible our successful new program of niobium measurements. I would also like to thank Dr. J. C. Swihart and Dr. Sang Boo Nam for discussions which were helpful in the computer implementation of the strong-coupling attenuation calculation. I am grateful to Dr. Victor Korenman for his constructive comments on the theoretical section.

I appreciate the assistance and good cheer afforded by my colleagues Mr. Fred Smith, Mr. Edward Alexander and Dr. Edward Page. I appreciate also the valuable laboratory help of Mr. Steve Dyal and Mr. Joel Fate.

I am indebted to Mrs. Noele Silverman who braved domestic turmoil to type the final manuscript. I would also like to thank Mrs. Florence Decker and Mrs. Eloise Mange for typing earlier drafts and the many communications associated with this work.

I am grateful for the devotion and sacrifice of my parents that made it possible for this work to begin and for the enduring patience of my wife that helped it to finally end.

Support by the Advanced Research Projects Agency is gratefully acknowledged.

TABLE OF CONTENTS

Chapter			Page
ACKNOWLEDGEMENTS			ii
LIST OF FIGURES			iv
CHAPTER	I.	INTRODUCTION	1
	II.	AMPLITUDE-INDEPENDENT DISLOCATION EFFECTS	8
	III.	OUTLINE OF STRONG-COUPLING LONGITUDINAL ATTENUATION DERIVATION	23
	IV.	STRONG-COUPLING INTERPRETATION OF EXPERIMENTAL RESULTS	28
	V.	INTERMEDIATE STATE AMPLITUDE EFFECT	70
	VI.	EXPERIMENTAL METHODS	75
		A. Preparation of Lead Samples	75
		B. Ultrasonic Probe Design	77
		C. Attenuation Measurements	81
	VII.	CONCLUSION	84
REFERENCES			87

FIGURES

1. Attenuation versus temperature for longitudinal sound along the [100] axis in lead for three signal amplitudes at 150 MHz.

2. Solid line shows stress strain law for a dislocation model which assumes a single loop length. The elastic strain has been subtracted out so that only the dislocation strain is shown. Point C is the point of breakaway from dislocation pinning points. For breakaway the path ABCDEF is followed for increasing stress while the path FA is followed for decreasing stress. The dashed line curve is that curve which would result for a distribution of loop lengths. After Granato and Lücke?

3. Table of temperature step locations at the three possible frequency paris with ratios of damping coefficients used to solve for possible resonant frequencies $f_o(+)$ and $f_o(-)$. The underlined resonant frequency solutions form a consistent set.

4. This figure shows the exercise of obtaining estimates for α_D from the data of Fig. 1. The electronic attenuation α_o is estimated by assuming that the ratio $(\alpha_1 - \alpha_o)/(\alpha_2 - \alpha_o)$ is approximately constant.

5. (a), (b), (c), (d). The effective mean-free-path ratio ℓ_s/ℓ_n for temperature points near T_c computed from the measured attenuation ratio α_s/α_n of Fate et al[9] at 12.8, 32, 51 and 90 MHz. The strong-coupling prediction, ℓ_{st}/ℓ_{nt} is also shown.

6. The effective mean-free-path ratio ℓ_s/ℓ_n for temperature points in a broad superconducting temperature region at several frequencies computed from the measured attenuation ratio α_s/α_n of Fate et al.[9]

7. (a), (b), (e), (d). Measured attenuation ratio α_s/α_n from Fate et al[9] at temperature points immediately below T_c. These points are compared with the BCS and strong-coupling predictions.

8. Thermal conductivity ratio k_s/k_n from experiment and theory. Present theory refers to Ambegaokar and Woo.[9]

9. (a), (b). Electron mean free path versus electron energy in the normal(a) and superconducting (b) states.

10. Pippard function $F(q\ell)$ for several ultrasonic frequencies in the normal state versus electron energy at $T/T_c = 0.9535$.

11. Pippard function $F(q\ell_{st})$ for several ultrasonic frequencies in the superconducting state versus electron energy at $T/T_c = 0.9535$.

12. Strong-coupling phonon-limited normal state electron mean free path $\bar{\ell}_{npt}$ versus temperature at several ultrasonic frequencies. The Fermi zero temperature velocity v_{F0} is adjusted to give agreement with the estimated normal state mean free path ℓ_{npF} of Fate[39] at 90 MHz. Fate's predicted ℓ_{npF} is constant for all frequencies.

13. Estimated infinite -ql attenuation $\alpha'(f)$ estimated from Fate's $\alpha_{T_c}(f)$ and Pippard theory with a frequency constant mean-free-path assumed. From Fate[38].

14. Estimated infinite -ql attenuation $\alpha'(f)$ estimated from Fate's $\alpha_{T_c}(f)$[38] and strong-coupling theory. A zero temperature Fermi velocity $v_{FO} = 1.3 \times 10^8$ cm/sec is assumed.

15. Estimated infinite -ql attenuation $\alpha'(f)$ estimated from Fate's $\alpha_{T_c}(f)$[38] and strong coupling theory. A zero temperature Fermi velocity $v_{FO} = 8.0 \times 10^7$ cm/sec is assumed.

16. Our normal state attenuation α_n for temperature points above T_c at several frequencies. Solid line shows Fate's[38] Pippard theory prediction. The experimental points, lacking a determined zero point, are adjusted to match Fate's prediction at T_c.

17. (a), (b), (c), (d). Our measured attenuation ratio α_s/α_n compared with the BCS and strong-coupling predictions at 90, 150, 210, and 510 MHz. At 150 MHz the experimental curve corrected for the estimated α_D is shown. The correction is not significant compared with the strong-coupling influence on the ratio α_s/α_n.

18. Attenuation versus temperature for a broad temperature range at 510 MHz.

19. Attenuation α_s versus temperature near T_c for two signal amplitudes at 510 MHz.

20. Attenuation drop $\alpha_{(T_c)} - \alpha_s(T)$ versus frequency for sample 3 at several temperatures near T_c.

21. Intermediate state amplitude-magnetoaccoustic effect compared with observations of Traüble and Essman[42].

22. Table of lead samples.

23. Lower part of ultrasonic probe.

24. Block diagram of electronics for measuring ultrasonic attenuation.

CHAPTER I

INTRODUCTION

Many of the previous reports of low temperature longitudinal ultrasonic attenuation measurements in lead have been of anomalous and conflicting results. One problem has been a lack of an explicit computation of the electronic attenuation to be expected in lead, a strong-coupling superconductor. Another problem has been a failure to recognize fully the attenuation in the superconducting state due to dislocations. In this thesis the strong-coupling theoretical normal and superconducting state attenuations are computed. These numerical results are compared with our attenuation measurements and those of previous work. Also, amplitude independent dislocation sources are reported and described. These sources, by their difficulty in being separated from the electronic attenuation, have quite possibly caused some of the previous anomalous results.

A review of past work will show the relevance of the present attenuation measurements in lead. Lead has been an interesting material for many investigators to study ultrasonically because of its departure from weak-coupling behavior predicted by the very successful Bardeen, Cooper, and Schrieffer theory of superconductivity.[1] According to theBCS theory the ratio of the electronic attenuation in the superconducting state α_s to that in the normal state α_n is given by

$$\frac{\alpha_s}{\alpha_n} = \frac{2}{e^{\Delta(T)/kT} + 1} \qquad (1)$$

where $2\Delta(T)$ is the temperature-dependent energy gap. Bömmel's pioneering ultrasonic attenuation measurements in lead[2] predated this theory. However, a later examination of these measurements in light of the BCS prediction

stimulated further investigation by Love, Shaw and Fate.[3] They analyzed Bömmel's results in terms of Eq. 1 and found that the drop in attenuation below T_c was anomalously rapid. The indicated zero temperature gap inferred from the data near T_c was $2\Delta(0) = 8.0\ kT_c$, quite large compared with the BCS weak-coupling result of $3.52\ kT_c$ or even the value $4.3\ kT_c$ measured in tunneling experiments. That the anomalously large apparent energy gap is not found in impure lead, was shown by Love, Shaw and Fate.[3,4] The measurements of Love, Shaw, and Fate, in addition to indicating a gap of about $4.1\ kT_c$ in impure lead, revealed an amplitude-dependent nature of the attenuation in the superconducting state. Tittman and Bömmel[5,6] made more measurements and explained this amplitude dependence in terms of dislocations: The damping of dislocation motion by free electrons is reduced in the superconducting state and an <u>amplitude-dependent</u> irreversible dislocation unpinning process is able to occur. This attenuation source had been treated theoretically by Granato and Lücke[7] for higher temperature normal-state measurements. Mason[8] then proposed that the anomalously rapid drop in the measured attenuation ratio as temperature is reduced below T_c could be explained in terms of an <u>amplitude-independent</u> dislocation attenuation which can be derived from a Granato-Lücke type model. This suggestion was disputed by Tittman and Bömmel[6] on theoretical grounds and by Fate, Shaw and Salinger,[9] who measured a far more rapid drop in the attenuation ratio near T_c than predicted by Mason.

Interest increased when Deaton[10] reported finding the attenuation ratio α_s/α_n near T_c to decrease with increasing frequency. He claimed to have no amplitude dependent behavior in his attenuation measurements and suggested that his results were a manifestation of the strong electron-phonon coupling in lead. At high ultrasonic frequencies he proposed that the situation was

the same as for thermal conductivity where anomalous behavior of k_s/k_n had been explained by Ambegaokar and Woo.[11] However, Ambegaokar[12] replied that, in fact, strong coupling theory predicted nothing but a return to the BCS attenuation behavior given in Eq. 1 for ultrasonic frequencies sufficiently high that $q\ell >> 1$, as was the case in Deaton's experiments. Here q is the phonon wave number and ℓ is the electron mean free path. Hence, the experimental or theoretical explanation of Deaton's findings was and is still missing.

Fate and Shaw,[13] working with deformed Pb samples to reduce amplitude effects, saw a frequency dependence in the rate of change of attenuation with temperature opposite to that observed by Deaton. They found that as frequency, and hence $q\ell$ increased at a given temperature, the attenuation ratio α_s/α_n increased also. Fate and Shaw explained their findings qualitatively in terms of an increase in the scattering rate Γ_s for electron excitations in the superconducting state over the Γ_n for electrons in the normal state, as found in strong-coupling calculations of Ambegaokar and Woo.[14] However, the drop in the mean-free-path ratio ℓ_s/ℓ_n, calculated from their data, was an order of magnitude larger than the calculated drop in Γ_n/Γ_s below T_c. This led to their suggestion that the electron energy distribution of ℓ_s and ℓ_n must also be accounted for.

To sum the situation preceding our work, there were conflicting reports of the frequency dependence of the longitudinal attenuation ratio α_s/α_n in lead. There were also conflicting explanations for the departure from the BCS temperature dependence by α_s/α_n. The most recent and best documented work prior to the present study, that of Fate et al, with strained lead samples, showed the attenuation ratio α_s/α_n to increase with frequency. This is in qualitative agreement with strong-coupling theory. However, no

asymptotic approach of the observed temperature dependence to Eq. (1) was achieved by Fate et al at their highest frequencies.

One of our initial experimental goals was to make measurements of α_s/α_n in unstrained pure lead at high enough frequencies that the expected asymptotic approach of the ratio α_s/α_n to Eq. 1 could be checked and compared with strong-coupling theory. The primary experimental obstacle was expected to be amplitude-dependent attenuations obscuring the true attenuation values in the superconducting state. The Granato-Lucke theory for dislocation attenuation, while qualitatively quite successful, is not practical for subtracting this attenuation source from measured values: the theory in itself is approximate and many of its parameters, such as the distribution of dislocation loop lenghts, are unpredictable and changeable even within a given experimental run. The alternative we pursued in attempting to eliminate amplitude-dependent attenuation was to work with low ultrasonic signal amplitudes below the dislocation breakaway threshold for which amplitude effects occur. If amplitude independence of the attenuation could be verified, then, in terms of previous results, it was expected that the remaining attenuation would be purely electronic.

Our technical experimental goal was achieved by designing a highly sensitive ultrasonic probe. Lack of amplitude dependence in the attenuation could be confirmed at low superconducting-state temperatures for frequencies up to 450 MHz. However, further examination of the data revealed that non-electronic sources of attenuation were still present. In Chapter II we describe a "shelf" feature of the attenuation versus temperature curve which was seen at 90, 150, and 210 MHz. We explain this shelf in terms of a temperature-dependent amplitude-independent dislocation attenuation model based on the Granato-Lücke dislocation damping theory. This interpretation

is formally different from that of Mason.[8] Evidence in support of our model is found also from our examination of the results of Simmons[15] for Nb and of Fate et al[16] for Pb. This source of attenuation, at least as described by the theory, does not pose a serious problem to analysis of strong-coupling attenuation features. It is almost negligible near T_c and vanishes, for our lower frequency range, near $T = 0$.

In Chapter III we outline briefly the derivation of the strong-coupling longitudinal attenuation formula. The derivation begins with a generalized expression for the attenuation in terms of correlation functions by Kadanoff and Falko.[25] The final result is the attenuation formula derived by Nam and others which is valid for the 10 to 510 MHz frequency region of our study.

Experimental attenuation results are compared with the computed strong-coupling theory prediction in Chapter IV. In the beginning of the chapter we describe the computer evaluation of the Nam attenuation formula. Values of the theoretical superconducting and normal state attenuation are found near T_c using the energy gap and renormalization factors $\Delta(\omega)$, $z_s(\omega)$, and $z_n(\omega)$ for difficult electron quasiparticle energies as calculated from tunneling data by Swihart, Scalapino, and Wada.[18] Using these computed attenuation values, we are in a position in the next section to compute the drop in the theoretical effective mean free path ratio $\bar{\ell}_s/\bar{\ell}_n(T)$ for $T < T_c$. Examining the low-frequency ($f \leq 90$ MHz) experimental results of Fate et al[9] for ℓ_s/ℓ_n in light of this calculation, we find good qualitative agreement. This is more than Fate et al have been able to claim in their more qualitative comparison of their data with strong coupling theory.

The frequency and temperature dependence of the normal state attenuation are discussed next. Fate's low frequency (12.8 - 90 MHz) data is fit extremely well with his assumed frequency-constant electron mean free

path ℓ_n. An attempt to fit his normal state data with a frequency-dependent ℓ_n from strong-coupling theory is less successful. Our own normal state data is then examined. It extends over a broader temperature range than Fate's and over a frequency range up to 510 MHz. This data is also consistent with the frequency constant phonon-limited mean-free-path of Fate.

In the remainder of Chapter IV we discuss our superconducting state attenuation data. For our lower frequency measurements, as with Fate's measurements, we find that the ratio α_s/α_n is consistent with strong-coupling theory within the accuracy of the theory. For our highest ultrasonic frequencies, a most disturbing non-electronic source of attenuation is detected and identified for the first time in our data for the superconducting state. This is a temperature dependent, amplitude independent attenuation, probably dislocation related and closely linear with frequency. It thus represents a very serious obstacle to the measurement of the electronic attenuation in pure undeformed lead at high frequencies. In our case it prevents a verification of an approach to a BCS temperature dependence by α_s/α_n as predicted by Ambegaokar.[12]

In Chapter V our intermediate state amplitude-dependent magneto-acoustic effect is reported. We relate this effect to the intermediate state structure as described by Traüble and Essman.[42] This effect has an advantage over thermal conductivity and ordinary ultrasonic measurements in that it is very sensitive to the onset of the intermediate state.

In Chapter VI our experimental methods and specialized equipment are discussed. Our principal technical achievement is the development of an internally tuned ultrasonic probe which operates sensitively in the 100 to 500 MHz frequency range for which one begins to achieve $q\ell >> 1$ in lead.

This is a hybrid frequency range, below the microwave range and yet high enough that one cannot use a straight-forward lumped model for circuit design. The vagaries of dislocation attenuation in lead prevented us from measuring the $q\ell >> 1$ asymptotic temperature dependence of α_s/α_n, even with the highly sensitive probe. However, the sensitivity of the instrument has made possible the positive identification of some of the pitfalls of amplitude-independent dislocation attenuation.

CHAPTER II

AMPLITUDE-INDEPENDENT DISLOCATION EFFECTS

A required first step in the investigation of the electronic attenuation in superconducting lead is the evaluation of dislocation-related background effects. It is desirable that they can be made to disappear as in the removal of amplitude-dependent attenuation through sample deformation by Fate et al.[9] Failing this, it becomes necessary to understand dislocation-related features in the attenuation to be aware of their effect on estimates of the electronic attenuation.

One puzzling feature of our attenuation measurements for undeformed lead was a ledge in the superconducting attenuation vs. temperature plot which appeared most strongly at 150 MHz and is shown in Fig. 1. This was characteristic of all experimental runs with all samples at 150 MHz, appearing less strongly at neighboring frequencies.

From sample to sample, or with sample history (temperature cycles or high sound amplitude) this ledge tended to shift in position, sharpness and magnitude. However, the effect was not dependent on high signal amplitude for its existence. With an ultrasonic probe capable of operating with input signals reduced 85db below a 50v transmitter pulse at 150 MHz, it was possible to verify absence of the usual type of amplitude effect:[3,6] over a 20 db increase in input signal from the lowest level, the attenuation difference between T_c and the lowest measured temperature, $\sim$2.0°K, remained constant within our experimental error. The damping of dislocation motion is minimal at the lowest temperatures; amplitude dependent dislocation attenuation should be strongest there. On the other hand, amplitude effects shou be minimal at T_c, where full normal electron density obtains. Hence, lack of any decrease in $[\alpha(T_c) - \alpha(2°)]$ over a factor of ten increase in signal amplitude is strong evidence for amplitude independence at the lowest temperatures for these runs at 150 MHz in lead. Also, a direct comparison of the effects

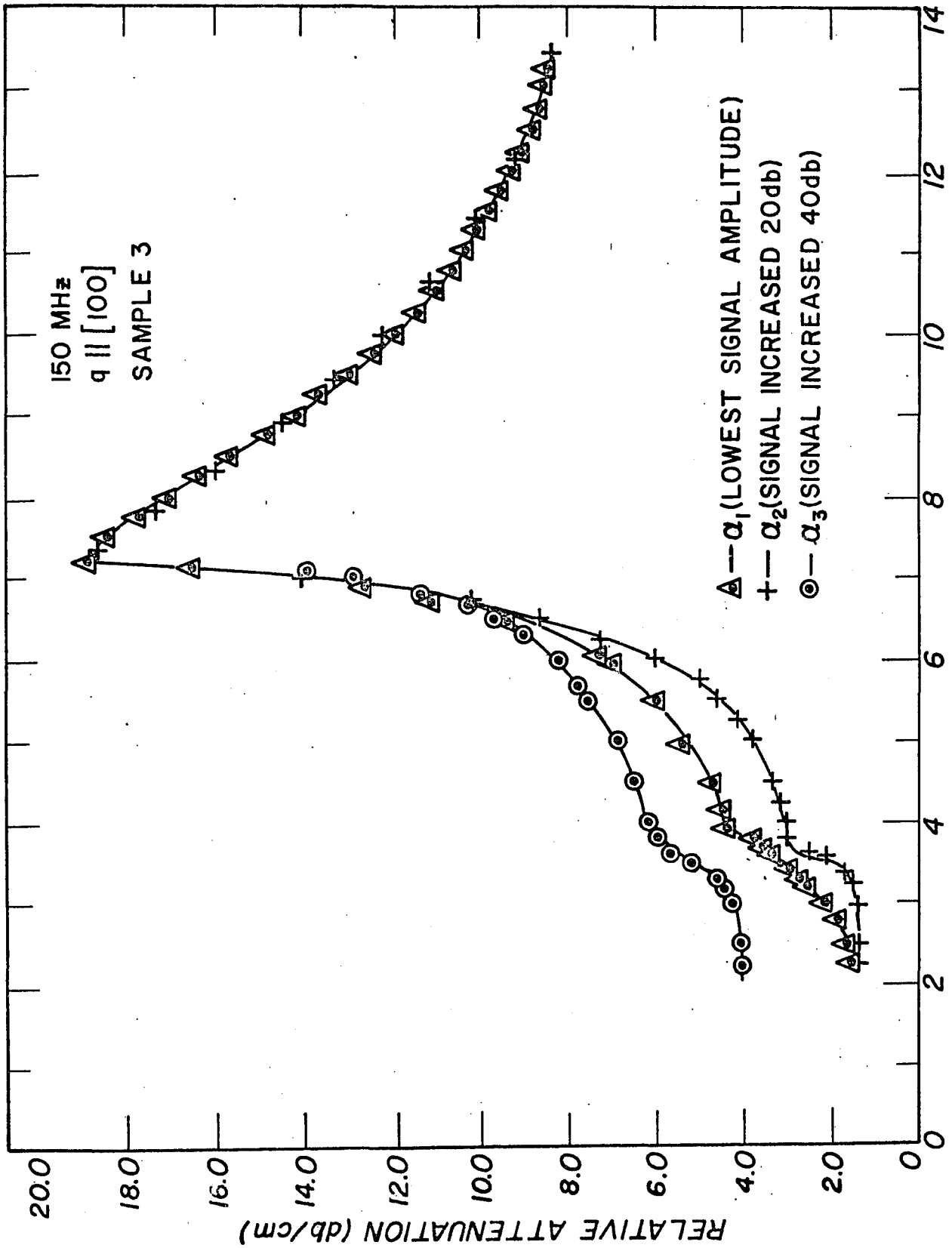
150 MHz
q || [100]
SAMPLE 3
Δ — α1 (LOWEST SIGNAL AMPLITUDE)
+ — α2 (SIGNAL INCREASED 20db)
⊙ — α3 (SIGNAL INCREASED 40db)
RELATIVE ATTENUATION (db/cm)
T (°K)
0
2.0
4.0
6.0
8.0
10.0
12.0
14.0
16.0
18.0
20.0
2
4
6
8
10
12
14

Figure 1

of adding 10db of attenuation to the transmitter line and into a comparison signal from a "T" in the receiver line revealed no consistent difference of either sign in measured attenuation.

From the evidence that the position and height of the step vary with sample history it is inferred that the step is dislocation related. Simmons, who reported a similar feature in niobium,[15] suggested that it was caused by collective mode absorption of the type investigated by Claiborne and Einspruch.[19] That absorption mechanism consists of excitation of resonant standing modes of pressure-density waves in the neutral Fermi gas. The absorption is particularly strong in the superconducting state because of the lack of damping of the low frequency density modulations. These waves are found to propagate with a temperature-dependent velocity

$$c = c_o\left[1 - a\left(\frac{T}{T_c}\right)^2 + b\left(\frac{T}{T_c}\right)^4\right]^{1/2} \qquad (2)$$

where c_o is the velocity at zero temperature and a and b depend on the thermodynamic properties of the electron system. Hence, a collective mode will be excited and an absorption peak will occur at a temperature T and frequency f for which

$$f = f_o\left[1 - a\left(\frac{T}{T_c}\right)^2 + b\left(\frac{T}{T_c}\right)^4\right]^{1/2} \qquad (3)$$

$$f_o = \frac{nc_o}{\ell_p}$$

where ℓ_p is the width of the excited region and n the order of the excited mode. The excited region may consist of the distorted neighborhood of an impurity atom, or a dislocation, or may be an entire single crystal of a pure specimen.

Attempts to explain the observed shelf in terms of this density modulation mechanism, letting the parameters f_o, a, and b vary freely, met with no

success. Taking the shelf as a single lop-sided peak or a merged series of peaks always resulted in predictions of peaks where they did not occur. Also, in the merged peak consideration, our observed shelf appears to be quite smooth as can be seen in Fig. 1 and unlike the bumpy attenuation vs. temperature curves observed by Claiborne and Einspruch in Nb-Zr[19] and Olsen et al in single crystal tin.[20] One other very important difference is that the position of the edge of the step changed with sample history. In the observations of Claiborne and Einspruch the position of the absorption peaks remained constant and only the magnitude of the peaks could be changed by annealing or damaging the sample.

Another possible cause of the step is dislocation damping. Tittman and Bömmel[6] explained amplitude dependence found in ultrasonic attenuation of superconducting lead in terms of the Granato-Lücke theory[7] for dislocation damping. This theory assumes that irreversible energy losses occur when dislocation lines break away from their impurity pinning points. With larger sound amplitudes more dislocation lines are able to break away. Hence, the amplitude dependence. In the normal state at low temperatures this source of attenuation is small because of the damping of dislocation motion by the conduction electrons. The dislocation loops behave like vibrating strings between their impurity pinning points. The conduction electrons, in their collisions with the distorted volume surrounding a dislocation line, tend to keep it at rest with the surrounding lattice. In the superconducting state, however, the number of normal electrons which may interact with the lattice (and dislocations) is decreased. The attenuation in that state is proportional to the damping force/velocity on the lattice by the electron system and is also proportional to the damping force/velocity on the moving dislocation lines. As the attenuation ratio α_s/α_n becomes small, the unpinning process may begin for large enough sound amplitudes.

In addition to the attenuation from this unpinning process, which has been reported previously in superconducting lead,[5,3] the Granato-Lücke model predicts an attenuation source independent of signal amplitude. The damping of the dislocation motion causes a shift in the phase lag between the applied stress and the resulting dislocation motion. This lag causes a net energy loss for each cycle as in Fig. 2 for amplitude-dependent attenuation.

We follow briefly the development of the Granato-Lücke theory for dislocation loop motion.[7] Stress σ and strain ε in the solid are related by an equation of motion

$$\frac{\partial^2\sigma}{\partial x^2} - \rho\frac{\partial^2\varepsilon}{\partial t^2} = 0 \qquad (4)$$

where ε is the sum of dislocation strain and elastic strain of the perfect crystal lattice.

$$\varepsilon = \varepsilon_{el} + \varepsilon_{dis} \qquad (5)$$

Let a be the Burgers vector of the dislocation. Then the strain introduced into a unit cube containing the dislocation loop of length ℓ is $\bar{\xi}\ell a$, where $\bar{\xi}$, the average displacement of a dislocation, is given by

$$\bar{\xi} = \frac{1}{\ell}\int_o^{\ell} \xi(y)dy, \qquad (6)$$

where y is the coordinate on the dislocation line. The dislocation strain becomes

$$\varepsilon_{dis} = \frac{\Lambda a}{\ell}\int_o^{\ell} \xi(y)dy, \qquad (7)$$

where Λ is the length of moveable dislocation line per unit volume. Granato and Lücke add to this the equation of motion for a dislocation line given by Koehler,[21]

$$A\frac{\partial^2\xi}{\partial t^2} + B\frac{2^2\xi}{\partial t} - C\frac{\partial^2\xi}{\partial y^2} = a\sigma \qquad (8)$$

where $A = \pi\rho a^2$ is the effective mass per unit length; B is the damping force

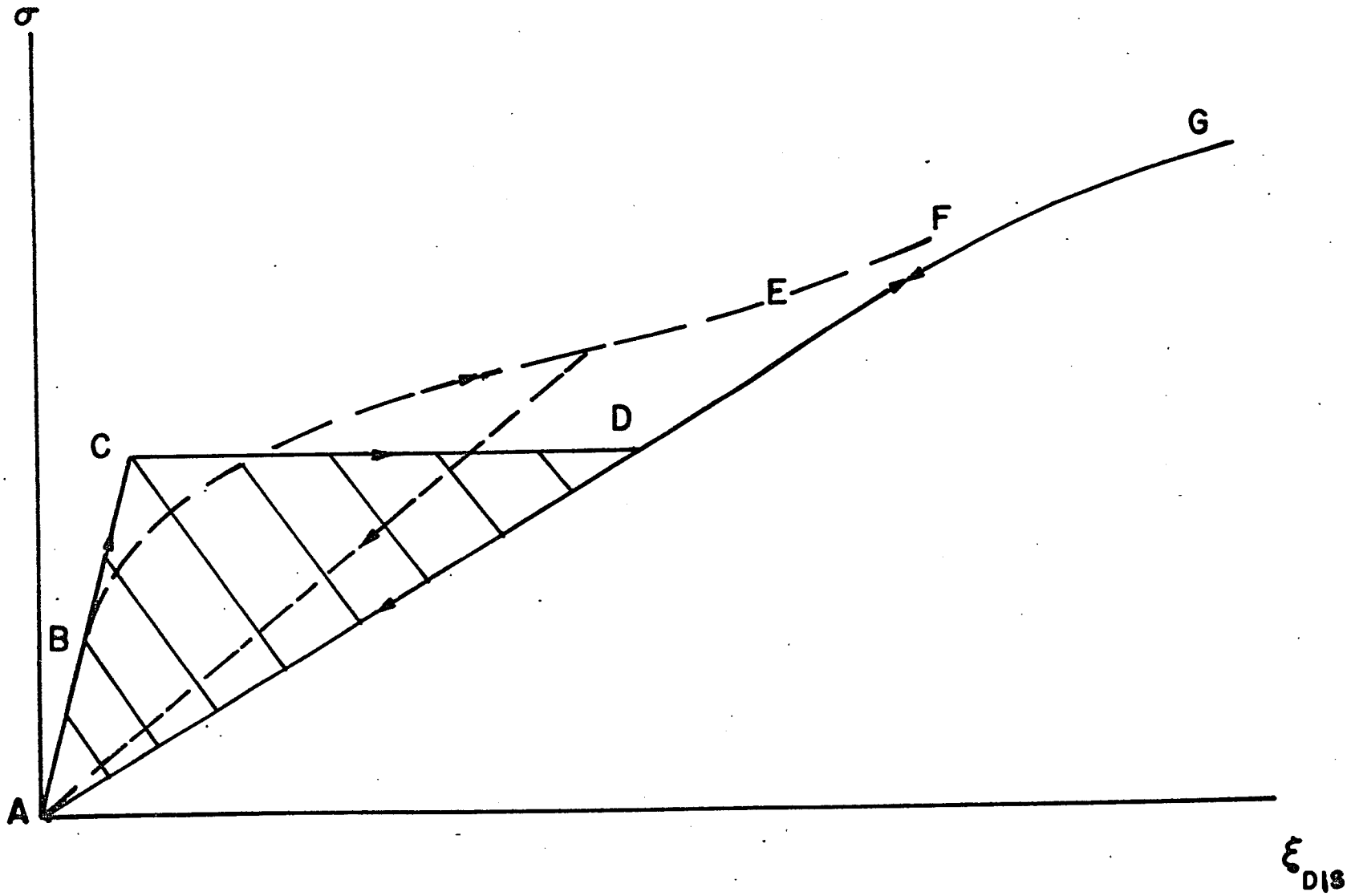

Figure 2

per unit length and velocity; and $c = 2Ga^2/\pi(1 - 2)$ is the force per unit length due to tension along the dislocation line. Here ρ is the density of the crystal, G is the shear modulus and ν is Poisson's ratio. Equation 8, together with the preceding equations, which become

$$\frac{\partial^2\sigma}{\partial x^2} - \frac{\rho}{g}\frac{\partial^2\sigma}{\partial t^2} = \frac{\Lambda pa}{\ell}\frac{\partial^2}{\partial t^2}\int_o^\lambda \xi dy \tag{9}$$

form a system of simultaneous partial differential integral equations. Further, there is the boundary condition that $\xi = 0$ at 0 and ℓ (the dislocation line remains pinned at both ends). Granato and Lücke propose the trial solution

$$\sigma = \sigma_o\, e^{-\alpha_o x}\, e^{i\omega(t - x/v)} \tag{10}$$

which leads to the series solution for the displacement

$$\xi = 4a\sigma \sum_{n=0}^{\infty} \frac{1}{(2n+1)}\frac{\sin(2n+1)\pi y}{\ell}\frac{e^{i(\omega t - \delta_n)}}{[(\omega_n^2 - \omega^2)^2 + (\omega d)^2]^{1/2}}$$

$$d = \frac{B}{A},\ \omega_n = (2n+1)\frac{\pi}{\ell}\left(\frac{C}{A}\right)^{1/2},\ \text{and}\ \delta_n = \tan^{-1}\frac{\omega d}{\omega_n^2 - \omega^2} \tag{11}$$

Most of the previous investigations of dislocation damping have been done at frequencies not greater than the resonant frequency ω_o. In this case, only the n = 0 term is important and the dislocation attenuation and velocity are given by

$$\alpha_D(\omega) = \frac{\omega}{2v}\frac{\Lambda\Delta_o\eta}{\pi}\frac{\omega d}{[(\omega_o^2 - \omega^2)^2 + (\omega d)^2]}$$

$$v(\omega) = v_o\left[1 - \frac{\Lambda\Delta_o\eta}{2\pi}\frac{\omega_o^2 - \omega^2}{[\omega_o^2 - \omega^2)^2 + (\omega d)^2]}\right] \tag{12}$$

where

$$v_o = \left(\frac{G}{\rho}\right)^{1/2}, \quad \Delta_o = \frac{8Gb^2}{\pi^2 c}, \quad \eta^2 = \pi C/A.$$

At a given frequency, the only temperature dependence of $\alpha_D(\omega)$ is through $d = \left(\frac{B}{A}\right)$. The damping force B is proportional to the amount of momentum transfer from the lattice to the electron system per given lattice momentum, as mentioned above. This is proportional to the superconducting ultrasonic attenuation. At the low temperatures where we observe low amplitude dislocation-related structure, a simple approximation may be made for d. At these temperatures the electron mean free path is mostly impurity limited and the normal state attenuation α_n nearly constant with temperature. Strong coupling effects due to phonon limitation should be unimportant. If we let d_o be the value of d in the normal state at T = 0, d(T) may be approximated by

$$d(T) = d_o[\alpha_s/\alpha_n]_{BCS}(T). \tag{13}$$

The attenuation ratio $[\alpha_s/\alpha_n]_{BCS}(T)$ is that prediced by the BCS theory.

$$[\alpha_s/\alpha_n](T) = 2/\left(1 + e^{\Delta(T)/kT}\right). \tag{1}$$

We take for the zero-temperature energy gap

$$2\Delta(0) = 4.3\ kT_c, \tag{14}$$

which has been verified by tunneling experiments in lead.[22] As a function of d, the attenuation due to dislocations, as in Eq. 12, takes on its maximum when $d = d_{res}$ which is given by

$$d_{res} = \left|\frac{\omega_o^2 - \omega^2}{\omega}\right| \tag{15}$$

For sample 3 the highest point of the "step" (or the position of the maximum value of the low amplitude dislocation attenuation) could be determined at three frequencies. At 90 and 150 MHz this feature was quite distinct. At 210 MHz the step edge could barely be seen in the noise.

However, the temperature sweep at this frequency was repeated six times in succession and the step edge was always present at the same temperature. It should be noted that the step positions were all determined before any data analysis was undertaken.

Using Eqs. 12 and 15 and examining the data in pairs of frequencies proves fruitful. Let f_1 and f_2 be the two frequencies and T_1 and T_2 the corresponding positions of the top of the step edge. The damping coefficients d_1 and d_2 should be at their resonant values at the respective temperatures and frequencies 1 and 2. Taking the ratios d_1/d_2 and solving for the resonant frequency $f_o = \frac{\omega_o}{2\pi}$ in the undamped case (T = 0 in the superconducting state), we obtain

$$f_{o(\pm)}^2 = \frac{f_1 f_2 \left[\pm \left(\frac{d_1}{d_2}\right) f_2 - f_1 \right]}{\left[\pm \left(\frac{d_1}{d_2}\right) f_1 - f_2 \right]} \tag{16}$$

where (d_1/d_2) may be obtained from 12:

$$\left(\frac{d_1}{d_2}\right) = [\alpha_s/\alpha_n]_{BCS}(T_1)/[\alpha_s/\alpha_n]_{BCS}(T_2) \tag{17}$$

The (+) sign in Eq. 16 arises when f_o lies outside the interval (f_1, f_2), the (-) sign otherwise. From Eqs. 13 and 15 we can solve for the T = 0 normal state damping coefficient;

$$d_o = 2\pi \left| \frac{f_o^2 - f^2}{f} \right| \Big/ [\alpha_s/\alpha_n]_{BCS}(T) \tag{18}$$

where T is the temperature at the top of the step edge at frequency f. For our three possible (two independent) frequency pairs, we have possible predictions for f_o and d_o given in Fig. 3.

It can be seen from the underlined solutions to Eq. 16 in the figure that an undamped resonant frequency f_o = 190 MHz and a normal state damping

Observed quency pair f_1 , f_2	Observed maxima of temperature steps T_1 , T_2 (^oK)	Ratio of Damping Coefficients d_1/d_2	Calculated undamped resonant frequency from dislocation loops $f_o(+)$	$f_o(-)$ (MHz)	Calculated normal state damping constant (B/A) T=0 - d_o ± 10%) from $f_o(t)$	from $f_o(-)$
)0 , 150	4.8 ,3.7 ± .05	3.3	191 ±10	132 ±10	1.57×10^{10}	5.90×10^{9}
50 , 210	3.7 ,3.1 ± .05	2.4	272 ±10	189 ±10	1.01×10^{10}	1.62×10^{10}
)0 , 210	4.8 ,3.1 ± .05	8.0	242 ±10	189 ±10	2.88×10^{10}	1.62×10^{10}

Figure 3

constant $d_o = 1.6 \times 10^{10}$ sec^{-1} is consistent with all pairs of our measurements. Thus, the position of the steps fits an amplitude-independent Granato-Lücke model with a faithfulness far exceeding both the completeness of the theory and the accuracy of our measurements. A comparison with other theoretical and experimental results adds further weight to these results.

Using Mason's[23] expression for the resonant frequency of a pinned dislocation line in lead with a length between pinning points $\ell_c = 10^{-4}$ cm, Granato and Lücke[24] obtain

$$f_o = \frac{1}{2\ell_c}\left(\frac{C}{A}\right)^{1/2} = \frac{1}{2\pi\ell_c}\left(\frac{2G}{\rho(1-\nu)}\right) = 200 \text{ MHz} \qquad (19)$$

Since G and ν are the shear modulus and Poisson ratio, the only variable parameter in determining f_o is ℓ_c. The value $\ell_c = 10^{-4}$ cm was found for lead 99.999% pure, the approximate p rity of our sample, from an analysis of amplitude dependent data by Granato and Lücke.[24] This impurity pinning length, which is approaching the length between nodes in the dislocation network represents some average over a distribution and depends on the state of anneal of the crystal. However, the averaging should be the same for both types of dislocation attenuation and it thus is reassuring that the magnitudes are the same.

T. Holstein, in a result reported by Tittmann and Bömmel,[6] calculated the damping force B of the electron system on a dislocation line using a deformation potential model. Near T = 0 in the normal state of lead he obtains $B = 6 \times 10^{-5}$ dyn sec cm^{-2}. This corresponds directly to the $d = 2.1 \times 10^{9}$ sec^{-1}. This is in fair agreement with our result of $d_o = 1.6 \times 10^{10}$ considering the theoretical approximations involved, such as the estimation of appropriate limits for the lattice distortion around a dislocation.

Mason[8] has attempted to use an electron viscosity model of dislocation damping to explain departures from the usual BCS behavior of ultrasonic attenuation in superconducting lead. His model, when applied to temperatures well below T_c, predicts qualitatively the same "step" features that we observe in the amplitude independent dislocation attenuation and this led to our consideration of this source. According to Mason, however, this attenuation is proportional to

$$(\omega^2/\omega_{oM}) \times [1 + (\omega/6\omega_{oM})]^{-1} \qquad (20)$$

where here $\omega_{oM} = Gb^2/Bl_c^2$ is temperature dependent through the damping force B. In Mason's theory, a step at a single frequency is sufficient to determine the value of the damped resonant frequency ω_{oM} at all temperatures. Assuming f_{oM} = 150 MHz at 3.7°K where we observed the step edge at that frequency, we obtain from Mason's calculation f_o = 366 MHz at 3.1° and f_o = 45 MHz at 4.8°. This is in poor agreement with our observations, since 3.1° and 4.8° are the observed positions of the step edges at 2.10 MHz and 90 MHz, respectively.

Other features remain to be discussed. Figure 4 shows the two lowest amplitude 150 MHz curves for α_s vs T and the theoretical electronic attenuation α_o curve obtained from subtracting out our estimated dislocation attenuation α_D. Differences are to be expected between this and the actual electronic attenuation because the lead sample has a distribution of loop lengths and more than one type of dislocation.

For example, suppose dislocation network lengths have a distribution sharply peaked at ℓ_1 and impurities are randomly scattered along the network length with average density on the order of one per dislocation loop. Then the spacing between dislocation pinning points will have a length distribution function of non-negligible value from 0 to ℓ_1. This would result in a fairly

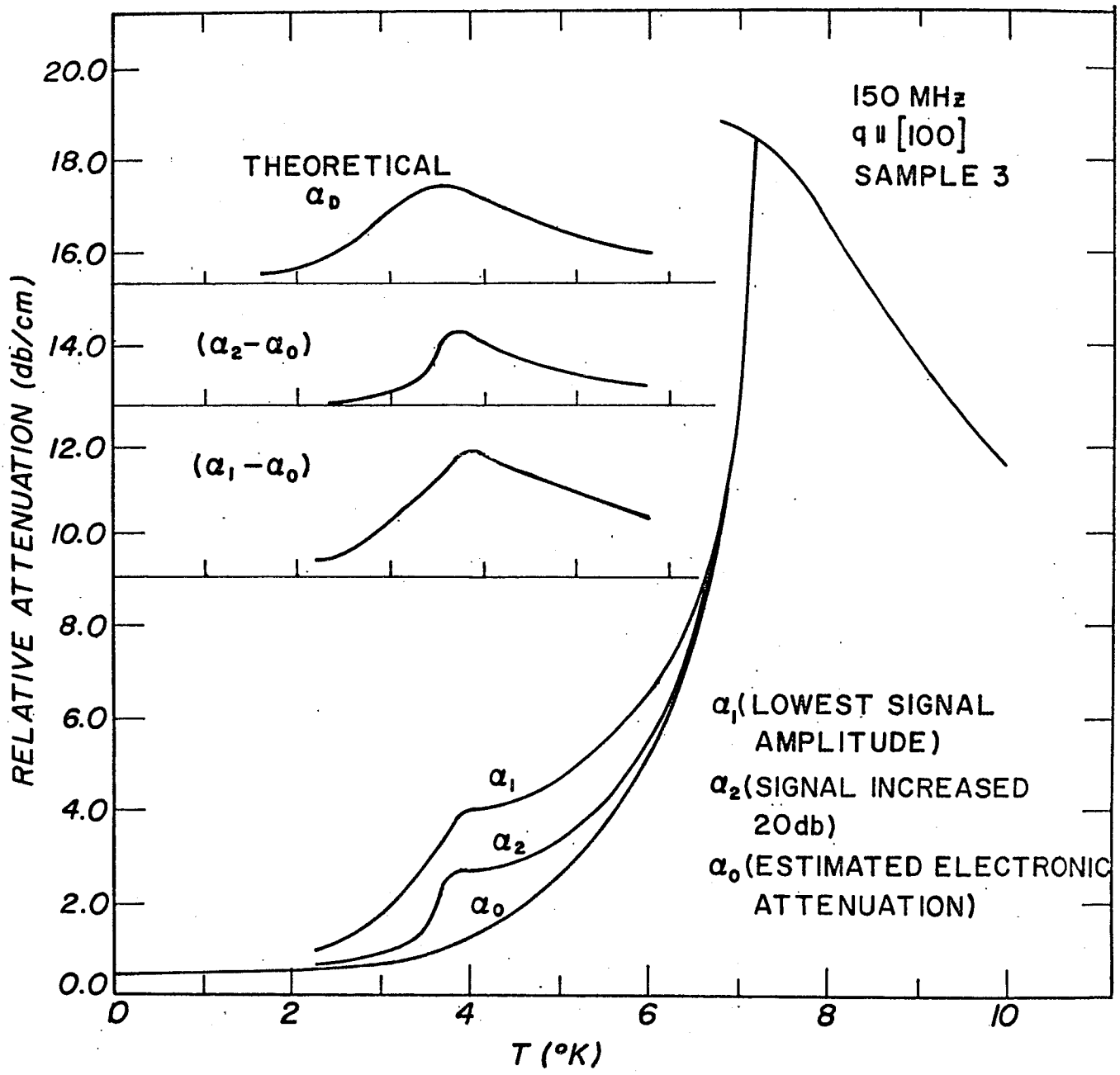
150 MHz
q ∥ [100]
SAMPLE 3
THEORETICAL
α_D
$(\alpha_2-\alpha_0)$
$(\alpha_1-\alpha_0)$
α_1(LOWEST SIGNAL AMPLITUDE)
α_2(SIGNAL INCREASED 20db)
α_0(ESTIMATED ELECTRONIC ATTENUATION)
α_1
α_2
α_0
RELATIVE ATTENUATION (db/cm)
T (°K)
20.0
18.0
16.0
14.0
12.0
10.0
8.0
6.0
4.0
2.0
0.0
0
2
4
6
8
10

Figure 4

sharp cutoff in α_D at temperatures below the resonant temperature T_1 corresponding to resonance of loops of length ℓ_1. Above T the attenuation α_D would taper off more slowly, being enhanced by loop lengths shorter than ℓ_1.

The α_o curve in Fig. 4 was estimated by assuming that $(\alpha_1 - \alpha_o)(T)$ and $(\alpha_2 - \alpha_o)(T)$ would have an approximately constant ratio; the curve for electronic attenuation α_o connects low and high temperatures smoothly. In absolute terms, the estimates of $(\alpha_i - \alpha_o)(T)$ must be crude, for their largest magnitude is about 4 times the estimated experimental error.

As sound amplitude is increased 20 db, as in Figs. 1 and 4, the step edge moves to a lower temperature and is reduced in height. The move to lower temperature may have a simple explanation. As some of the dislocation lines break loose from their pinning points, their average loop length becomes longer, and their resonant frequency lower, and the weaker damping found at lower temperatures is needed to resonante them at the driving frequency. This line of reasoning would seem to indicate a higher step at the higher amplitude, in line with form of the Granato-Lücke α_D in Eq. 12. Hence the reduction in step height with increased sound amplitude is difficult to explain. The possibility that amplitude-dependent attenuation was raising the level of the attenuation below the step was considered, but was inconsistent with the fact that the difference in attenuation between T_c and 2.0°K was constant within our 0.1 db experimental error over the 20 db signal amplitude change. The difference between $\alpha(T_c)$ and the attenuation at the top of the step was not constant within this error.

The diminishing of the maximum in α_D at higher sound amplitudes may explain its feebleness at 210 MHz. Here it was expected to be particularly large because of the proximity of the undamped resonant frequency $f_o = 190$ MHz.

Of primary and final importance is the effect of amplitude-independent dislocation damping on attenuation measurements near T_c. Although Mason[22] suggested this attenuation source as causing most of the anomaly seen there in lead, Fate et al[9] showed that an anomalously rapid fall in attenuation existed at temperatures closer to T_c than would be affected by Mason's prediction. With the approximation of a BCS dependence for the electronic attenuation ratio $[\alpha_s/\alpha_n]$ and a maximum α_D as observed at the step top, a calculated correction to α_s/α_n by α_D is plotted for 150 MHz in Fig. 17(b). At the transition temperature α_D is only as large as 1% of the electronic attenuation $\alpha_e(T_c)$ and $\alpha_D(6°)$ is only 3% of $\alpha_e(T_c)$. This predicted 2% alteration in the measurement is small compared with the strong-coupling anomalies to be discussed in the next sections.

CHAPTER III

OUTLINE OF STRONG-COUPLING LONGITUDINAL ATTENUATION DERIVATION

The derivation of the strong-coupling longitudinal acoustic attenuation formula begins with the general form derived by Kadanoff and Falko.[25]

$$\alpha_L(q,\omega) = A \; e\{\frac{q^2}{i\omega} <[n,n](q,\omega] - 2d[\tau_{zz},n](q,\omega) + d^2[\tau_{zz},\tau_{zz}](q,\omega)>\} \quad (21)$$

The operators n and τ_{zz} are the electronic density and stress tensor, respectively. The constants in Eq. 21 are

$$A = (\rho_F^2/3m)/\rho_{ion}\, V_{sound} \quad \text{and} \quad d = (3m/\rho_F^2).$$

The momentum space correlation functions are defined

$$<[A,B]>(q,z) = -i \int_{-\infty}^{t} dt' \int dr' \; e^{iz(t - t')} e^{-iq(r - r')} x<[A(r,t),B(r',t')]> \quad (22)$$

In order to apply Eq. 21 to the strong coupling superconductor case, the density and stress tensor correlation functions must be expressed in terms of the strong coupling Greens functions. In this regard it is appropriate to use the notation introduced by Nambu[26] to handle both one particle and pair correlations in a Green's function format which is formally the same as for weak couplers. The Matrix operators

$$\psi_k = \begin{pmatrix} C_{k\uparrow} \\ C^{\dagger}_{-k\downarrow} \end{pmatrix} \text{and} \quad \psi_k^{\dagger} = \left(C^{\dagger}_{k\uparrow},\; C_{-k\downarrow}\right) \quad (23)$$

are introduced. In terms of these operators, the four-current density becomes

$$j_\mu(q) = \begin{cases} (-e) \sum\limits_p \; \psi_p^{\dagger}(\vec{p} + \frac{\vec{q}}{2})_i \; \mathbb{1} \; \psi_{p+q} & \text{for } i = \mu = 1,2,3 \\ (-e) \sum\limits_p \; \psi_p^{\dagger} \tau_3 \; \psi_{p+q} & \text{for } \mu = 0 \end{cases} \quad (24)$$

where 1 and τ_3 are the usual 2 x 2 Pauli matrices.

To greatly ease the way, one can follow the procedure used by Schrieffer, computing quantities in the more simple T = 0 case and converting the final Green's function expressions to a form valid at finite temperatures.[27,31,32]

Equation 22 involves a retarded commutator. To evaluate it in terms of the Green's function formalism, it is best to express it in terms of time-ordered products. By comparing their spectral forms it is found that

$$\langle o|[n,n]|o\rangle(q) = \begin{cases} \frac{1}{e^{z}}\langle o|T\{j_o(q)j_o(-q)\}|o\rangle & \text{for } q_o > 0 \\ \frac{1}{e^{z}}\langle o|T\{j_o(q)j_o(-q)\}|o\rangle^* & \text{for } q_o < 0 \end{cases} \quad (25)$$

We continue the evaluation with the expression

$$\Lambda_\mu(x,y,z) = \langle o|T\{j_\mu(z)\psi(x)\psi^\dagger(y)\}|o\rangle . \quad (26)$$

The function Λ_μ is related to the vertex function Γ_μ which is defined by the integral

$$\Lambda_\mu(x,y,z) = e\int G(x,y)\Gamma_\mu(x,y',z)G(y',y)d^4x'd^4y' \quad (27)$$

where

$$G(x,x') = -i\langle o|T\{\psi(x)\psi^\dagger(x')\}|o\rangle \quad (28)$$

is the 2 x 2 Nambu Green's function. If we multiply $\Lambda_o(x,y,z)$ by τ_3, take the trace and reorder terms, we find, after transforming into momentum space,

$$\langle o|[n,n]|o\rangle(q) = \frac{1}{2}\sum_p T_r[\tau_3 G(p+q)\Gamma_o(p+q,p)G(p)] \quad (29)$$

At finite temperature the sum

$$\int_{-\infty}^{\infty} \frac{dp_0}{2\pi} \; \cdots \qquad (10)$$

$$p_0 = p_m = \cdots$$

The sum is converted to a contour integral. This contour is then opened up to pick up the poles for final evaluation of the integral.

Nam[28] begins his application of the ... action of an "undressed ... using the ... :

$$\frac{1}{m}(p = \frac{1}{p} \qquad (11)$$

$$\tau_3 \qquad \cdots = 1$$

The errors ... are neglecting ... are on the order of $\left(\frac{m}{M}\right)$ ... by Migdal's theorem ...

$$\cdots = \frac{1}{2} \sum_{p} \cdots \qquad (12)$$

Nam finds the Green's function for the ... to be formally the same as ... the weak-coupling ... have the form

$$\cdots = [z(p)]p_0 - \cdots$$

$$= \frac{1}{2}\left[\frac{\cdots = p(p)\tau_1 + \cdots}{\cdots - \tilde{\varepsilon}(p)} + \cdots \right]$$

where

$$\varepsilon(p) = Z(p)[p_o^2 - \Delta^2(p)]^{1/2} = \varepsilon_o + i\Gamma$$

$$N(p) = Z(p)p_o/\varepsilon(k) = p_o/[p_o^2 - \Delta^2(p)]^{1/2} \qquad (33)$$

$$P(p) = Z(p)\Delta(p)/\varepsilon(p) = \Delta(p)/[p_o^2 - \Delta^2(p)]^{1/2}$$

$Z(k)$, $\Delta(k)$ and $\bar{\varepsilon}_k$ are the wave function renormalization, gap parameter and the renormalized quasiparticle energy, respectively.

Equations 33 are inserted in Eq. 32 and the indicated sums performed.[27,28,29] Taking the limit in which the ultrasonic energy q_o is small compared with the gap energy ω_g, the attenuation due to the density-density correlation term in Eq. 21 becomes

$$\int_{\omega_g}^{\infty} \frac{\beta}{2} d\omega \left(A \cdot \frac{m^2 q}{\pi}\right) \cdot \{N^+N^- - P^+P^- - 1\} \cdot \left\{\frac{q\ell \tan^{-1} q\ell}{q\ell - \tan^{-1} q\ell}\right\} \tanh \frac{\beta\omega}{2} \qquad (34)$$

[1] [2]

Factor [1] is the coherence factor. It would be identically 1 if the gap function $\Delta(\omega)$ were not complex. The signs on N and P are related to the particular cut of the p_o integral which contributes the terms. The factor [2] comes from the angular sum over the energy denominator of the Green's function. Vertex corrections due to impurity scattering are added. This is done by replacing the relaxation time with an effective relaxation time for transport.[16,28] The gap energy, $\omega_g = \Delta(\omega_g)$, is solved for implicitly.

Including also contributions involving the stress tensor τ_{zz} which are calculated in a similar manner, the longitudinal ultrasonic attenuation becomes

$$\alpha_L = \int_{\omega_g}^{\infty} \frac{\beta}{2} d\omega \, \mathrm{sech}^2 \frac{\beta}{2}\omega \, \alpha_N(q\ell(\omega)) \cdot \frac{1}{2}\left\{1 + \frac{(\omega^2 - |\Delta(\omega)|^2)}{|\omega^2 - \Delta^2(\omega)|}\right\} \qquad (35)$$

where

$$\alpha_N = \left(\frac{N_m v_F q}{\rho_{ion} v_s}\right)\frac{1}{q\ell}\left\{\frac{(q\ell)^2 \tan^{-1} q\ell}{(q\ell) - \tan^{-1} q\ell} - 1\right\}. \qquad (36)$$

The electronic mean free path $\ell(\omega)$ includes both impurity and electron-phonon scattering. This is essentially the same result as that obtained by Pippard.[30] The differences are the inclusion of the superconducting coherence factor and the fact that the energy dependence of the mean free path over the effective energy range requires separate handling of each energy group of electrons. All electrons are not treated as "on the Fermi surface" and an integral over energies is used. The coherence factor $\frac{1}{2}\left\{1 + \frac{(\omega^2 - |\Delta(\omega)|^2)}{|\omega^2 - \Delta^2(\omega)|}\right\}$ is only negligibly different from 1 in the contributing integrand at our ultrasonic frequencies in lead. It may be taken as 1 to the accuracy which strong coupling effects, at the ultrasonic frequencies used in our experiment, have been described by the rest of the theory. However, it has been included in all computer calculations.

CHAPTER IV

STRONG-COUPLING INTERPRETATION OF EXPERIMENTAL RESULTS

The discussion of experimental and theoretical results begins with equations detailing the strong-coupling predictions for longitudinal-ultrasonic attenuation in lead.[14,16] We label the theoretical attenuation values $\alpha_{nt}(f,T)$ and $\alpha_{st}(f,T)$ in the normal and super states for ultrasonic frequency F and temperature T. Subscripts designating the mode of attenuated ultrasound are omitted since all our experiments and computations for lead concern longitudinal waves propagating along the [100] axis.

$$\alpha_{st}(f,T) = \int_{\omega_g}^{\infty} d\omega \, \frac{\beta}{2} \, \mathrm{sech}^2 \left(\frac{\beta}{2}\omega\right) \alpha_N(q \cdot \ell_{st}(\omega,T)) \cdot \frac{1}{2}\left[1 + \frac{(\omega^2 - |\Delta|^2)}{|\omega^2 - \Delta^2|}\right] \quad (36)$$

$$\alpha_{nt}(f,T) = \int_{\omega_g}^{\infty} d\omega \, \frac{\beta}{2} \, \mathrm{sech}^2 \left(\frac{\beta}{2}\omega\right) \alpha_N(q \cdot \ell_{st}(\omega,T)) \quad (37)$$

where

$$\alpha_N(q\ell) = \left(\frac{N m v_F q}{\rho_{ion} v_s}\right) \frac{1}{(q\ell)} \left\{\frac{1}{3} \frac{(q\ell)^2 \tan^{-1}(q\ell)}{(q\ell) - \tan^{-1}(q\ell)} - 1\right\} \quad (38)$$

and

$$\omega_g(T) = \mathrm{Re}\{\Delta(\omega_g(T))\} \quad (39)$$

is found implicitly at each temperature in the superconducting range. The electron mean free path is the variable of critical importance in the strong-coupling properties of lead. It depends upon electron energy and differs in the normal and superconducting states. If ℓ_o is the residual impurity-limited

electron mean free path, we have[11,28]

$$\ell_{st}^{-1}(\omega,T) = \left[\frac{v_e(\omega,T)}{2\mathrm{Im}\{z_s(\omega,T)(\omega^2 - \Delta^2)^{1/2}\}}\right]^{-1} + \ell_o^{-1} \tag{40}$$

$$\ell_{nt}^{-1}(\ ,T) = \left[\frac{v_e(\omega,T)}{2\omega\ \mathrm{Im}\{z_n(\omega,T)\}}\right]^{-1} + \ell_o^{-1} \tag{41}$$

where

$$v_e(\omega,T) = v_{F0}\cdot\left(\frac{m^*(0,0)}{m^*(\omega,T)}\right) = v_{F0}\cdot\left(\frac{z_n(0,0)}{z(\omega,T)}\right) \tag{42}$$

The integrals 36 and 37 were evaluated numerically using values of the renormalization constants and gap parameter $z_s(\omega)$, $z_n(\omega)$ and $\Delta(\omega)$ computed by Swihart, Scalapino and Wada,[17,18] hereafter referred to as SSW. Tunneling data[22,33,34] was used as a basis of their numerical description of the phonon density of states. The only remaining parameter not directly determined experimentally is the zero temperature Fermi velocity v_{F0}. It is dependent upon the particular region of the Fermi surface picked out by the direction of ultrasound propagation and is best determined in a fit to the attenuation data. For an approximate estimate it is pertinent to note that Anderson and Gold[35] find the zero temperature Fermi velocity $v_{F0} = 1.28 \times 10^8$cm/sec from de Haas-van Alphen measurements in lead. From the coherence length one finds $v_{F0} = \pi\Delta(0)\xi_o/h = 5.27 \times 10^7$ cm/sec. We must be reminded that the Anderson-Gold value of v_{F0} pertains to an averaged v_{F0} over a particular cross-sectional area of the Fermi surface, so their value provides, at best, only a rough indication of the particular v_{F0} appropriate to this work.

Attenuation integrals were evaluated by Simpson's rule and cutoff at 10 mev in our computer program. To check the accuracy of the integration and the validity of the cutoff, the coherence factor $\frac{1}{2}\left[1+\frac{(\omega^2-|\Delta|^2)}{|\omega^2\ \Delta^2|}\right]$ and α_N were both set equal to 1.0 for one computer integration run. The resulting $\alpha_S(T)$ was found to equal $f(\beta\omega_g)$, the expected Fermi function, to 4 decimal places.

In evaluating ultrasonic attenuation due to electrons, it is customary to speak in terms of the product $q\ell$, where $q = 2\pi f/v_s$ is the phonon wave number and ℓ is the electron mean free path, usually taken to be constant for all ultrasonic frequencies. The value of $q\ell$ may be determined from high-field magnetoacoustic measurements or from a least squares fit of $\alpha_n(T)$ versus frequency for a constant temperature T. Strict application of both of these methods is prone to inaccuracies as both are based upon a weak-coupling, free-electron model which is not a proper description of strong-coupling lead. If the attenuation is to have the form of α_N as derived by Pippard,[30] then

$$\alpha_N(f,T) = A\cdot f\cdot\left\{\frac{6/\pi}{q\ell}\left(\frac{1}{3}\cdot\frac{(q\ell)^2\ \tan^{-1}q\ell}{q\ell-\tan^{-1}q\ell}-1\right)\right\} \tag{43}$$

where f is the ultrasonic frequency, A is a constant for the material, and ℓ depends upon the purity and temperature of the sample in question.

It should be remembered that the assumption of a constant A is not completely consistent with our renormalization of all parameters. Blount,[36] including the effects of renormalization in the Pippard formula for α_N, found that the leading factor Af becomes A $\left(\frac{m}{m^*}\right)$f. However, in the actual computed values of α_n less than a 1% shift results from the assumption of a constant A in fitting the theoretical mean free path to its measured value at T_c. The shifts in attenuation ratios between different frequencies, temperatures or

between the normal and superconducting states are affected only negligibly. Hence, in order to keep the interpretation of the data and theory on an intuitive level we make the necessary assumption of an A, which is constant over electron energy, and which may then be moved outside the attenuation integral.

Usually $\alpha'(f)$ is defined as the attenuation at a frequency f for infinite $q\ell$ and $F(q\ell)$ the free-electron theoretical ratio of the attenuation to the maximum $a'(f)$ at that frequency. From Eq. 43 we have

$$\alpha'(f) = A \cdot f$$

$$F(q\ell) = \frac{6/\pi}{q\ell} \left(\frac{1}{3} \frac{(q\ell)^2 \tan^{-1} q\ell}{q\ell - \tan^{-1} q\ell} \right) - 1 \Bigg) \tag{44}$$

If we assume the attenuation is correctly described by the strong-coupling formalism in Eqs. 36 and 37, an "effective normal state ultrasonic mean free path" may be defined:

$$\bar{\ell}_{nt}(f,T) = \left(\frac{1}{q}\right) F^{-1} \left(\int_0^\infty d\omega \, \frac{\beta}{2} \, \mathrm{sech}^2 \left(\frac{\beta\omega}{2}\right) F(q\ell_{nt}(\omega,T)) \right) \tag{45}$$

where $\ell_{nt}(\omega,T)$ is given in 41. This is the mean free path which would be computed by the experimentalist if he were to measure the strong-coupling calculated attenuation and interpret it under the usual Pippard theory. Similarly, if we assume the approximation used by Fate and Shaw.[13]

$$\alpha_s(f,T) \simeq A \cdot f \cdot F(q\ell_s) \cdot 2f(\beta\omega_g), \tag{46}$$

to be exactly true, we may define an "effective superconducting ultrasonic

mean free path" to be

$$\bar{\ell}_{st}(f,T) = \frac{1}{q} F^{-1} \left(\frac{\int_{\omega_g}^{\infty} d\omega \, \frac{\beta}{2} \, \mathrm{sech}^2\left(\frac{\beta\omega}{2}\right) \cdot F(q\ell_{st}(\omega,T)) \cdot \frac{1}{2}\left[1 + \frac{(\omega^2 - |\Delta|^2)}{|\omega^2 - \Delta^2|}\right]}{2f(\beta\Delta(T))} \right) \quad (47)$$

In addition to the Pippard theory the experimentalist is assuming that the superconducting attenuation follows a BCS temperature dependence. This assumption involves a free-electron gap $2\Delta(T)$ as tabulated by Mühlschlegel[37] with the zero temperature gap $2\Delta(0) = 4.3\ kT_c$.[22] However, $\bar{\ell}_{st}(f,t)$ does include allowance for different mean free paths in the normal and super states.

Figures 5 show the "experimental effective mean free path ratio" $\bar{\ell}_{se}/\bar{\ell}_{ne}$ at several frequencies as measured by Fate et al and as given by our strong-coupling theory calculation fitted to their normal state mean free path at 90 MHz. Here, $\bar{\ell}_{se}$ and $\bar{\ell}_{ne}$ are defined for experimental attenuation values the same way that $\bar{\ell}_{st}$ and $\bar{\ell}_{nt}$ were related to the strong-coupling theory predictions:

$$\bar{\ell}_{ne}(f,T) = \frac{1}{q} F^{-1}(\alpha_n(f,T)/A \cdot f)$$

$$\bar{\ell}_{np}^{-1} = \bar{\ell}_{ne}^{-1} - \bar{\ell}_o^{-1} \quad (48)$$

$$\bar{\ell}_{se}(f,T) = \frac{1}{q} F^{-1}\left(\left[\frac{\alpha_s(f,T)}{2f(\beta\omega)}\right] \Big/ A \cdot f \right)$$

$$\bar{\ell}_{sp}^{-1} = \bar{\ell}_{se}^{-1} - \bar{\ell}_o^{-1}$$

Fate et al observed that more than a simple temperature dependence of

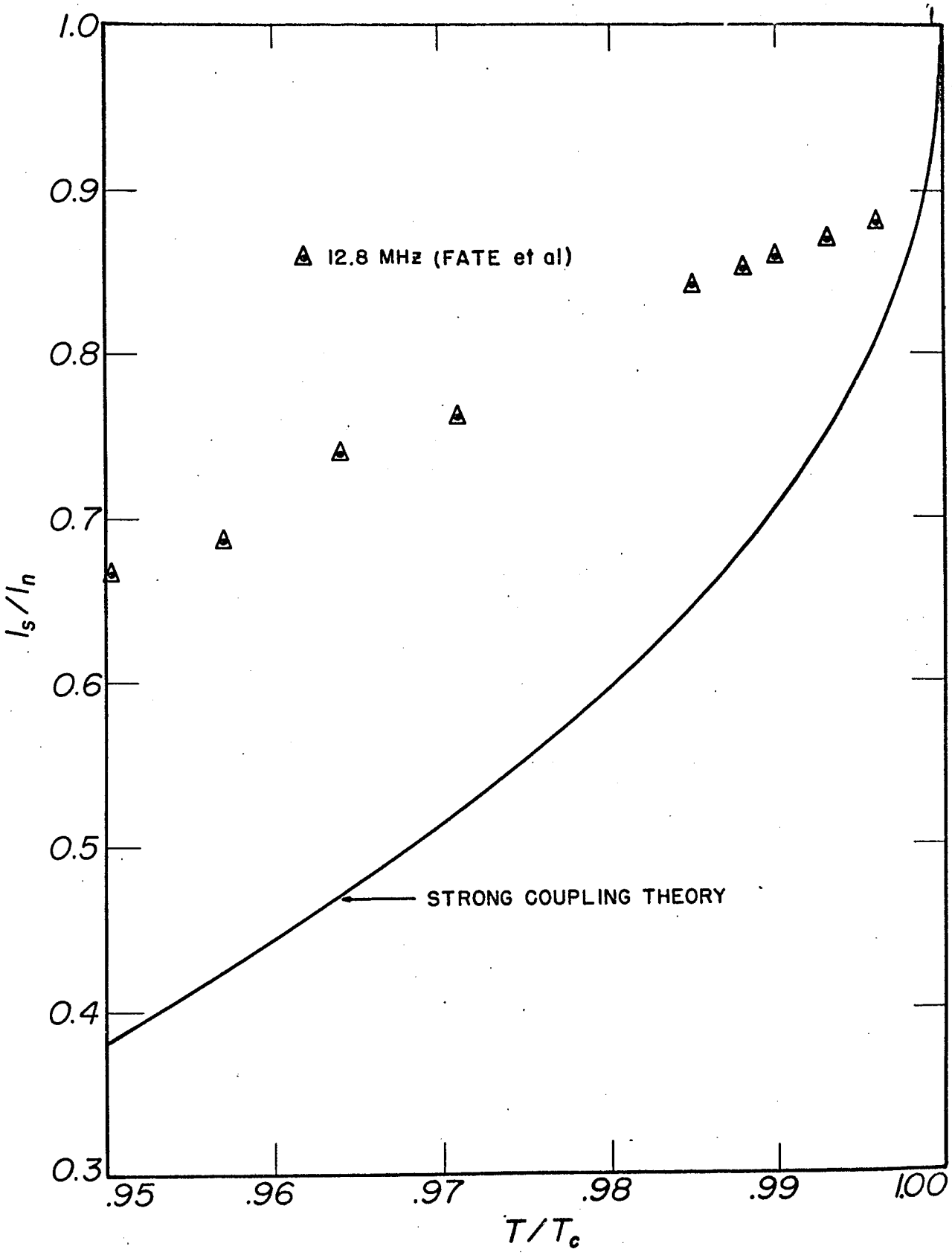
1.0
0.9
0.8
0.7
0.6
0.5
0.4
0.3
I_s/I_n
12.8 MHz (FATE et al)
STRONG COUPLING THEORY
.95
.96
.97
.98
.99
1.00
T/T_c

Figure 5(a)

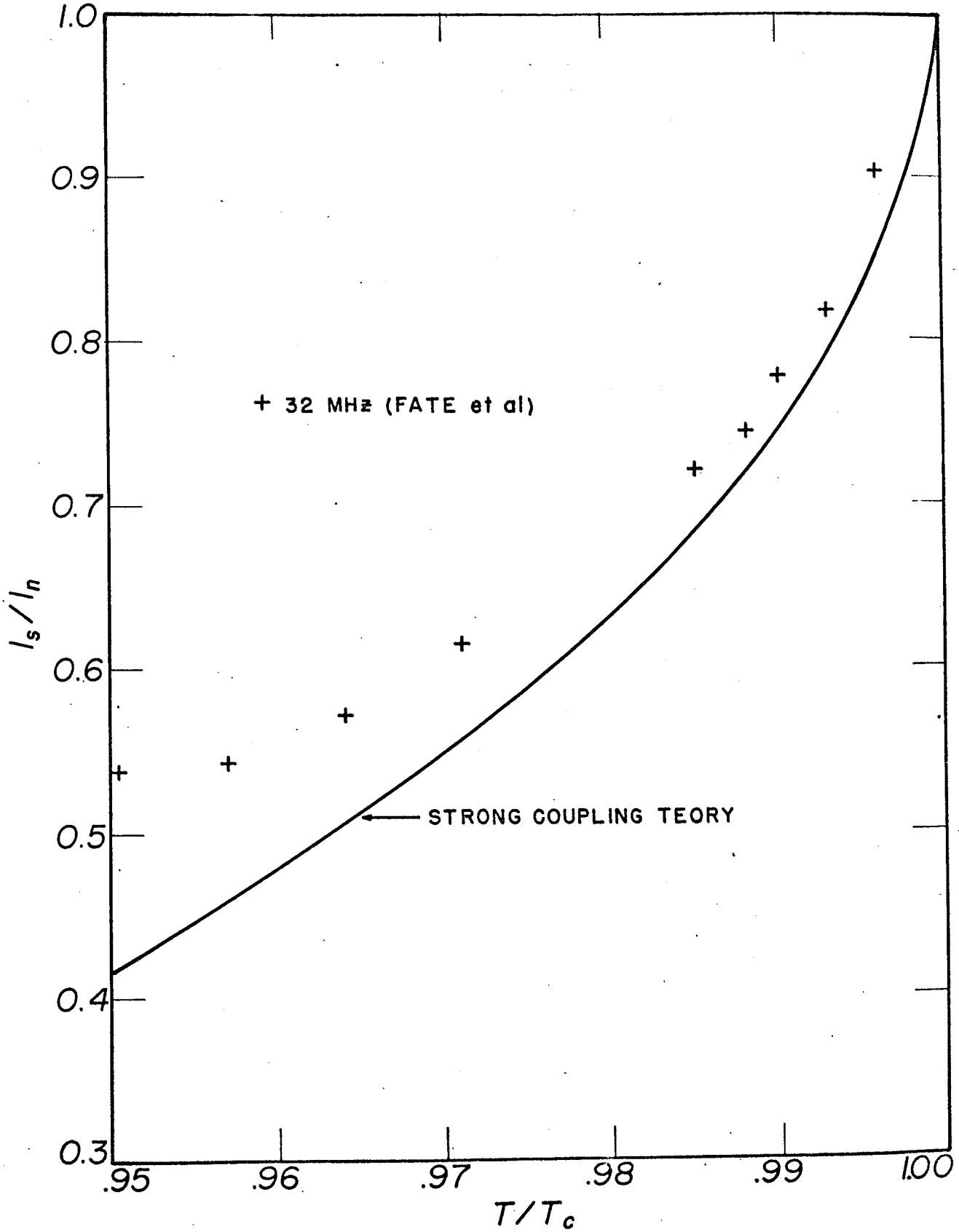
1.0
0.9
0.8
0.7
0.6
0.5
0.4
0.3
I_s / I_n
+ 32 MHz (FATE et al)
STRONG COUPLING TEORY
.95
.96
.97
.98
.99
1.00
T / T_c

Figure 5(b)

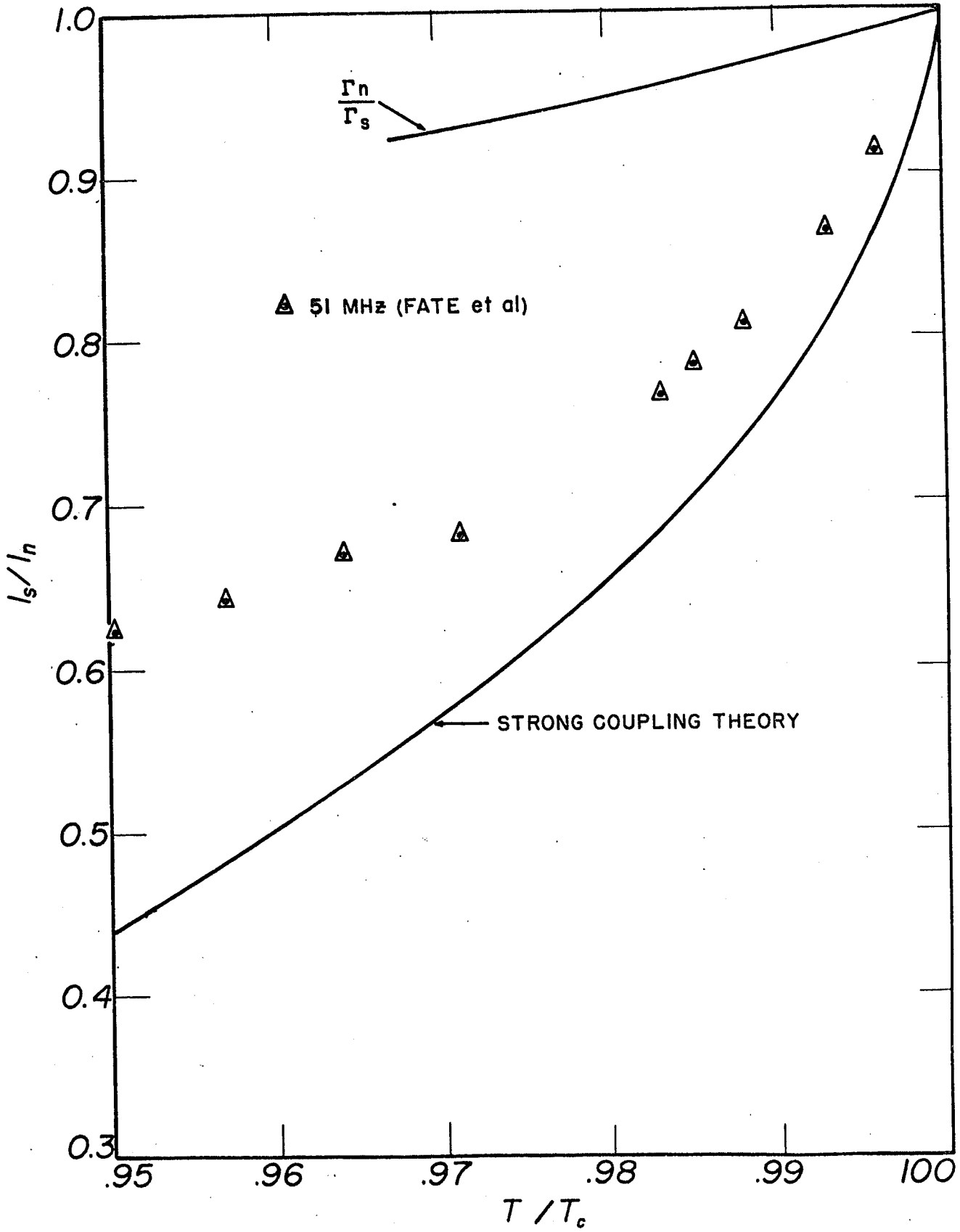
1.0
0.9
0.8
0.7
0.6
0.5
0.4
0.3
$\frac{\Gamma n}{\Gamma s}$
51 MHz (FATE et al)
STRONG COUPLING THEORY
I_s / I_n
.95
.96
.97
.98
.99
100
T / T_c

Figure 5(c)

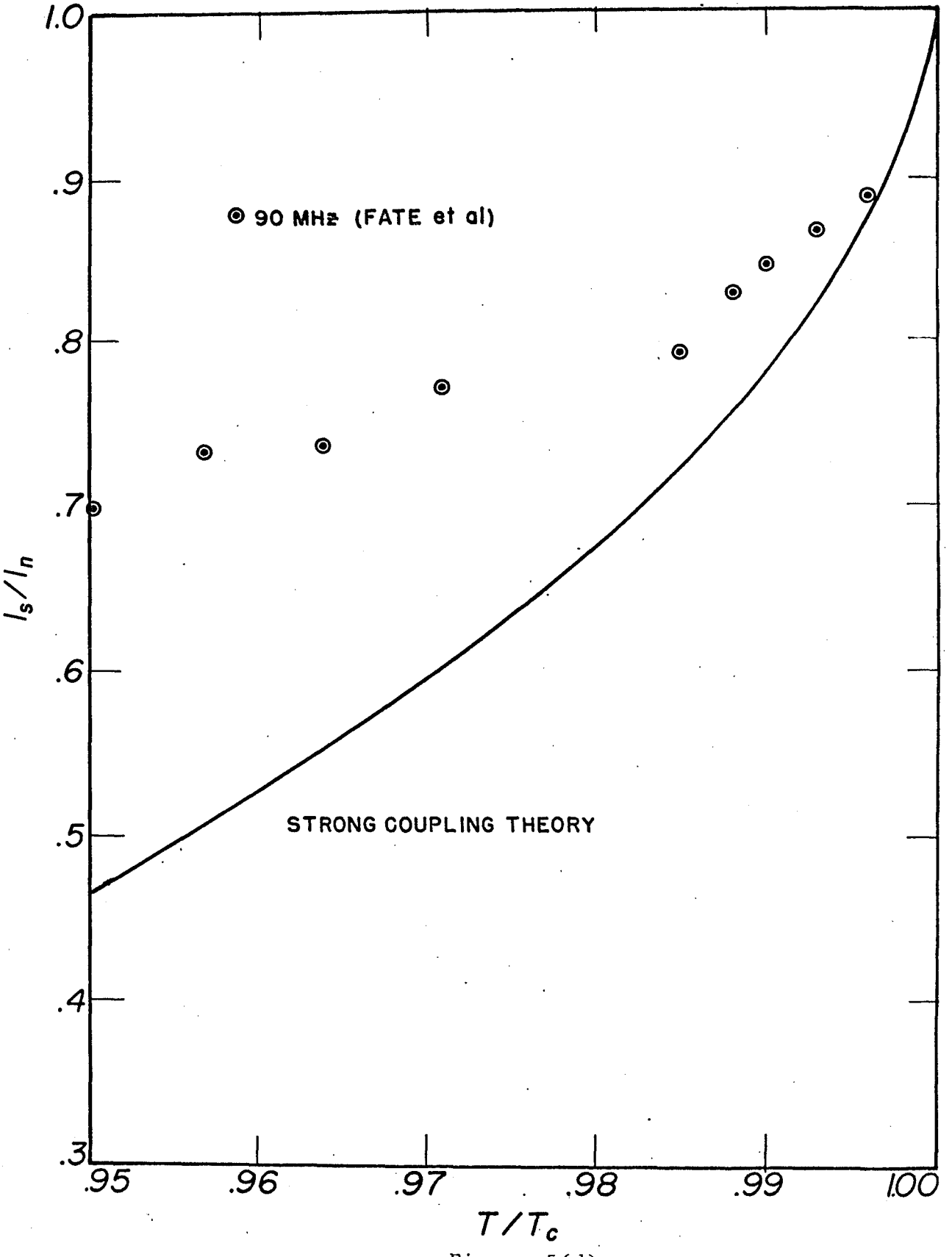
1.0
.9
.8
.7
.6
.5
.4
.3
I_s/I_n
⊙ 90 MHz (FATE et al)
STRONG COUPLING THEORY
.95
.96
.97
.98
.99
1.00
T/T_c

Figure 5(d)

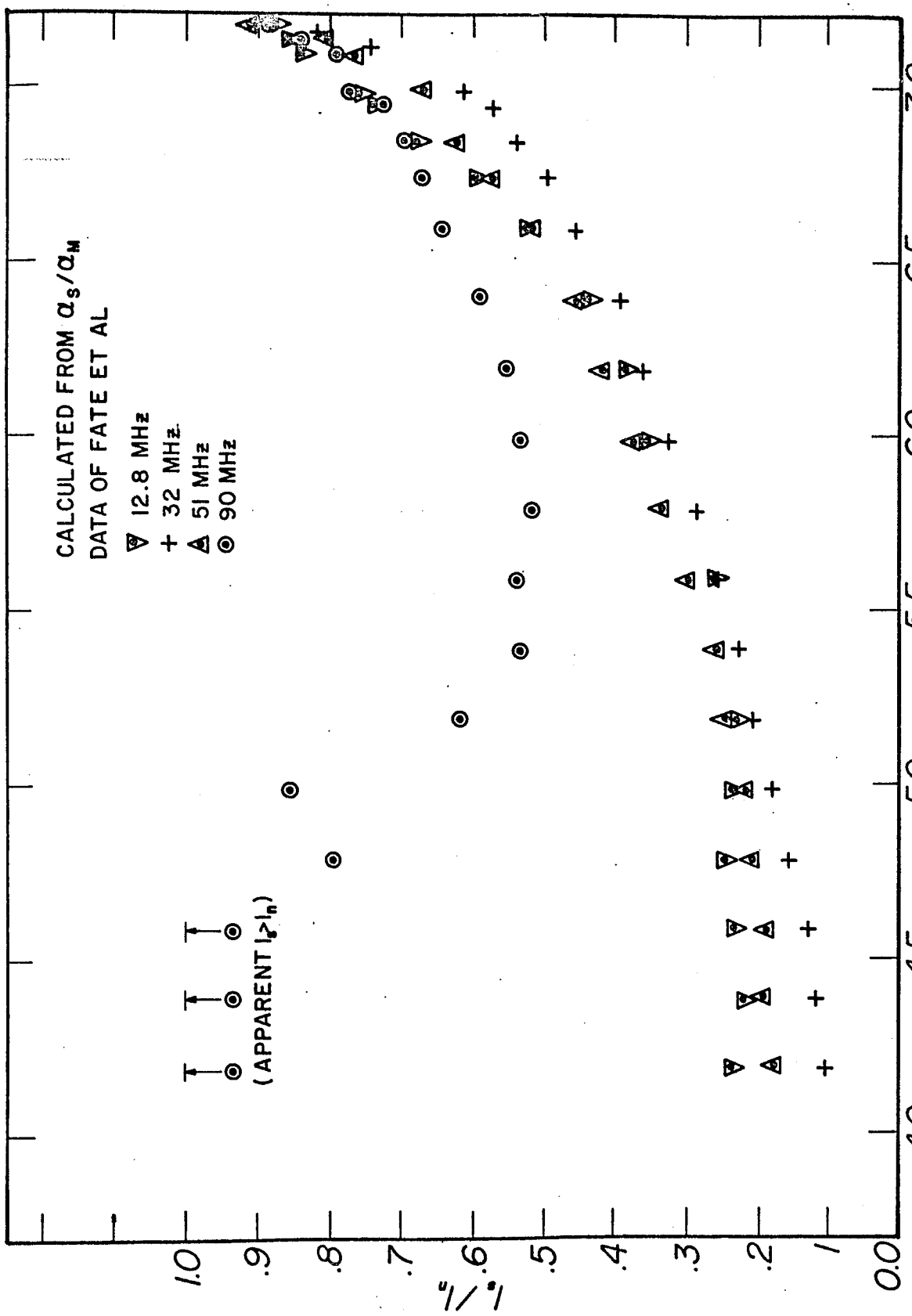
CALCULATED FROM α_s/α_M
DATA OF FATE ET AL
12.8 MHz
32 MHz
51 MHz
90 MHz
(APPARENT $I_s > I_n$)
I_s/I_n
T(°K)
0.0
.1
.2
.3
.4
.5
.6
.7
.8
.9
1.0
4.0
4.5
5.0
5.5
6.0
6.5
7.0

Figure 6

the electron-phonon scattering rate Γ might be involved in the drop in attenuation below the transition temperature. The reason they made this observation is shown in Fig. 5c constructed from their data at 51 MHz. The quantity Γ_n/Γ_s, as calculated by Ambegaokar and Woo from the SSW numerical results at electron energy 0.6 mev, shows a drop which does not compare with that in the $\bar{\ell}_{sp}/\bar{\ell}_{np}$ curve below T_c. The agreement of $\bar{\ell}_{se}/\bar{\ell}_{ne}$ with our computed strong-coupling effective mean free path ratio $\bar{\ell}_{st}/\bar{\ell}_{nt}$ is much better. It includes changes over the whole electron quasiparticle energy spectrum. The superstate mean free path $\ell_{st}(\omega,T) = v_e(\omega)/2$ Im $\{Z_s(\omega^2 - \Delta^2)^{1/2}\}$ is largest for electrons in low energy states as pointed out by Ambegaokar and Woo,[11] and these electron states are the first to disappear as the gap opens up below T_c. Hence, we show that a much larger drop in the effective $\bar{\ell}_{sp}$ is predicted by strong-coupling theory and observed experimentally in Fig. 5 for all of Fate's frequencies. Figure 7 shows the resulting attenuation ratio α_s/α_n compared with Fate's measurements. The strong-coupling theory predicts a drop-off in the attenuation below T_c somewhat stronger than that which is measured. This is not surprising. Essentially the same computations by Ambegaokar and Woo, using the same SSW calculations for the region below T_c, yielded a drop in the thermal conductivity ratio (K_s/K_n) somewhat greater than has been measured.[11] This is shown in Fig. 8. The ultrasonic measurements confirm the direction in which the strong-coupling calculation must be improved.

The dependence of longitudinal attenuation on ultrasonic frequency shown in Figs. 5, 6, and 7 in both theory and experiment can be explained in terms of a shift in emphasis from one part of the electron quasiparticle energy spectrum to another. This is demonstrated in Figs. 9, 10 and 11. At lower ultrasonic frequencies $F(q\ell) \propto q\ell$ and long-lived low energy quasiparticles

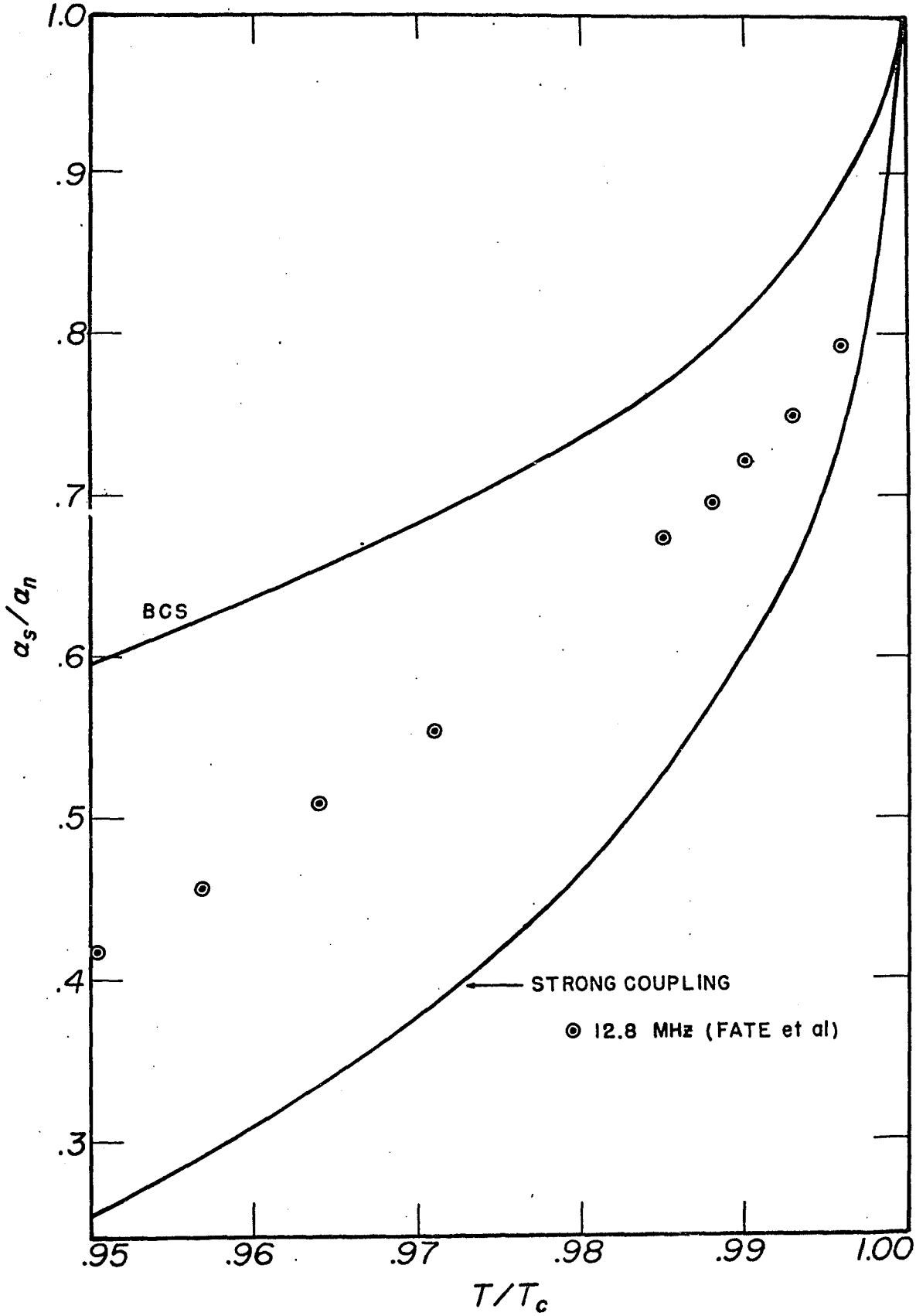
1.0
.9
.8
.7
.6
.5
.4
.3
a_s/a_n
BCS
STRONG COUPLING
12.8 MHz (FATE et al)
.95
.96
.97
.98
.99
1.00
T/T_c

Figure 7(a)

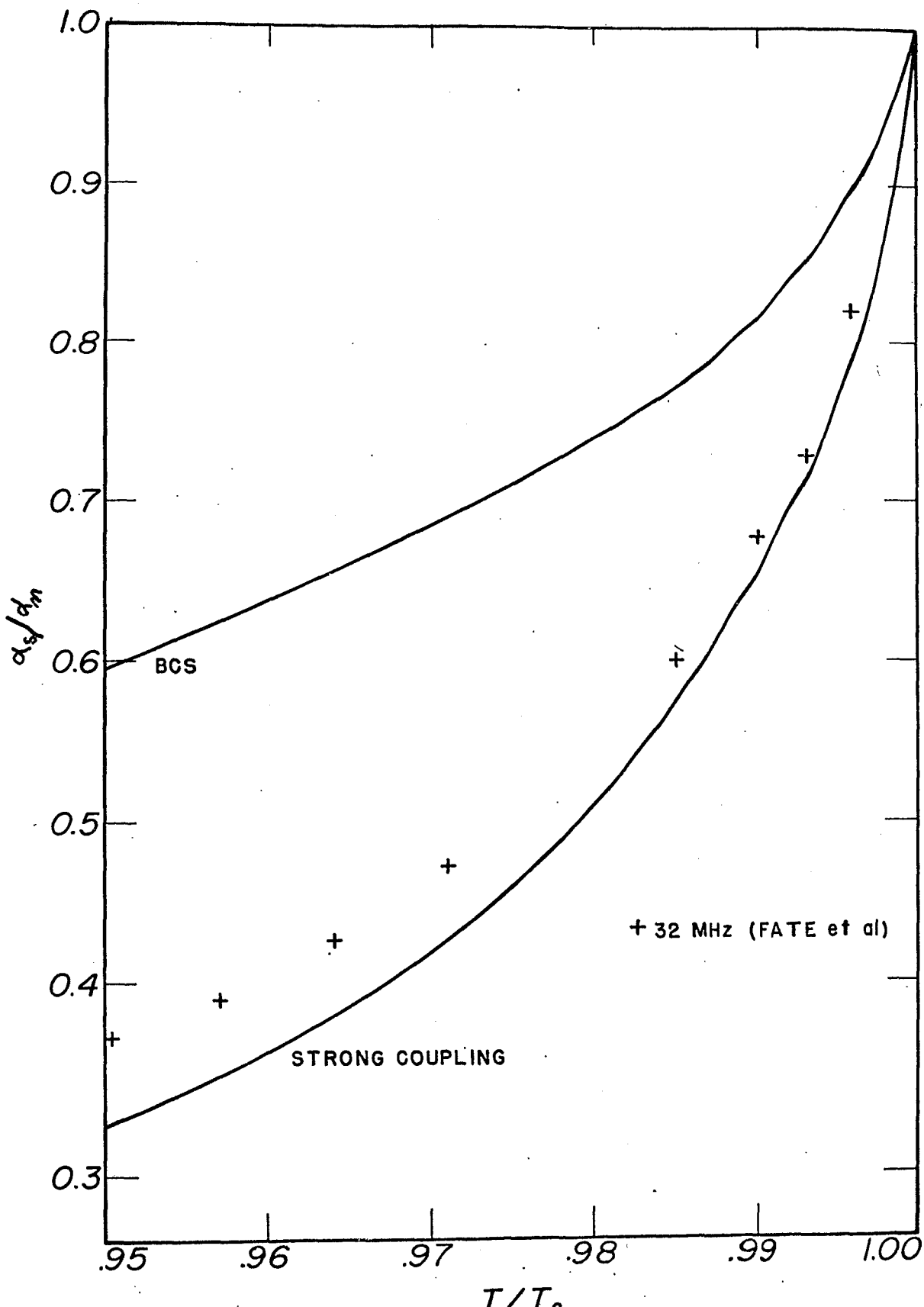
1.0
0.9
0.8
0.7
0.6
0.5
0.4
0.3
α_s/α_n
BCS
STRONG COUPLING
+ 32 MHz (FATE et al)
.95
.96
.97
.98
.99
1.00
T/T_c

Figure 7(b)

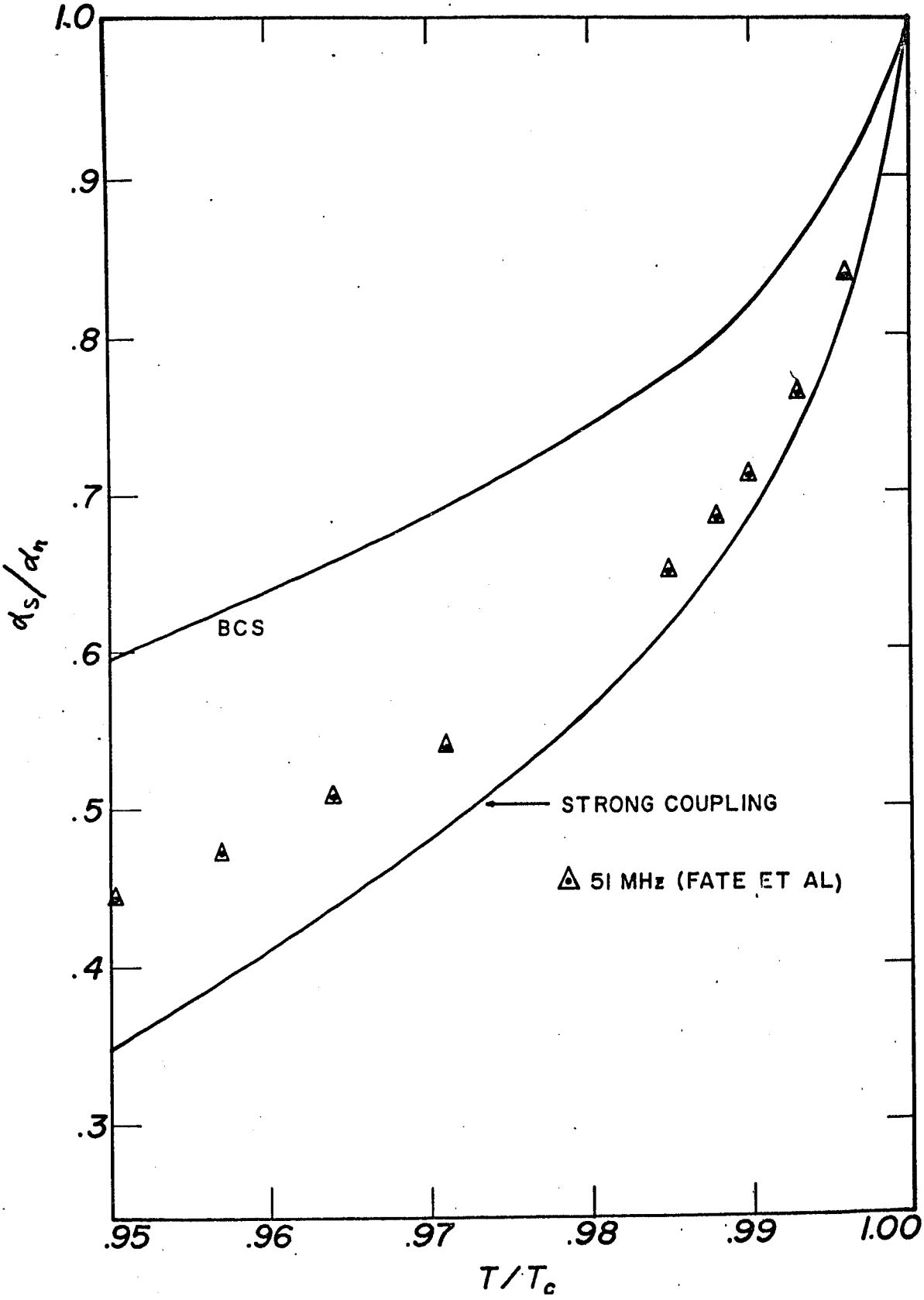
1.0
.9
.8
.7
.6
.5
.4
.3
d_s/d_n
BCS
STRONG COUPLING
51 MHz (FATE ET AL)
.95
.96
.97
.98
.99
1.00
T/T_c

Figure 7(c)

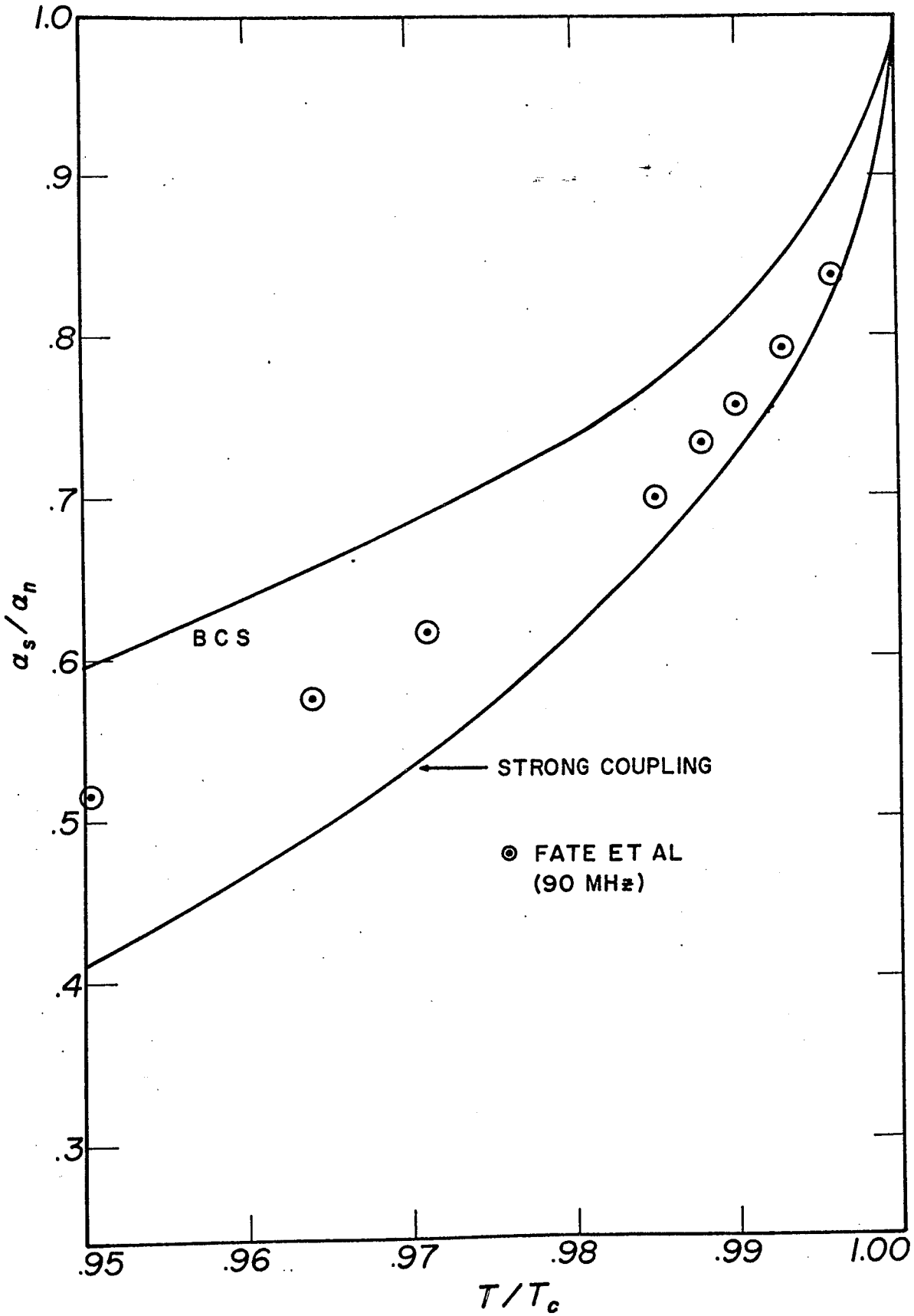
1.0
.9
.8
.7
.6
.5
.4
.3
α_s / α_n
BCS
STRONG COUPLING
FATE ET AL
(90 MHz)
.95
.96
.97
.98
.99
1.00
T / T_c

Figure 7(d)

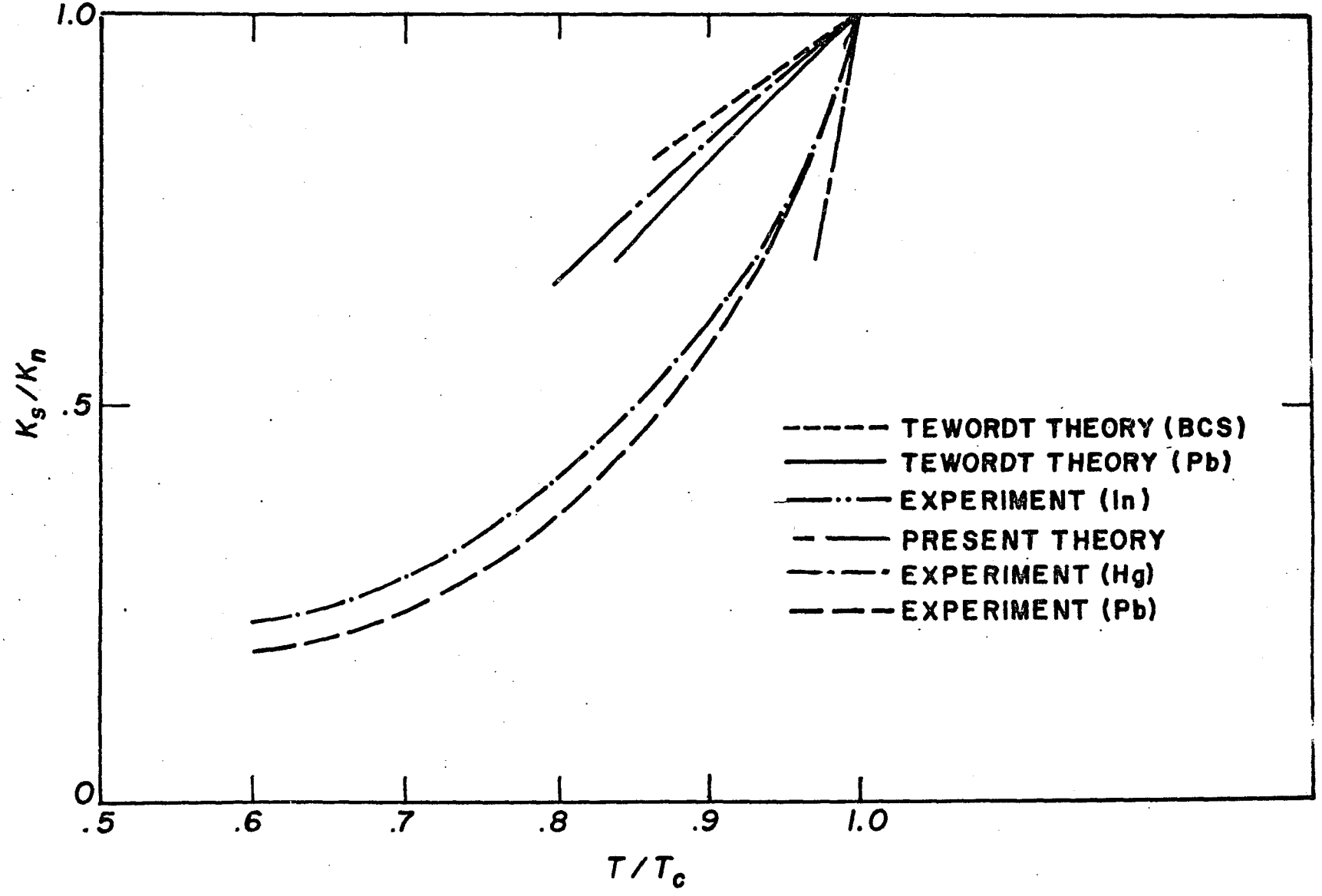
1.0
.5
0
K_s/K_n
.5
.6
.7
.8
.9
1.0
T/T_c
TEWORDT THEORY (BCS)
TEWORDT THEORY (Pb)
EXPERIMENT (In)
PRESENT THEORY
EXPERIMENT (Hg)
EXPERIMENT (Pb)

Figure 8

are emphasized in the attenuation. At the higher frequencies, more electrons of shorter mean free path come into play and the average mean free path must drop. This is obviously true in both the normal and superconducting states. However, in the superconducting state the longest living quasiparticle states have been eliminated by the opened gap and the remaining energy states have lifetimes more nearly the same. Hence, $\bar{\ell}_{st}$ decreases proportionately more slowly than $\bar{\ell}_{nt}$ with increasing f, and the ratio $\bar{\ell}_{st}/\bar{\ell}_{nt}$ increases with f as seen in Fig. 5.

Both theory and experiment show this frequency behavior, except for the 12.8 MHz experimental case. The measurements of α_s at this frequency are less accurate than those at other frequencies, according to FSS.

Figure 6 shows another interesting feature of $\bar{\ell}_{se}/\bar{\ell}_{ne}$ as calculated from the α_s/α_n ratio measured by Fate et al. At 90 MHz the ratio $\bar{\ell}_{sp}/\bar{\ell}_{np}$ actually begins to rise as T drops below 5.5°K and becomes greater than 1.0 for $T < 4.5$°K. This is incompatible with the strong-coupling electronic attenuation predictions. Lacking an obvious explanation for this in terms of electronic attenuation, we naturally turn to dislocation. Confirmed amplitude independence was one of the important features of the Fate data. Hence, amplitude dependent dislocation attenuation should be ruled out as the source of this distortion. Amplitude independent dislocation attenuation of the "shelf" type reported here cannot be ruled out. Fate's measured attenuation must fall back to the BCS prediction at $T = 0$ where superconducting electronic attenuation disappears. Hence, a bump of some sort is necessary. Amplitude dependent dislocation attenuation was regarded as unnecessary for the explanation of their results by Fate et al, but this 90 MHz case may be an exception.

We find the agreement of the measurements of Fate et al with strong-coupling theory and, through it, with other measurements, to be more extensive

than they have claimed. It is pleasing to find this kind of agreement between measured ratios for two different transport processes, α_s/α_n and K_s/K_n, through a strong-coupling calculation based upon another transport process, electron tunneling. Also, the multiple frequencies available for ultrasonic measurements bring another dimension to the qualitative confirmation of the theory.

The effective normal state mean free path $\bar{\ell}_{nt}$ has been plotted in Fig. 9 for several ultrasonic frequencies. In this computation the Fermi velocity at zero temperature v_{F0} has been adjusted as a sliding parameter at 90 MHz to give approximate agreement with the high-field magnetoacoustic mean free path measurements of Fate et al at that frequency.[38] His measurements were made at temperatures below 5°K and were extrapolated to 7.2°K according to his fitted exponential law for the phonon-limited mean free path,

$$\ell_{npF} = 2.27 \times T^{-4.02} \text{ cm} \tag{49}$$

Magnetoacoustic measurements actually made by Fate at 7.2°K diverged from this low temperature fit.

The figure shows that a strong frequency dependence in the effective mean free path is expected even in the normal state. This should show itself in ultrasonic measurements if the formulation has any meaning at all. Fate, on the other hand, found that his normal state attenuation data agreed well with the frequency dependence predicted by Pippard[30] for a frequency-independent electron mean free path. In comparing his data with Pippard theory, Fate set A = 0.18 dB/cm MHz. The quantity A · f is compared with that indicated from experimental measurements of $\alpha_n(T_c)$. That is, for $\ell_{nF}^{-1} = \ell_{npF}^{-1} + \ell_o^{-1}$,

$$(Af)_{exp} = \alpha_n(T_c)/F\left(q\ell_{nF}(T_c)\right). \tag{50}$$

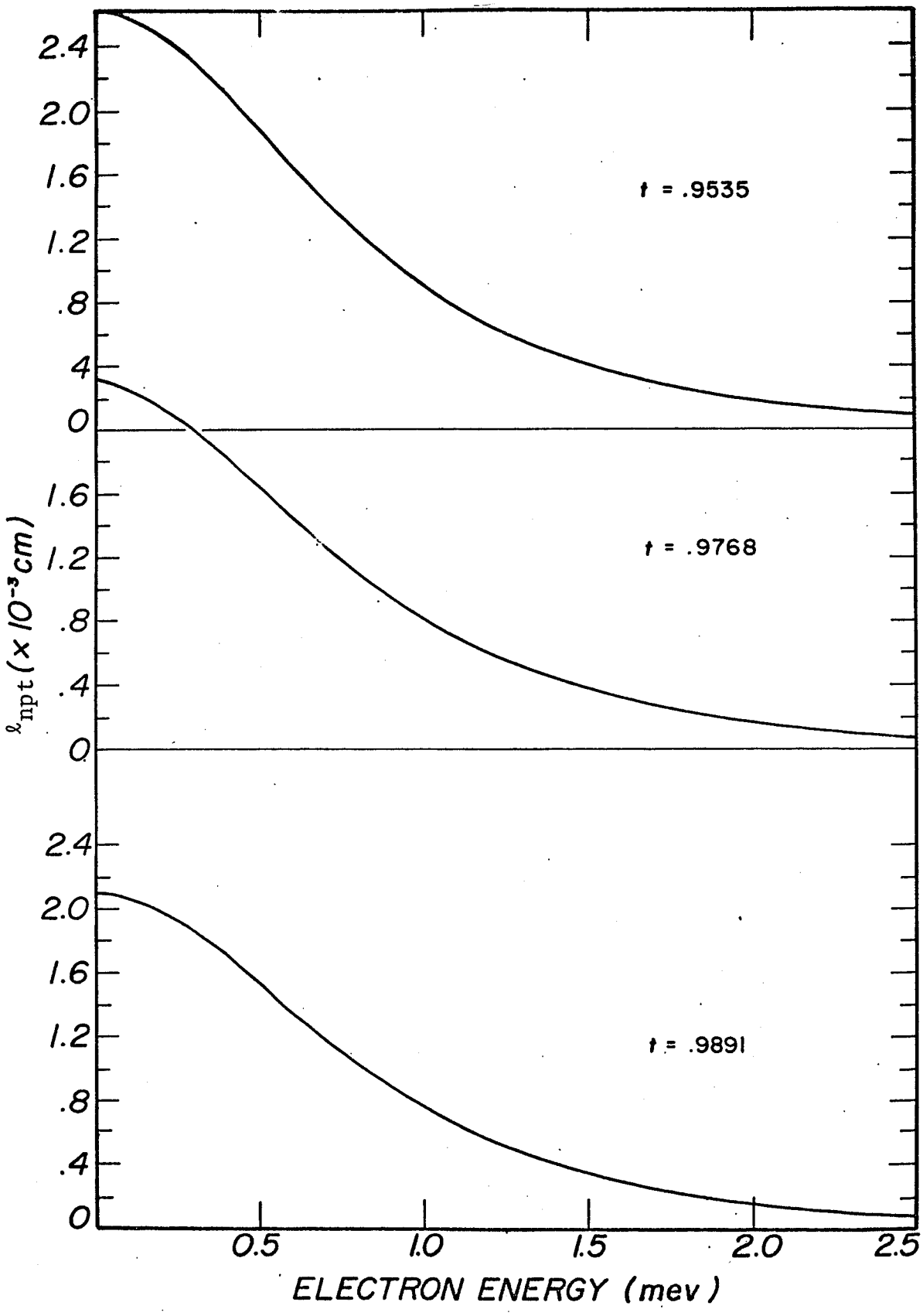
2.4
2.0
1.6
1.2
.8
4
0
t = .9535
1.6
1.2
.8
.4
0
t = .9768
2.4
2.0
1.6
1.2
.8
.4
0
t = .9891
ℓ_{npt} (x 10^{-3} cm)
0.5
1.0
1.5
2.0
2.5
ELECTRON ENERGY (mev)

Figure 9(a)

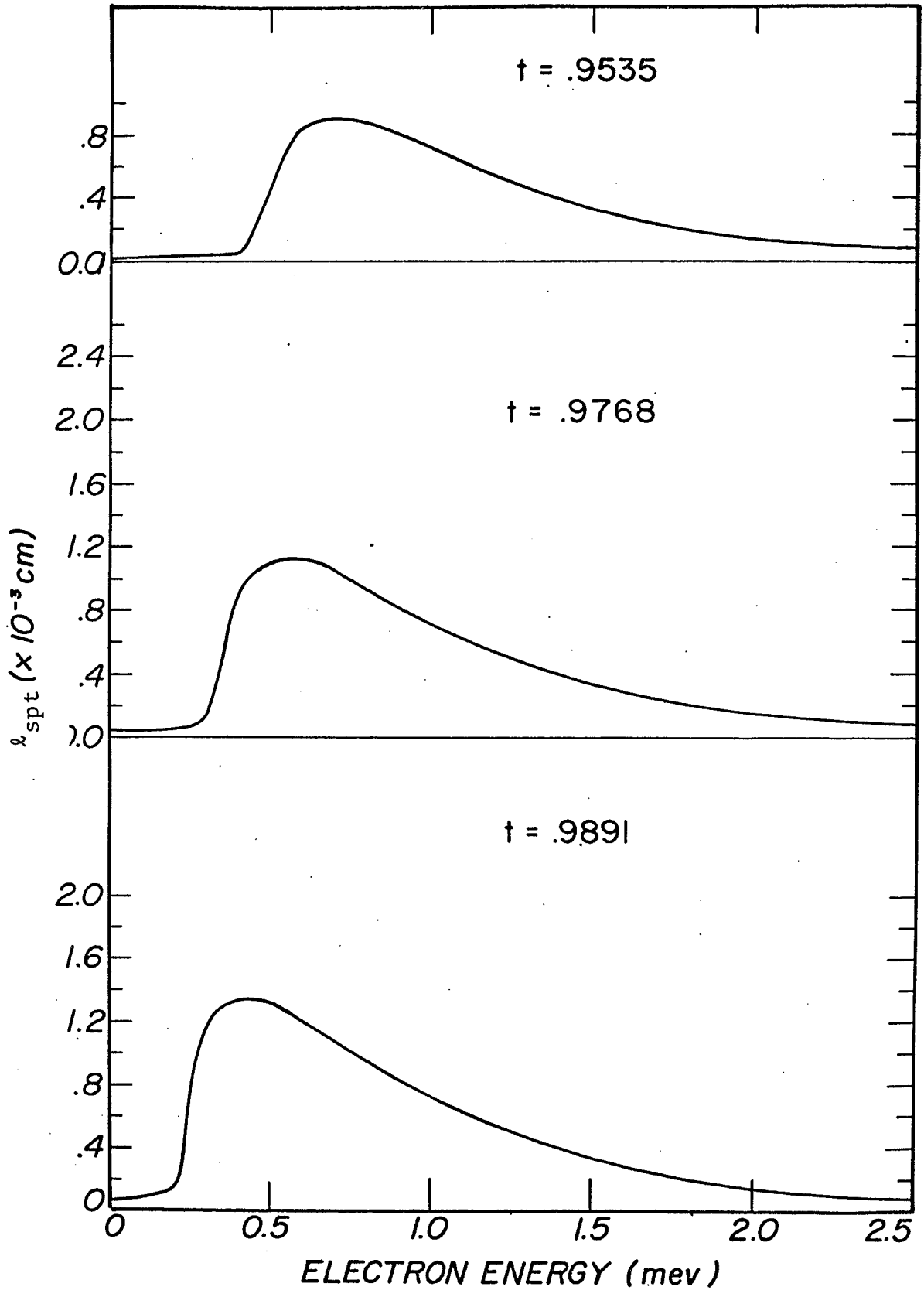
t = .9535
.8
.4
0.0
2.4
2.0
t = .9768
1.6
1.2
.8
.4
0.0
t = .9891
2.0
1.6
1.2
.8
.4
0
0
0.5
1.0
1.5
2.0
2.5
ELECTRON ENERGY (mev)
ℓ_{spt} (x 10^{-3} cm)

Figure 9(b)

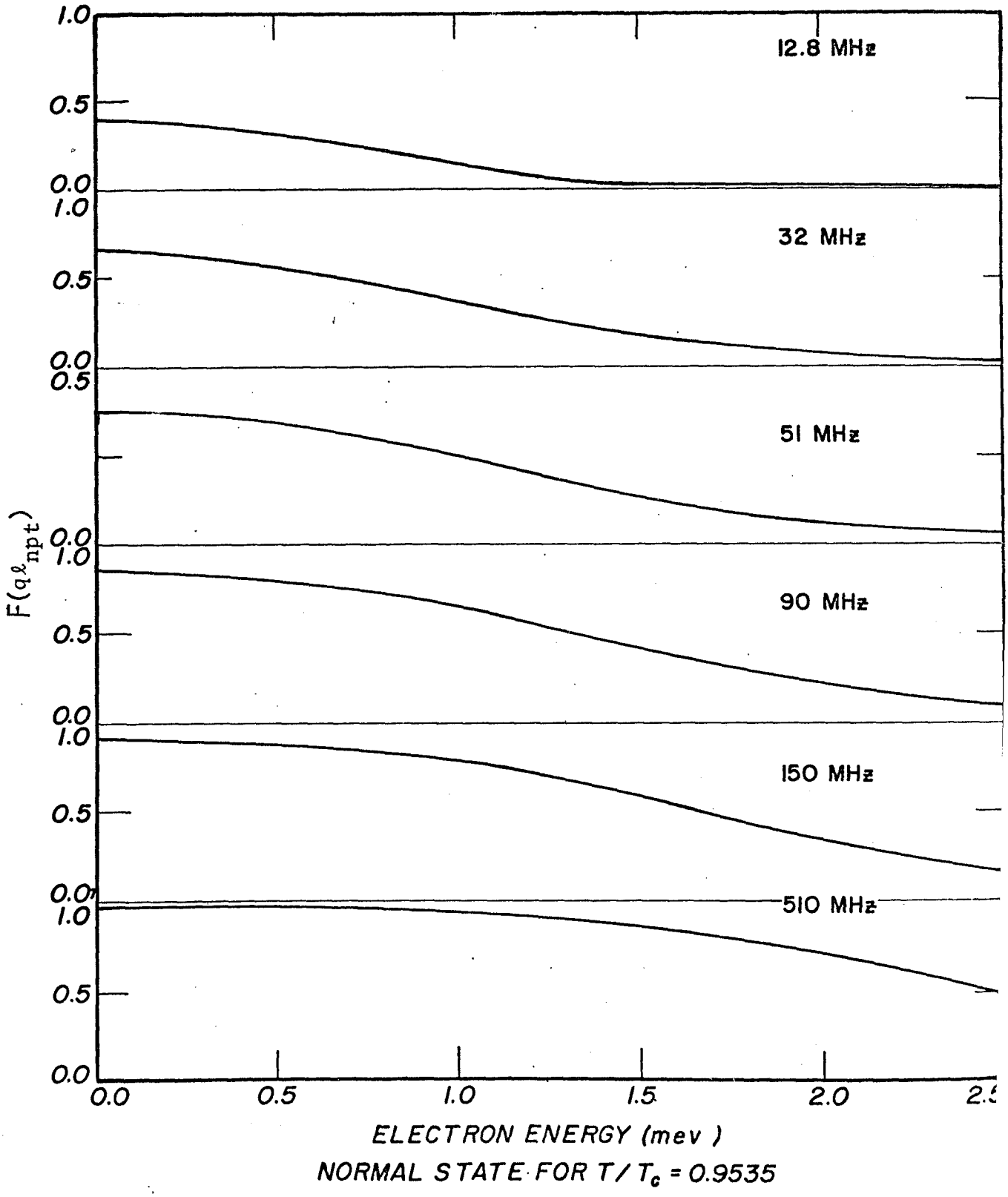
12.8 MHz
32 MHz
51 MHz
90 MHz
150 MHz
510 MHz
1.0
0.5
0.0
F(qℓnpt)
0.0
0.5
1.0
1.5
2.0
ELECTRON ENERGY (mev)
NORMAL STATE FOR T/Tc = 0.9535

Figure 10

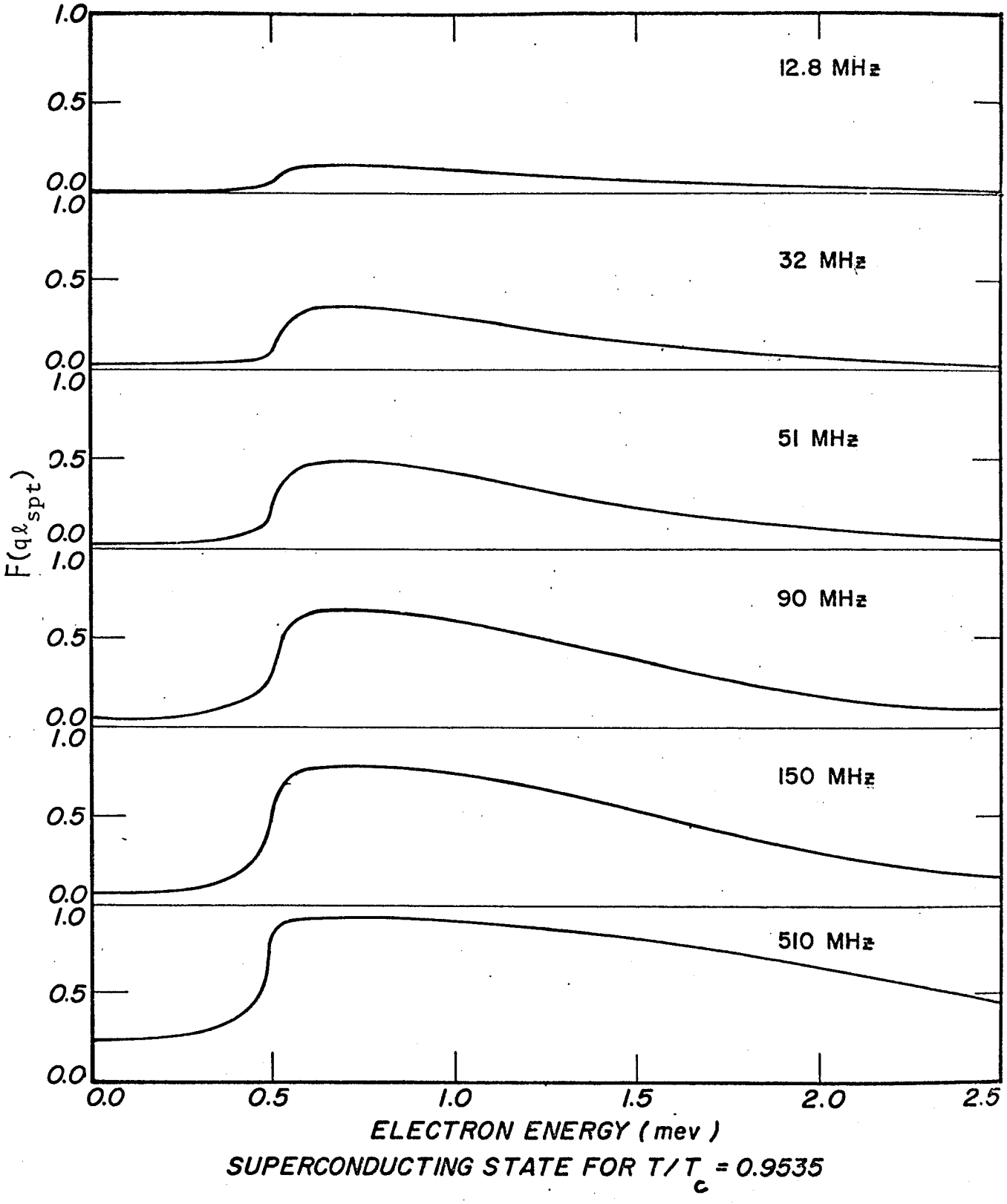
1.0
0.5
0.0
12.8 MHz
32 MHz
51 MHz
90 MHz
150 MHz
510 MHz
F(qℓspt)
0.0
0.5
1.0
1.5
2.0
2.5
ELECTRON ENERGY (mev)
SUPERCONDUCTING STATE FOR T/Tc = 0.9535

Figure 11

The success of this fit is shown in Fig. 13. It would seem from this figure along that a more complicated picture of the electron mean free path is not needed. However, the temperature dependence of the attenuation in the superstate was seen in the earlier discussion to require the energy dependence of the electron mean free path from the discussion above. This, in turn, indicates that $\bar{\ell}_{npt}^{1}$, defined by $\bar{\ell}_{npt}^{-1} = \bar{\ell}_{nt}^{-1} - \bar{\ell}_{o}^{-1}$, should be frequency dependent, as in Fig. 12. Thus, we attempted to fit Fate's data with a frequency-varying $\bar{\ell}_{npt}$.

In our derivation of $(Af)_{exp}$, $F(q\ell)$ in Eq. 50 is replaced by its normal state strong-coupling version, $\int_{o}^{\infty} d\omega \frac{\beta}{2} \operatorname{sech}^2\left(\frac{\beta\omega}{2}\right) F(q\bar{\ell}_{nt}(\omega,T))$. Figure 14 shows the result of this calculation, assuming that $\bar{\ell}_{npt}(T_c)$ is as estimated by Fate at 90 MHz and, as a result, again A = 0.18 dB/cm MHz. Figure 15 shows that an improved fit at all frequencies results from letting $\bar{\ell}_{npt}(T_c)$ be a free parameter at 90 MHz. Here the zero temperature Fermi velocity in Eq. 42, effective for longitudinal attenuation along [100], was allowed to assume a different value than the $v_{F0} = 1.3 \times 10^8$ cm/sec obtained in a fit to Fate's extrapolated value $\bar{\ell}_{npF}(T_c)$. The value obtained in this exercise is $v_{F0} = 8 \times 10^{-7}$ cm/sec. Changing this parameter also changes the fitting value of A, which becomes 0.22 dB/cm MHz. As seen in Fig. 15, the improved fit is excellent, except at 32 MHz, which lies outside the stated experimental error of Fate et al. The question of which frequency dependence of $\bar{\ell}_{np}$ holds hinges on the value which may be accepted for $\bar{\ell}_{np}(T_c)$. This quantity, in turn, depends upon the choice of an appropriate value of v_{F0}. The Fate extrapolation $\bar{\ell}_{np}$ derived from magnetoacoustic measurements at lower temperatures appears to work up to 8°K for their normal state data, but is really a semi-emperical fit, albeit a very successful one. Perhaps one way of measuring the mean free path, or the Fermi velocity effective for zero field ultrasonic

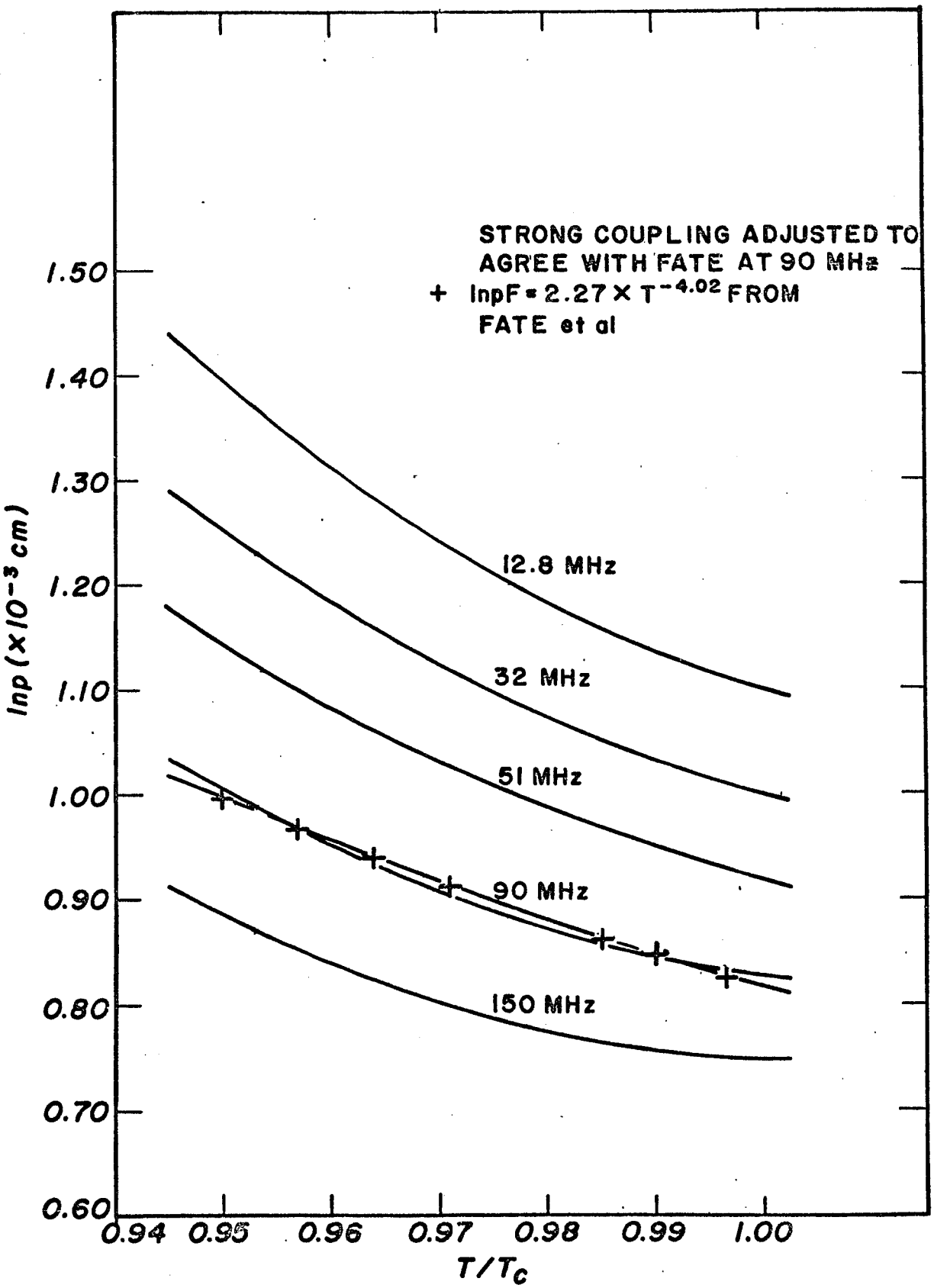
STRONG COUPLING ADJUSTED TO
AGREE WITH FATE AT 90 MHz
+ lnpF = 2.27 X T^-4.02 FROM
FATE et al
12.8 MHz
32 MHz
51 MHz
90 MHz
150 MHz
lnp (X 10^-3 cm)
1.50
1.40
1.30
1.20
1.10
1.00
0.90
0.80
0.70
0.60
0.94
0.95
0.96
0.97
0.98
0.99
1.00
T/Tc

Figure 12

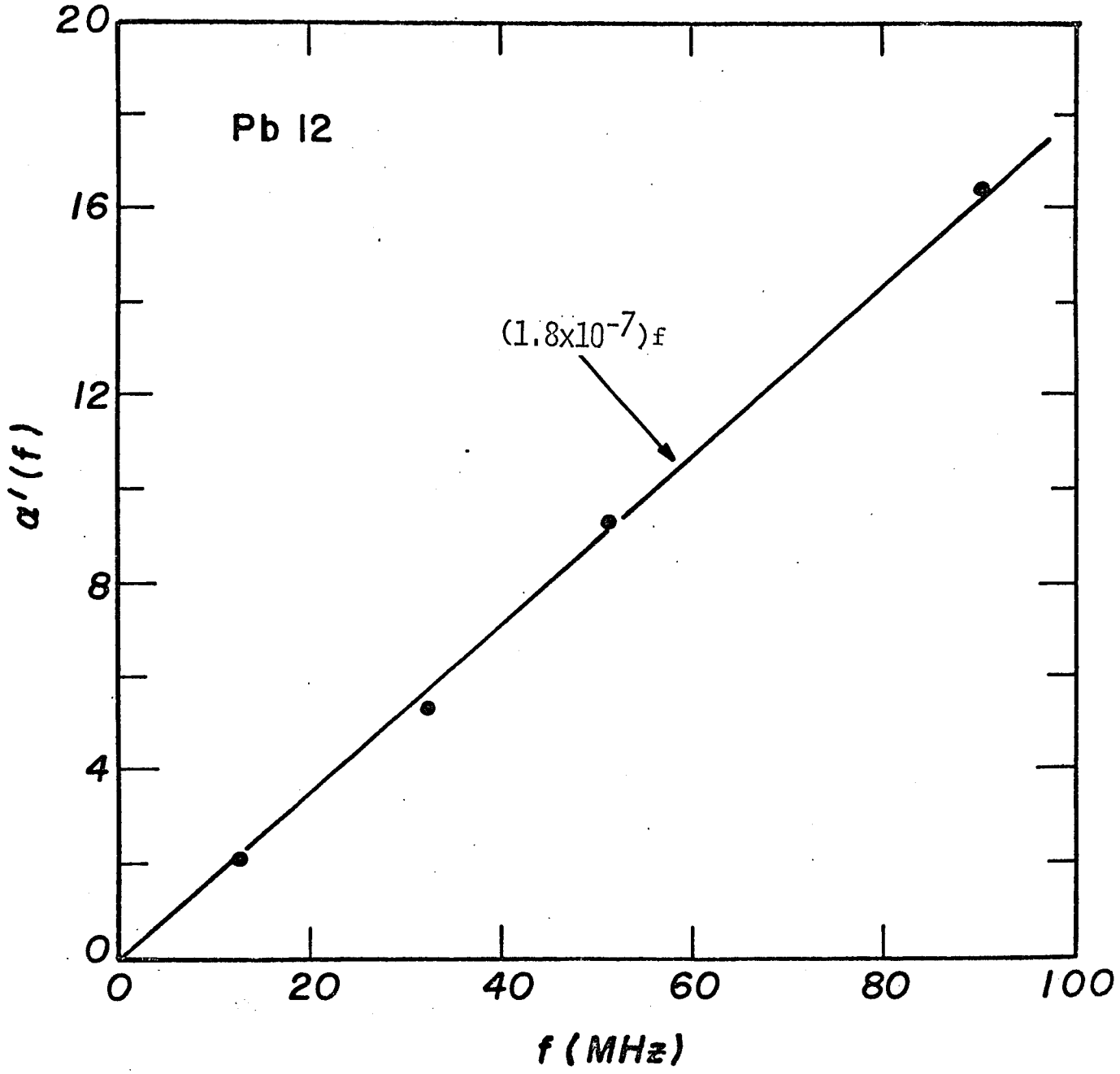

Figure 13

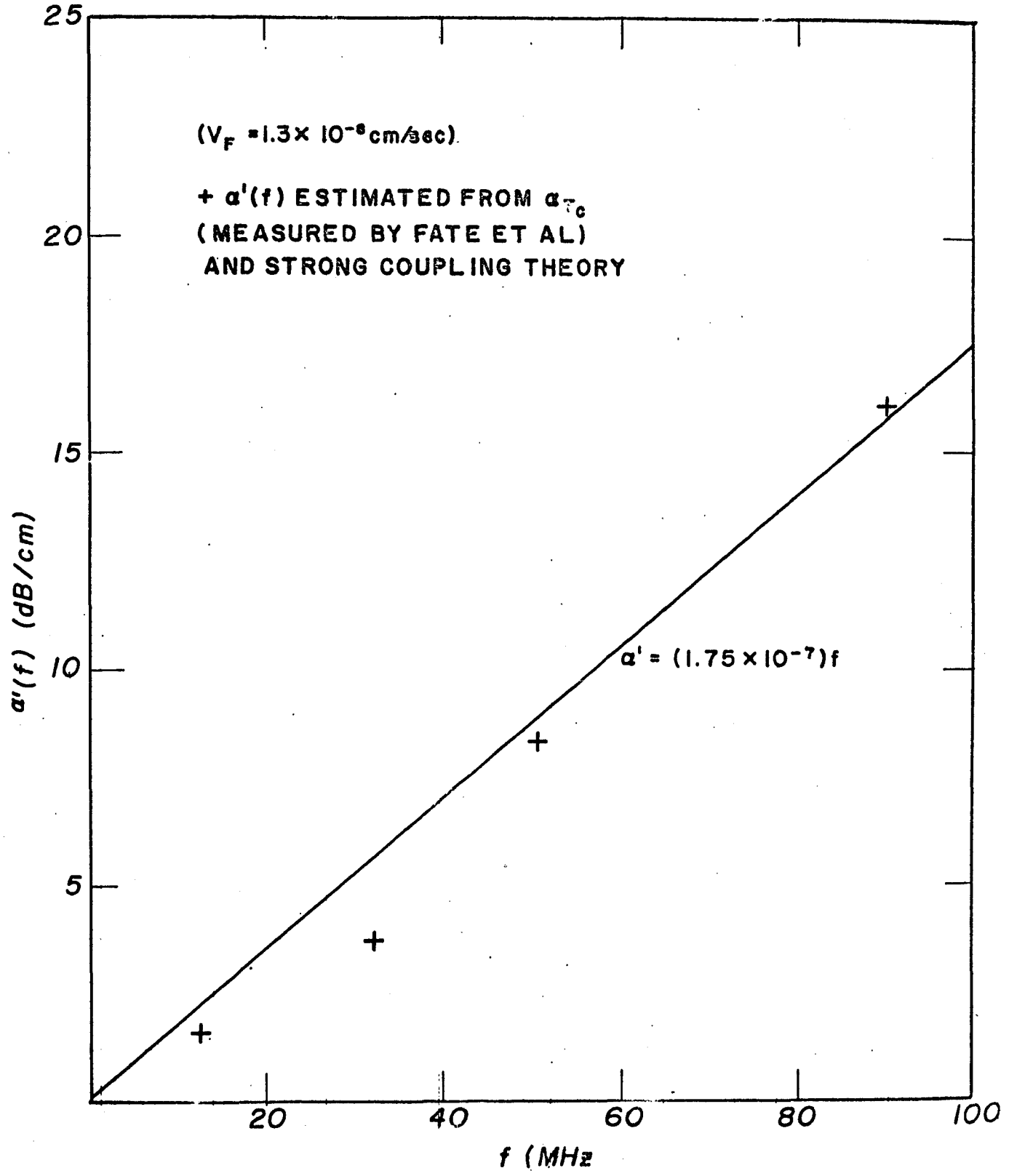
25
20
15
10
5
$(V_F = 1.3 \times 10^{-8}$ cm/sec)
+ $\alpha'(f)$ ESTIMATED FROM α_{τ_c}
(MEASURED BY FATE ET AL)
AND STRONG COUPLING THEORY
$\alpha' = (1.75 \times 10^{-7})f$
$\alpha'(f)$ (dB/cm)
20
40
60
80
100
f (MHz

Figure 14

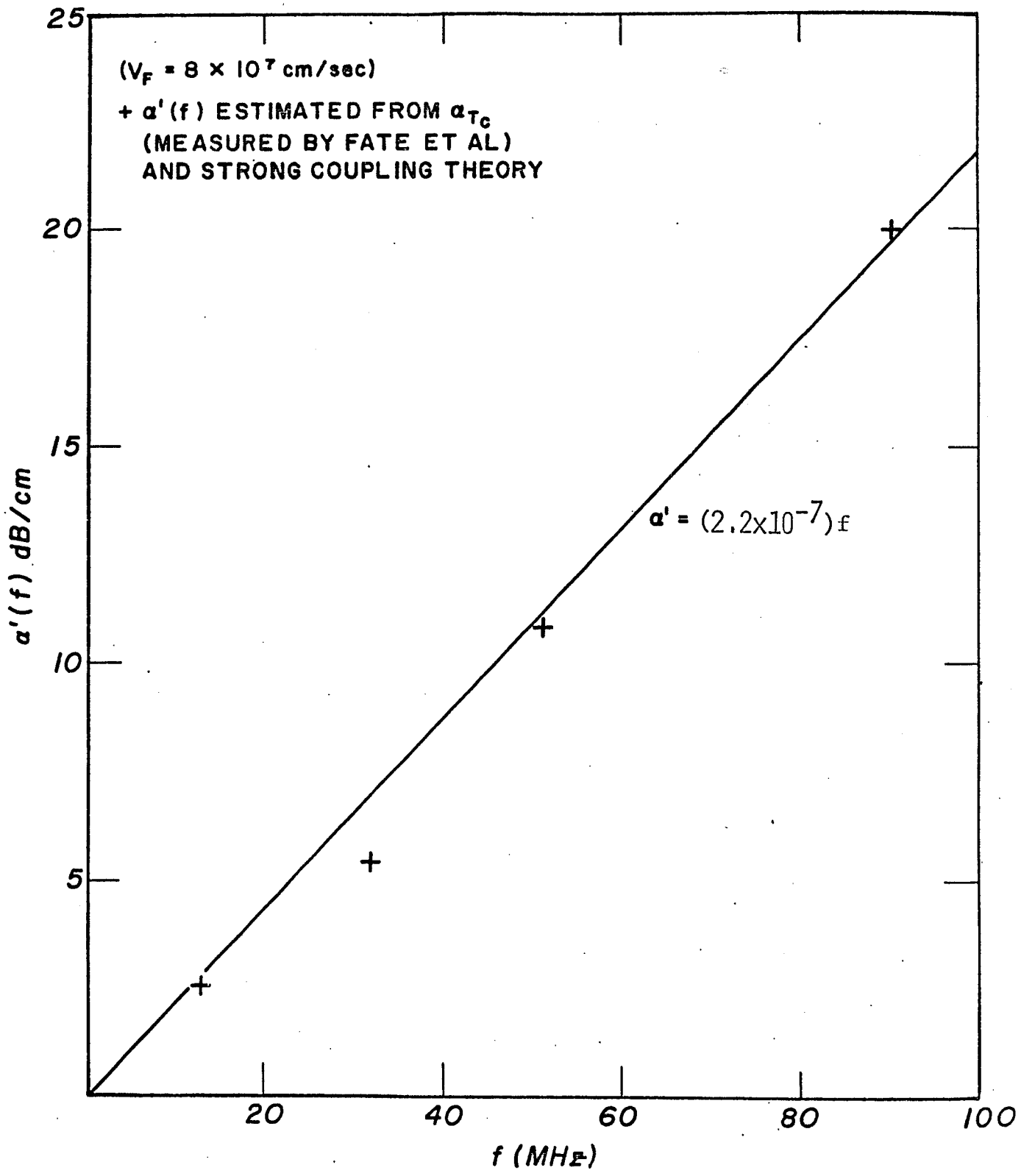
25
20
15
10
5
20
40
60
80
100
α'(f) dB/cm
f (MHz)
(V_F = 8 × 10^7 cm/sec)
+ α'(f) ESTIMATED FROM α_Tc
(MEASURED BY FATE ET AL)
AND STRONG COUPLING THEORY
α' = (2.2x10^-7)f

Figure 15

attenuation in lead, is a careful study of the frequency dependence of the attenuation in the 6°K to 10°K temperature region where ℓ is strongly phonon-limited for pure samples.

Our results for the normal state are consistent with those of Fate et al as far as they may be interpreted. The analysis of our normal state attenuation data at frequencies other than 150 MHz is complicated by the impossibility of directly measuring the zero electronic attenuation level near T = 0°K. These measurements were obscured by dislocation related attenuation in the superconducting state as described below. Using Eq. 49 for ℓ_{npF} in the normal state and the measured value of $\alpha(T_c)$ at 150 MHz to evaluate the impurity-limited mean free path, we found $\ell_o = 1.4 \times 10^{-3}$ cm for sample 3. At other frequencies, lacking a direct experimental measurement of $\alpha(T_c)$, we set this attenuation equal to the value predicted for a frequency-constant mean free path. With the normal state attenuation at T_c so determined, the measured values are compared with the theoretical prediction (from $\ell_{npF} = 2.27\ T^{-4.02}$) in Fig. 16. Above 10°K the measured attenuation is greater than the predicted electronic attenuation, reflecting a growing non-electronic residual attenuation.[39] Below 10°K, where these sources are much reduced, the usual Pippard frequency-constant mean-free-path theory finds no contradiction. The agreement is particularly good at 510 MHz. At this frequency the change in attenuation with temperature is large and, hence, measurable with more relative accuracy. Also, as will be seen below, amplitude effects are diminished from those present in the 210-390 MHz range if a linear frequency dependence of electronic attenuation is assumed. (Some temperature-dependent amplitude effects are expected in the normal state above T_c as a temperature-dependent mean free path modifies the electron damping of dislocation line motion.[8])

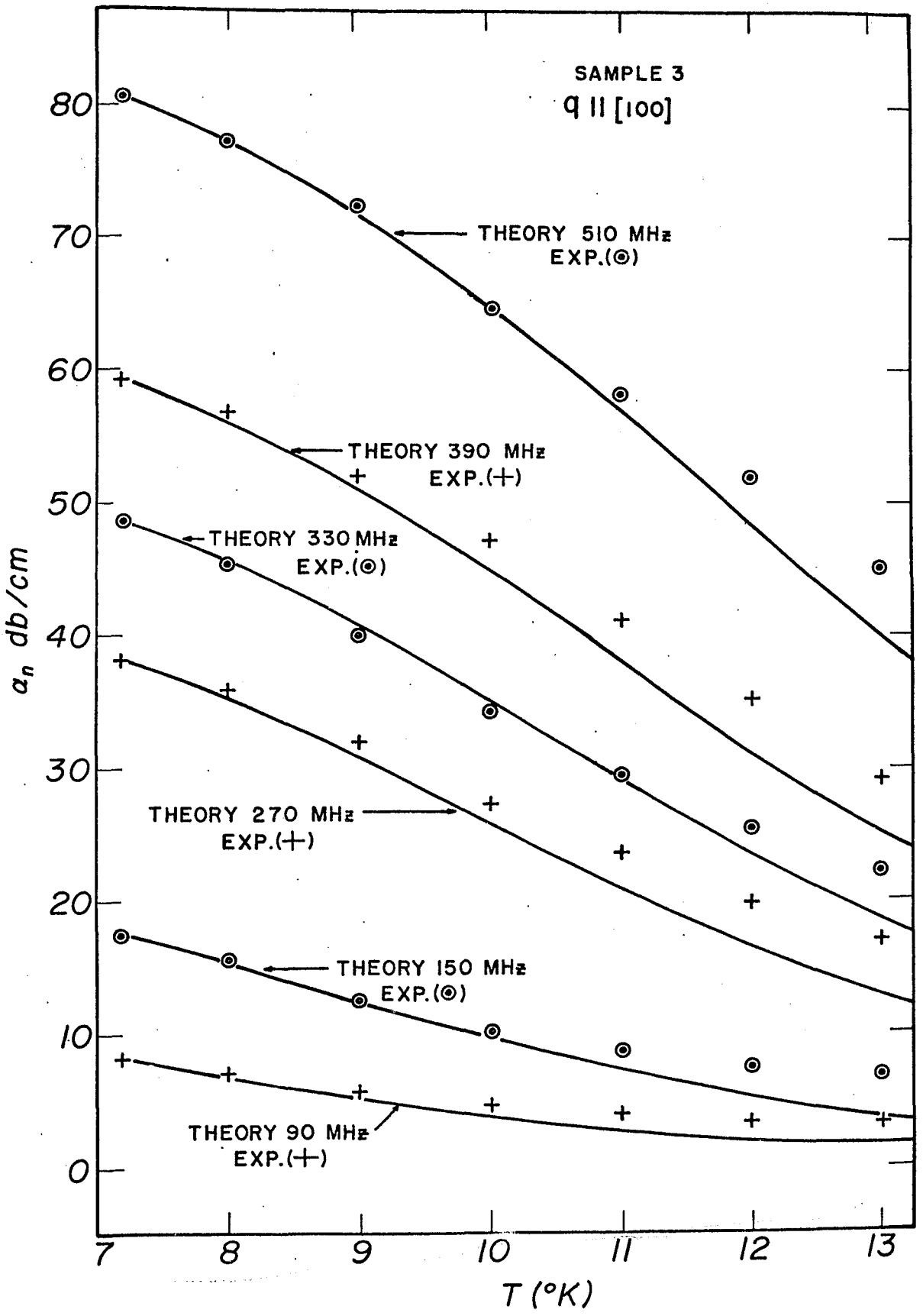
SAMPLE 3
q II [100]
THEORY 510 MHz
EXP.(⊙)
THEORY 390 MHz
EXP.(+)
THEORY 330 MHz
EXP.(⊙)
THEORY 270 MHz
EXP.(+)
THEORY 150 MHz
EXP.(⊙)
THEORY 90 MHz
EXP.(+)
α_n db/cm
T (°K)
0
10
20
30
40
50
60
70
80
7
8
9
10
11
12
13

Figure 16

It is unfortunate that no theoretical strong-coupling calculations are available for the normal state between T_c and 10°K. The temperature dependence here is not so dramatic as in the superconducting state. However, ultrasonic measurements in this region have an increased credibility and repeatability over those taken in the superconducting state. Also, the temperature and frequency dependence of the mean free path can be put to the test without the additional complication of a superstate. A good preliminary test for any strong-coupling attenuation calculation should be a fit to this normal state region.

Note the 90 MHz curves in Fig. 12. The difference in the shape of the $\bar{\ell}_{npt}$ (90 MHz,T) calculation over a very narrow temperature region shows that some qualitative gap exists between theory and experiment. This disagreement extends also to the frequency dependence of $\bar{\ell}_{npt}$ as seen in the same figure. Perhaps the most recent calculations of SSW have removed some of this discrepancy.[40]

The results of Fate et al described here were for a strained pure sample for frequencies up to 90 MHz. Our experiments examined the attenuation in lead for unstrained pure Pb samples at frequencies 90 MHz and above. In both the work of Fate et al and the present, sound propagation was along the [100] crystallographic axis. At 90 MHz, the highest $q\ell$ possible is about 2 at T_c because of thermal phonon limitation of the mean free path. For a definite test of strong-coupling properties, measurements should be taken in unstrained samples. The effect of dislocations on the attenuation is not completely understood. No large differences in electronic attenuation are to be expected between this and strained sample data, however, for the network of dislocation lines occupies a small portion of the lead single crystal volume, as is assumed in computations for dislocation damping here and elsewhere.[6,7,8] The

dislocation network itself might be a sizable separate source of attenuation, but as far as the electronic attenuation is concerned, most of the sample is undisturbed. The two sources are simply additive. If the dislocation attenuation were all amplitude-dependent, disappearing at low sound signal levels, then it would be sufficient to test for amplitude independence to confirm the absence of dislocation sources. Fate et al[9] used this method to check the removal of dislocation attenuation sources by their samples straining method. By this same means amplitude independence has been confirmed in some of our unstrained sample attenuation measurements at the lowest temperatures we reached in the superconducting state (∿2°K) and at frequencies up to 450 MHz. In order to achieve this amplitude independence it was necessary to work at very low signal levels. This was achieved in our experiments by using tuned circuits within our ultrasonic probe as described in the experimental section. One drawback of this method is that, as in the case of impedance matching by stub tuners, there are only periodic frequency ranges of good tunability. Also, at low frequencies, below 90 MHz, the transmitted signal is almost completely shorted out by the circuit which is appropriate for a broad high frequency (150-510 MHz) tuning range. Added to this problem is the very history-dependent behavior of the attenuation in unstrained Pb which we observed in our measurements and which has been reported by others.[6] This behavior caused us to treat the data from each helium temperature experiment run as if it were from a distinct sample. This was done even though a great number of runs may have been made on one lead specimen without allowing it to rise above liquid nitrogen temperature. Hence, with our high frequency data, no accompanying low frequency ($f < 90$ MHz) results are presented since none were obtained which would validly extend the high frequency data.

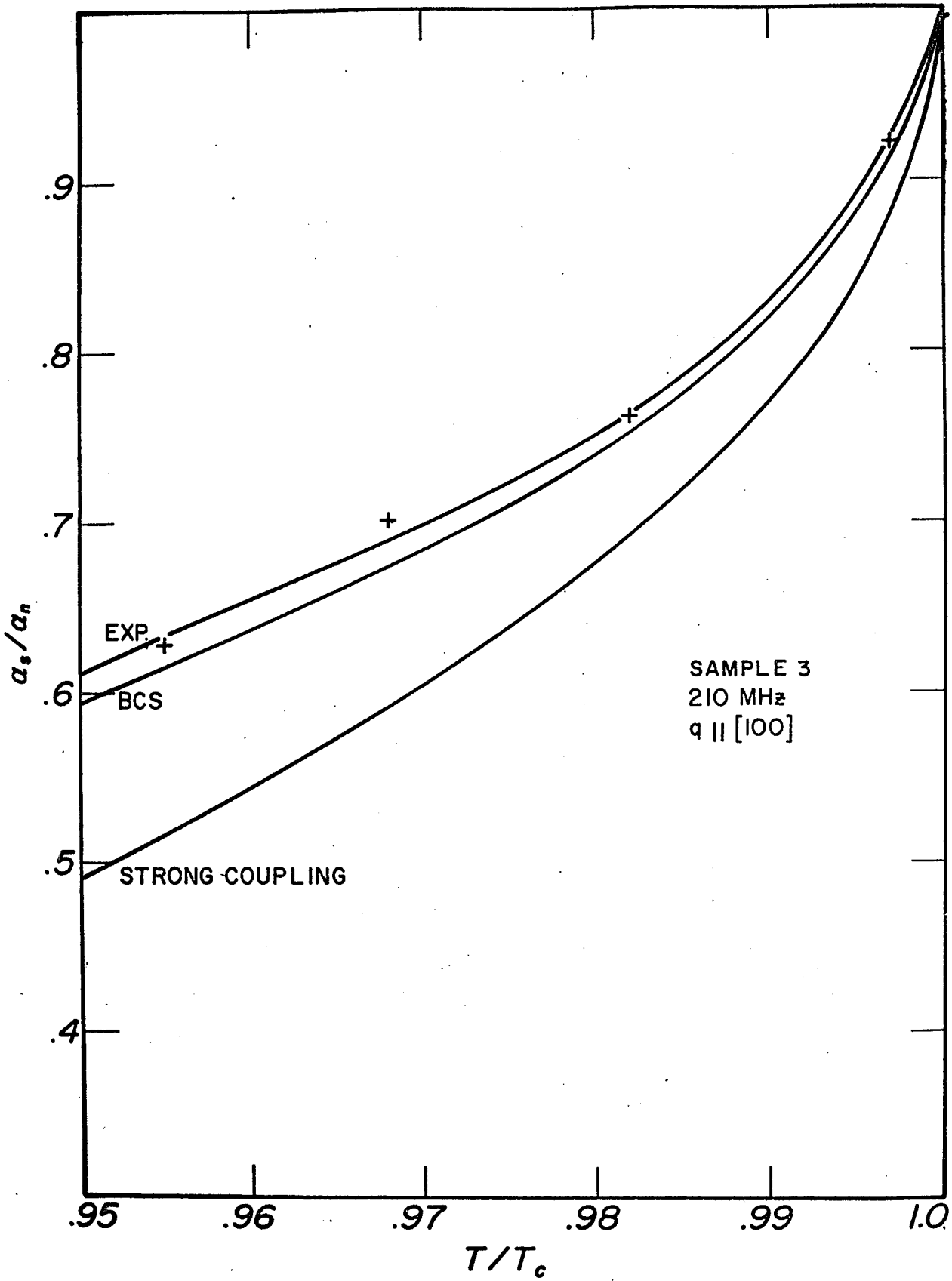
.9
.8
.7
.6
.5
.4
α_s/α_n
EXP.
BCS
STRONG COUPLING
SAMPLE 3
210 MHz
q || [100]
.95
.96
.97
.98
.99
1.0
T/T_c

Figure 17(c)

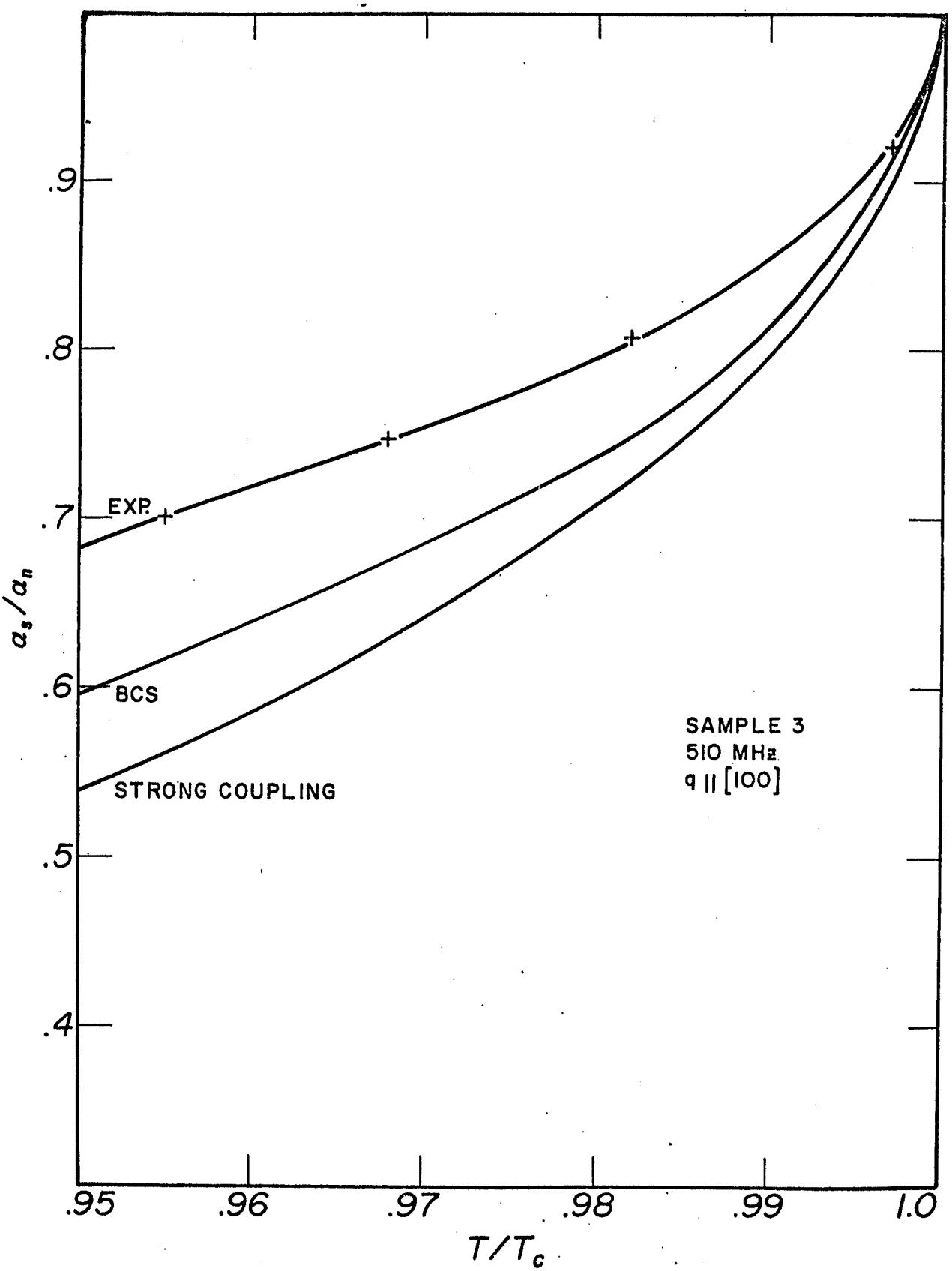
.9
.8
.7
.6
.5
.4
EXP.
BCS
STRONG COUPLING
SAMPLE 3
510 MHz
q ll [100]
α_s/α_n
.95
.96
.97
.98
.99
1.0
T/T_c

Figure 17(d)

The extensive and well-documented[38] measurements by Fate et al, which have been reviewed, will serve as well as any of our measurements for the low frequency range.

Using the results of Fate et al to obtain $v_{F0} = 1.3 \times 10^8$ cm/sec, as described above, we examine our results for sample 3. The sacredness of this value is in question, it should be remembered, even in view of the close agreement with $v_{F0} = 1.28 \times 10^8$ cm/sec by Anderson and Gold. The closeness of agreement is of less importance because the de Haas-van Alphen effect measures a different part of the Fermi surface than an ultrasonic measurement. We keep in mind, as we use this especially successful v_{F0}, the possibility that, as in the exercise above, a complete fit of a more precise strong-coupling theory to the data may require another value for v_{F0}. The present strong-coupling computation is not complete and accurate enough in its normal state predictions for us to use to overrule the mean free path results of Fate et al. The factor A remains 0.18 dB/cm MHz at 150 MHz. Our measurements give

$$\alpha_n(T_c) = 3.60 \text{ dB}/0.206 \text{ cm},$$

$$\alpha'(150 \text{ MHz}) = 150 \cdot 0.18 = 27 \text{ dB/cm},$$

and hence,

$$\left(\alpha_n/\alpha'\right)_{150 \text{ MHz}} (T_c) = 0.15 \qquad (51)$$

It is a simple matter to vary the impurity limited mean free path ℓ_o in Eq. 37 to satisfy Eq. 51. Using this method, $\ell_o = 1.5 \times 10^{-3}$ cm is found for sample 3. The results for α_s/α_n compared with experiment are shown in Fig. 17(b). The 150 MHz data were used for the match to strong-coupling theory because of the high sensitivity of our ultrasonic equipment at that

frequency. As described in the section on dislocation effects, a change of 20 dB (a factor of 10 in signal amplitude) resulted in no measurable change in the quantity $\alpha(T_c) - \alpha_s(2°)$ at 150 MHz. Thus, any amplitude effects of the type previously reported appeared to be gone at the lowest attainable signal levels. Also, amplitude independent dislocation attenuation should be absent from α_s near 2°K: if the amplitude independent attenuation follows the Granato-Lücke theory at 150 MHz, as it appears to do from our analyses, the ultrasonic frequency is far from the resonant frequencies of the dislocation loops near 2°K and the dislocation absorption should be insignificant.

Figs. 17(a-d) show our results for $\alpha_s/\alpha_n(T)$ at 90, 150, 210, and 510 MHz compared with strong-coupling theory and the parameter ℓ_o, as determined from the 150 MHz quantity $\alpha(T_c)$. Also plotted at 150 MHz is the curve for α_s/α_n corrected slightly by subtracting out the amplitude independent dislocation attenuation. This contribution is estimated from the Granato-Lücke theory via Eq. 12 based upon the amount of dislocation attenuation seen at its low temperature maximum. This source of attenuation may be underestimated somewhat. A single dislocation loop length ℓ_c was used in the estimate. The distribution of loop lengths, including lengths shorter than ℓ_c would tend to increase the dislocation absorption tail observed near T_c. The corrected measured attenuation at 150 MHz gives the same kind of agreement with strong-coupling theory as is seen in the results of Fate et al. The results at other frequencies are more worrisome. At 90 MHz the measured drop in α_s below T_c is larger than predicted by strong-coupling theory; at frequencies above 150 MHz the opposite is true and the measured drop appears small.

Another approach to fitting the parameter ℓ_o to the experimental results would have been to use the highest frequency results as a base and set the parameter there to fit the α_{se}/α_{ne} data to a BCS curve for a gap of $2\Delta(0) = 4.3\ K\ T_c$. This suggests itself because, according to strong-coupling

theory,[12] the attenuation ratio should approach a BCS curve in the superconducting state, not exceed it greatly as in our results. However, this approach results in even poorer agreement with strong-coupling theory at the lower frequencies. Unless an additional source of attenuation is considered, no single ℓ_o is appropriate for a good fit to the strong-coupling theory. Two possibilities are apparent, amplitude dependent and amplitude independent dislocation attenuation.

Amplitude dependent dislocation attenuation, increasing with frequency as observed by many investigators,[6,38] would produce qualitatively the same effect. However, at 150 MHz the quantity $\left(\alpha(T_c) - \alpha(2°)\right) \simeq \alpha(T_c)$ upon which the fit to strong-coupling theory is based, is amplitude independent, so any amplitude dependence present in the 90 - 150 MHz pair should be present at the lower frequency and produce the opposite of the observed trend. Further, measurements of the normal state attenuation above T_c as seen in Fig. 18 show that features in the strong-coupling electronic attenuation cannot account for all the high frequency behavior: the low temperature attenuation does not reach the low level measured high above T_c, even though additional attenuation sources are known to be present above 10°K[39] and less than 1% of the superconducting attenuation drop should remain at our lowest measured temperatures. Hence, we conclude that some non-electronic attenuation was measured in the superconducting state, presumably due to dislocations.

While an attenuation contribution attributable to dislocations is strongly indicated, the evidence suggests that the important dislocation contributions at the highest frequencies are not amplitude dependent. As a check for amplitude effects, runs were made at several amplitudes at the highest frequencies for sample 3. Two plots of α_s vs T from such runs at 510 MHz are shown in Fig. 19 and reveal some weak amplitude dependence which diminishes near T_c. An

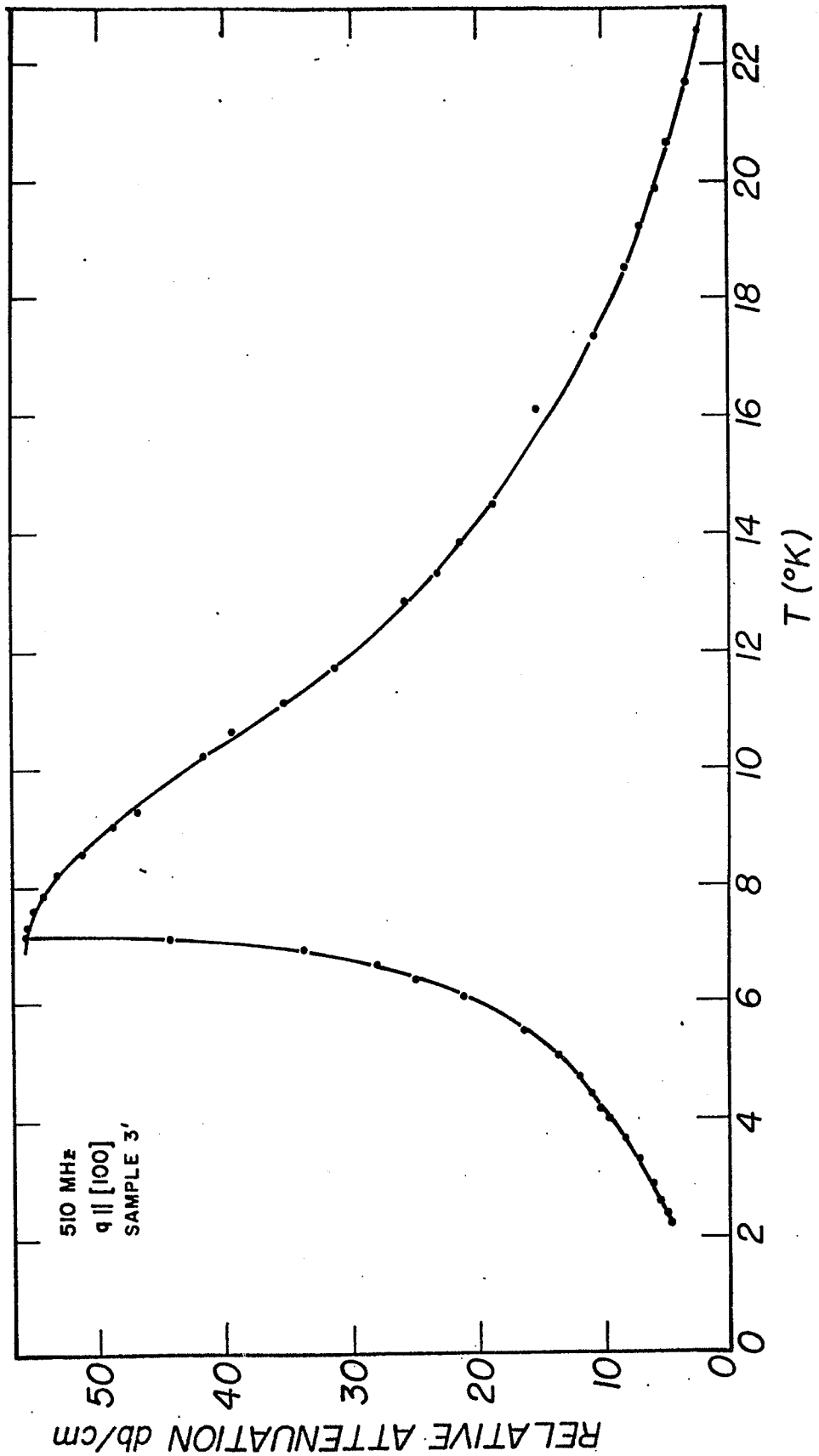
RELATIVE ATTENUATION db/cm
0
10
20
30
40
50
0
2
4
6
8
10
12
14
16
18
20
22
T (°K)
510 MHz
q ∥ [100]
SAMPLE 3'

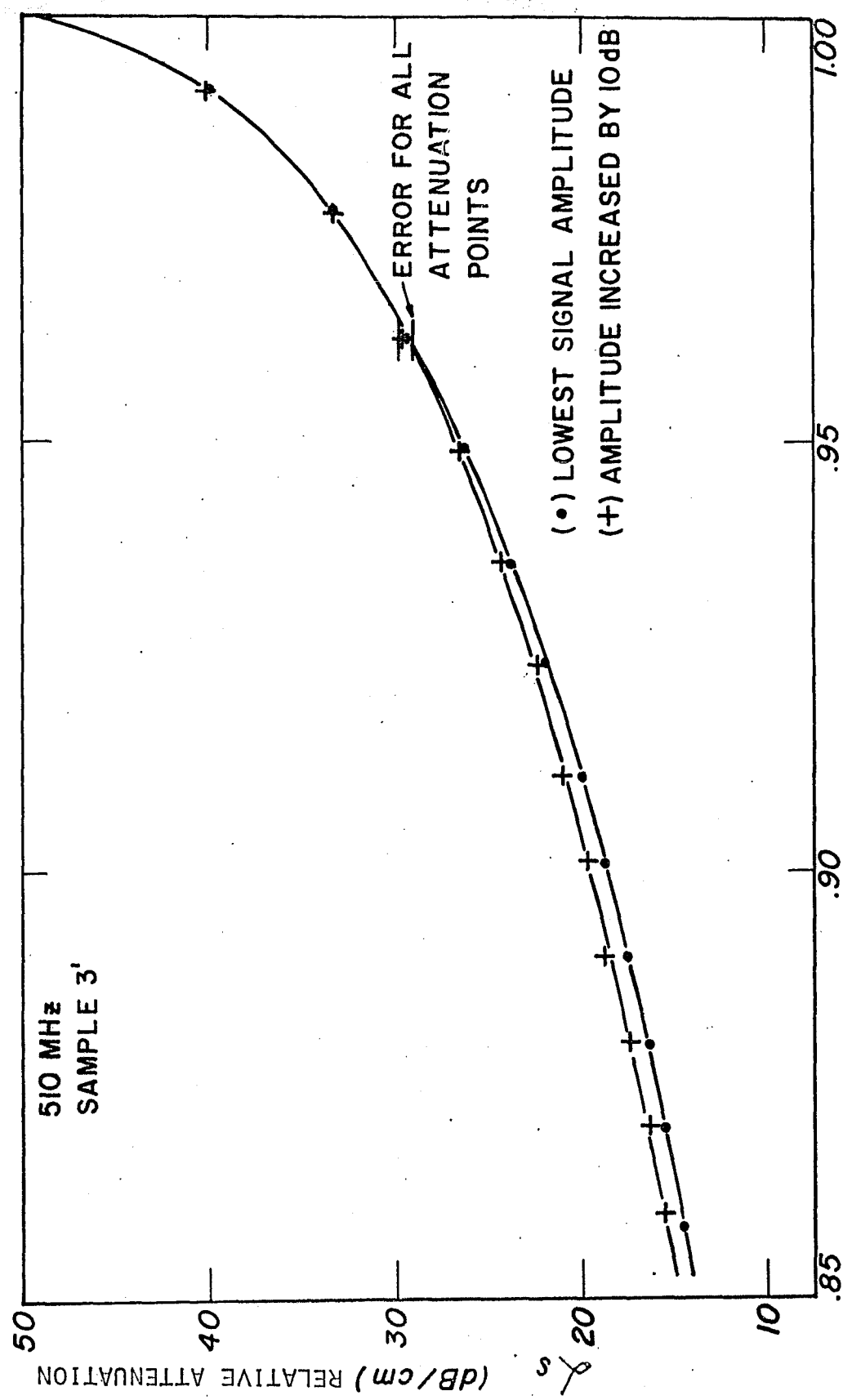
510 MHz
SAMPLE 3'
ERROR FOR ALL ATTENUATION POINTS
(•) LOWEST SIGNAL AMPLITUDE
(+) AMPLITUDE INCREASED BY 10dB
RELATIVE ATTENUATION (dB/cm)
α_s
50
40
30
20
10
.85
.90
.95
1.00
T/T_c

Figure 19

unevenness in the quantity $\{\alpha(T_c) - \alpha_s(T)\}$ vs frequency as in Fig. 20 is also characteristic of amplitude dependent attenuation being added to α_s and is a result of differences in our ability to tune the ultrasonic probe at the different frequencies. The sensitivity of the probe, as adjusted for this particular experimental run, was relatively weak in the region from 270 to 390 MHz and considerably more signal strength was necessary for data taking. The increased power resulted in more amplitude-dependent attenuation. Amplitude effects appear to lessen as frequency increases above 390 MHz in Fig. 20 and the attenuation drop $\{\alpha(T_c) - \alpha_s(T)\}$ again approaches the linear extrapolation from lower frequencies. In light of this and the very weak amplitude dependence observed directly at 510 MHz, we cannot use amplitude effects to explain the anomalously small attenuation drop near T_c in Fig. 17(d). The electronic attenuation is in the high $q\ell$ region and should be approaching the BCS temperature dependence from below as shown by the theoretical curves in the figure.

It appears that non-electronic attenuation - temperature dependent, amplitude independent and increasing linearly with frequency - is included in α_s. The amplitude independent dislocation attenuation α_D from Eq. 12 does not have the appropriate linear ultrasonic frequency dependence. This theoretical α_D was derived by assuming that only the lowest frequency dislocation mode is excited. Because of the shift of dislocation mode frequencies by electron damping, several modes should be excited at our highest ultrasonic frequencies. Thus, a less restricted formulation for α_D is required and may explain the frequency dependence near T_c of this attenuation source.

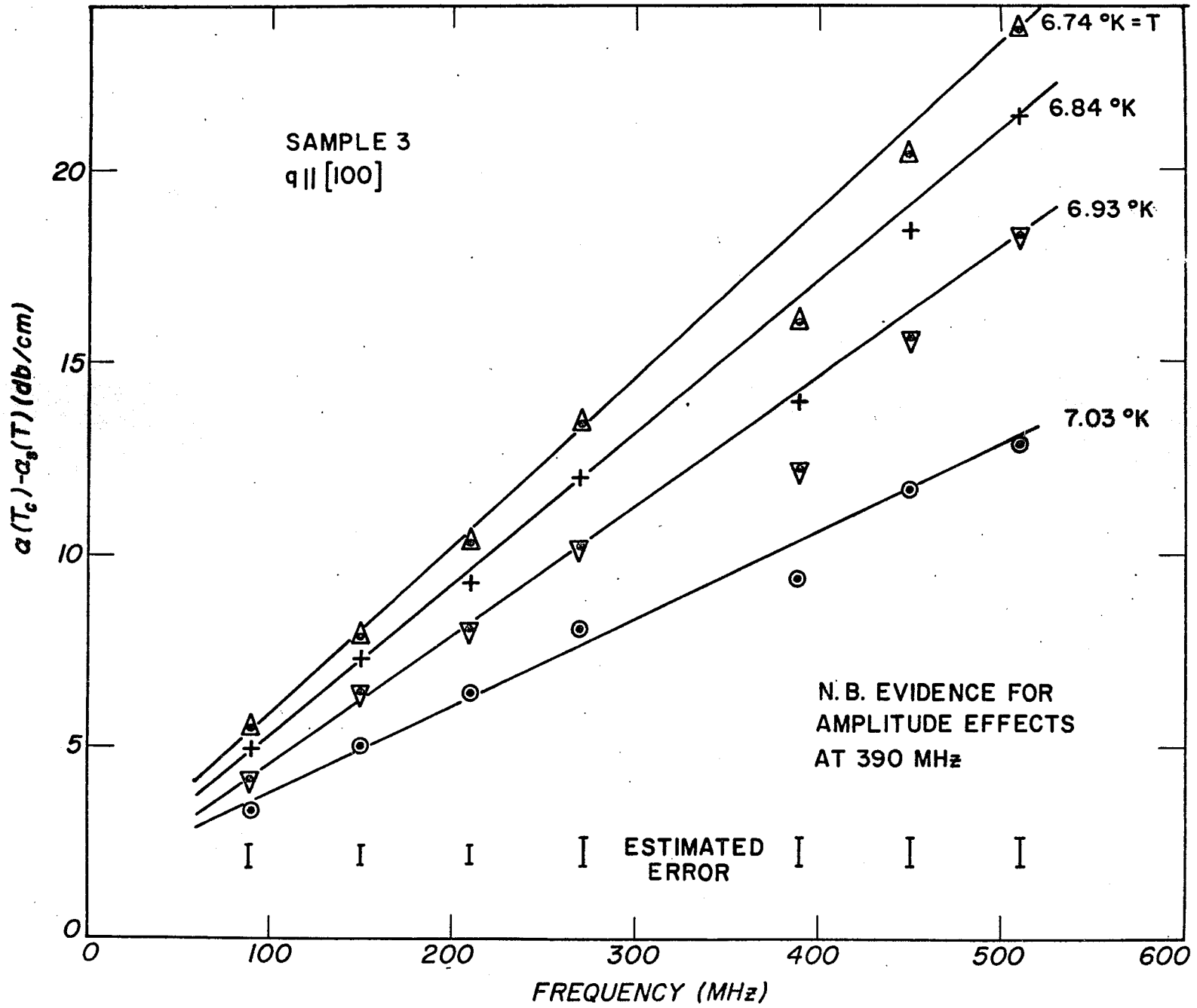
SAMPLE 3
q || [100]
6.74 °K = T
6.84 °K
6.93 °K
7.03 °K
N. B. EVIDENCE FOR
AMPLITUDE EFFECTS
AT 390 MHz
ESTIMATED
ERROR
α (T_c) - α_s (T) (db/cm)
FREQUENCY (MHz)
0
5
10
15
20
0
100
200
300
400
500
600

CHAPTER V

INTERMEDIATE STATE AMPLITUDE-MAGNETOACOUSTIC EFFECT

Our study of amplitude effects in ultrasonic attenuation measurements in lead has revealed an effect which has potential for aiding observations of the intermediate state. This is a magnetic field-dependent amplitude effect which we are able to relate to direct electron microscope observations of the intermediate state by Traüble and Essman.[42]

The measurements were made in sample 1, a lead disc 5.9 mm in diameter and 1.68 mm thick. As in the experiments described previously, the ultrasound was propagated normal to the disc face along the [100] axis of the crystal. The applied magnetic field was also parallel to the [100] axis. The measurements to be described were made at 4.66°K in a high vacuum ($\sim 10^{-7}$ mm Hg) and for the pulsed ultrasound frequency of 390 MHz.

For low signal amplitudes the usual pattern of attenuation α vs applied magnetic field H_o is observed: the attenuation remains at the superconducting level for $0 < H_o < H_2$ (dashed in Fig. 21(a)) until normal regions occupy a detectable portion of the crystal. The attenuation then increases approximately linearly until the crystal becomes fully normal at H_c.

At increased amplitudes, as expected, the attenuation in the superconducting state is increased by amplitude-dependent dislocation attenuation, as described by many investigators.[3,5] However, we observe an interesting pattern of α vs H_o. The attenuation remains at approximately the enhanced value up to a field value which we label H_1. It then drops sharply to a minimum at H_2 before rising linearly between H_2 and H_c. This is shown in Fig. 21(a) for ultrasound amplitude 15 dB above the level at which the attenuation minimum first appears. For moderate sound amplitude, as in Fig. 21(a), we find $H_1 = 0.35\ H_c$ on the average, with values of H_1 lying between $0.32\ H_c$

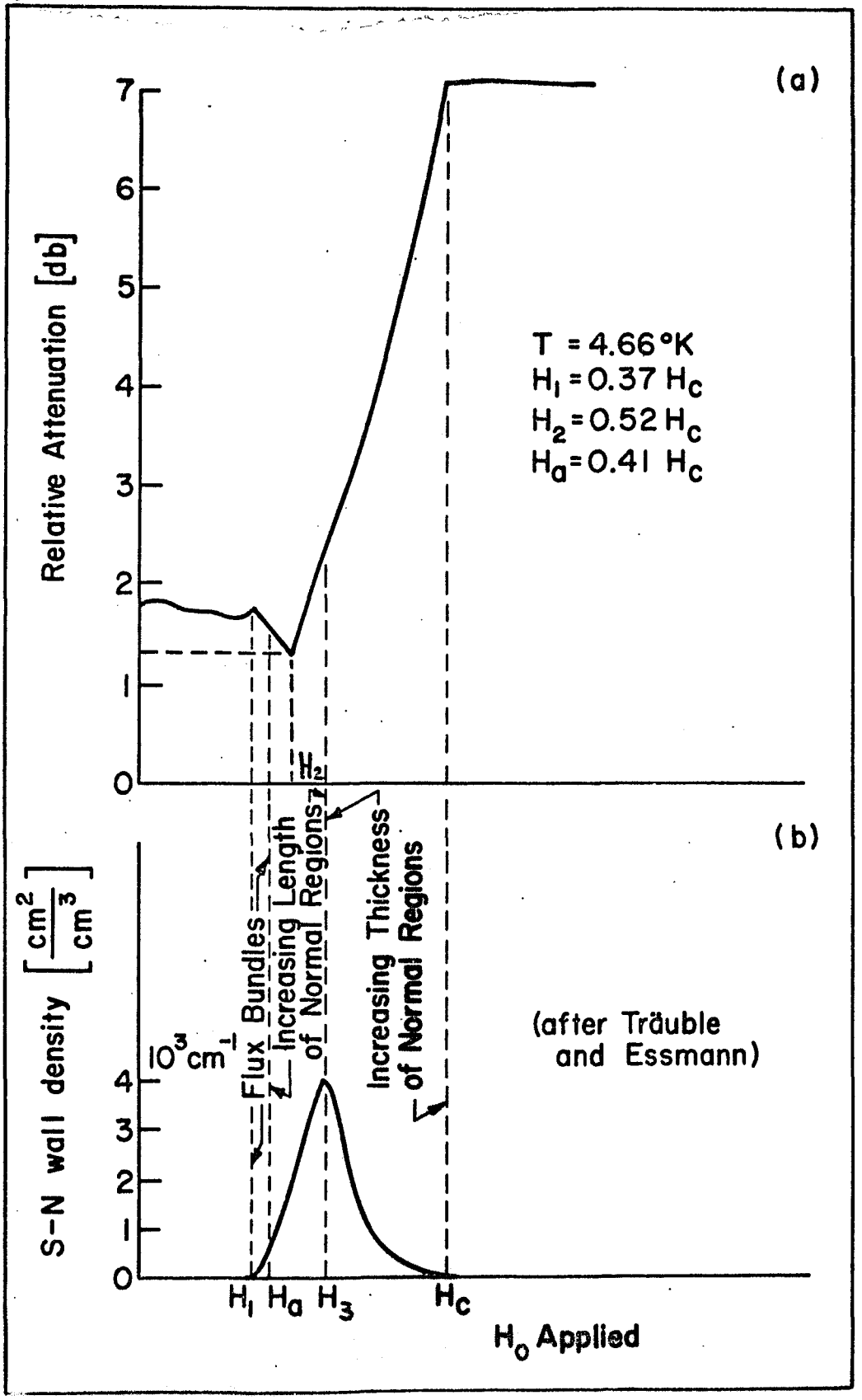
(a)
Relative Attenuation [db]
7
6
5
4
3
2
1
0
T = 4.66°K
H1 = 0.37 Hc
H2 = 0.52 Hc
Ha = 0.41 Hc
H2
(b)
S-N wall density [cm²/cm³]
10³cm⁻¹
4
3
2
1
0
Flux Bundles
Increasing Length of Normal Regions
Increasing Thickness of Normal Regions
(after Träuble and Essmann)
H1 Ha H3
Hc
H0 Applied

Figure 21

and 0.40 H_c. This is significant since in an ellipsoid approximation[41] of our sample, the theoretical onset of the intermediate state is 0.33 H_c. It might be noted that this ellipsoid approximation is in excellent agreement with direct visual detection of the intermediate state in lead: in a sample of nearly the same geometry as that used in the current experiments, with an effective demagnetization factor in the ellipsoid approximation corresponding to $H_o = 0.37\ H_c$ for the onset. Trauble and Essman[42] detected the first appearance of normal regions when $H_o = 0.37\ H_c$.

For higher sound amplitudes (10 to 15 dB greater) H_1 decreases with increasing amplitude to values as low as 0.15 H_c. This remains to be explained for, as has already been noted: field exclusion should persist in the given specimen for applied fields twice as large. Changes in magnetic field at these low field values are thus expected to have no effect whatsoever on the attenuation of the bulk of the sample.

The amplitude threshold of this effect and the exact value of H_1 can be changed by cycling the sample to liquid nitrogen temperature or by transmitting high amplitude sound through the sample. Since only the dislocation structure of the sample could be affected by these operations, this suggests that the observed minimum may be caused by a reduction of the dislocation attenuation of the ultrasound. In the envisioned model excessive motion of dislocations and subsequent irreversible breakaway from their pinning points are reduced by the presence of thin normal regions. This reduction in loop motion could be accomplished by free electron damping in the normal regions as in the widely accepted model for the bulk normal state.[6] Excessive loop motion might also be reduced by the added effective mass of attached interphase walls.[19] In either case, the normal regions must be dense enough to affect a significant number of dislocation loops, which have a density[8] on

the order of 3×10^{-4} cm^{-2}. Also, in order not to contribute a significant amount of the higher normal state attenuation, these normal regions must consist of a small fraction of the total volume in the field range $H_1 < H_o < H_2$.

Traüble and Essman[2] see conditions essentially as required, as shown in Fig. 21(b). The strong decrease in attenuation occurs in the region of flux bundles and the first lengthening of the normal laminae, H_1 to H_a and H_a to H_2, respectively. At H_a, the upper limit of applied field for flux bundles, Essman finds only 2 percent of the sample to be normal. Consequently, negligible contribution to the attenuation from normal electronic attenuation is to be expected. At the same time, the appearance of decreasing attenuation in this field region may be forced by the preference of the normal superconducting walls to lie on dislocations.

In this connection, Sarma and Moon[45] suggest that the Landau parameter κ may be increased (and hence S-N wall energy decreased) by the scattering of electrons in the neighborhood of dislocations, favoring the proliferation of S-N interfaces there. There is much experimental evidence for this: in type II superconductors dislocations impede the motion of fluxoids and distort fluxoid lattices;[46,47] cold working some type I materials causes them to exhibit type II behavior.[48] Also, a preference of S-N walls to lie on grain boundaries is observed.[43]

The appearance of field-dependent attenuation for anomalously low field values also fits this explanation. Some thin, normal regions may be allowed to follow the dislocation network through the sample at lower fields than those associated with the bulk intermediate state in the Landau model. Essman reported seeing no such regions for fields below the theoretical onset value for the intermediate state.[43] In light of this, we conclude that the

presence of high-amplitude sound must somehow serve to aid the entry of normal regions into the interior of the sample. We know that the lowering of H_1 for high sound amplitudes is not a simple heating effect, for the magnetic field values H_2 and H_c remained constant with changing signal amplitudes.

The observed field-dependent amplitude effect below H_c has a high correlation with the visual observations of low field structure for the intermediate state. The decrease in attenuation (see Fig. 21) appears strongly at applied magnetic fields H_o for which the normal regions occupying an insignificant volume of the lead specimen, and no significant normal-state electronic attenuation is expected. At the same time the injection of flux bundles (at H_1) is detectable ultrasonically in our experiments due to their influence in immobilizing dislocation and producing a consequent attenuation decrease. Thus, the effect represents a sensitive diagnostic tool for sensing the onset of flux structure in the intermediate state. Summarizing, from comparison of the visual and ultrasonic data (Figs. 21 (a and b)) we make the following qualitative assignments: field H_1 represents the onset of the intermediate state; H_2 corresponds to a field value for which dislocations have been effectively immobilized by field, and thus, as field is increased further the only consequence is an increase in normal-state electronic attenuation attributable to the growing normal volume; and, finally, H_c corresponds to that field for which the entire volume has become normal. We more readily appreciate the possibility of finding a field region H_1 to H_2 where dislocation immobilization is effected while at the same time, no significant electronic attenuation obtains, if we note that the dislocation loop length is 10^{-3} to 10^{-4} cm while the ultrasonic wavelength in this series of experiments was approximately 10^{-3} cm ($f \tilde{\sim} 390$ MHz). As has been noted, the observation which remains to be adequately understood is the shift of H_1 to lower values as sound amplitude is made very large.

CHAPTER VI

EXPERIMENTAL METHODS

A. The Sample Preparation

All our lead samples were cylinders with diameters on the order of 0.65 cm and thicknesses varying from 0.1 to 0.2 cm. They were oriented so that a [100] axis of the crystal was normal to the sample face within (2°), the estimated error for our procedure of aligning the samples on the X-ray goniometer and planing them on the "agitron" spark-erosion machine.

Because of the small sample thickness a quartz delay rod was used. An X-cut quartz transducer with a fundamental frequency of 30 MHz was indium-bonded onto one end of the delay rod. This delay rod, the sample, and a second transducer were bonded together using "Nonaq" stopcock grease. Cleanliness was very important for the "Nonaq" bonding procedure. The surfaces to be bonded were cleaned carefully with a cotton swab using acetone followed by distilled water. Allowing the sample surface to etch a few seconds was found to be quite useful, especially when residue remained from spark planing or previous bonding.

The Nonaq was heated on a microscope slide before applying. This removed water which would crystallize and destroy the bond at low temperatures. The delay rod and sample were warmed on a hot plate to a temperature above the boiling point of water and below the melting point of indium during the bonding. At this temperature the "Nonaq" spread easily so that a very thin bond could be made. After the delay rod-sample-transducer system had cooled, it was installed in the probe and the electrode positioned and pressure-adjusted on the transducer to maximize the first transmitted pulse. This final step probably compensated for any non-parallelism between the two faces of the lead disc.

FIGURE 22

TABLE OF LEAD SAMPLES

Sample Number	Thickness (mm.)	Experimental Use
1	1.68	Amplitude Dependent Intermediate State Effect
2	1.10	Strong Coupling Investigation
2'	1.10	Strong Coupling Investigation
3	2.06	Strong Coupling Dislocation Effects
3'	2.06	Strong Coupling Dislocation Effects

All samples were discs $\sim$ 0.6 cm in diameter with the [100] crystal axis normal to the disc face.

The probe was maintained at a high vacuum at liquid nitrogen temperature between experimental runs. Even in this controlled environment dislocation and mean-free-path related features in the attenuation of lead varied from one helium temperature experimental run to the next. For this reason, the measurements in a given experimental run were as extensive as possible, some requiring as long as 35 consecutive hours, and data from one run to the next were treated as if distinct samples had been used. Figure 22 is a table of the lead samples used.

B. The Ultrasonic Probe

The ultrasonic probe was a result of the particular requirements of the experiment, the need for experimental versatility and an adjustment to existing equipment. Its outstanding features are the systems for temperature control and ultrasonic tuning. Measurements had to be made at temperatures covering a range of 0 - 20°K, the approximate extent of electromagnetic attenuation in lead and niobium. Preliminary experiments revealed that use of a light exchange gas $\sim 10^{-3} - 10^{-4}$ mm Hg, was a source of instability in the ultrasonic signal level, since it varied with level of the vacuum, which could not be accurately controlled. Also, inaccuracies in temperature readings, specifically varying readings for T_c, revealed an uneven cooling effect of the exchange gas on the germanium thermometer and the lead samples. Hence, the experiments wereconducted in a moderately high vacuum, $10^{-7} - 10^{-8}$ mm Hg, with the ultrasonic probe shown in Fig. 23.

The high vacuum introduced a problem of pinning the germanium thermometer leads to low temperatures. This was solved by bringing the high thermal resistance "Advance" wire leads down a tubing on the outside of the vacuum can and bonding them to a copper cylinder on the inside of the bottom of the can

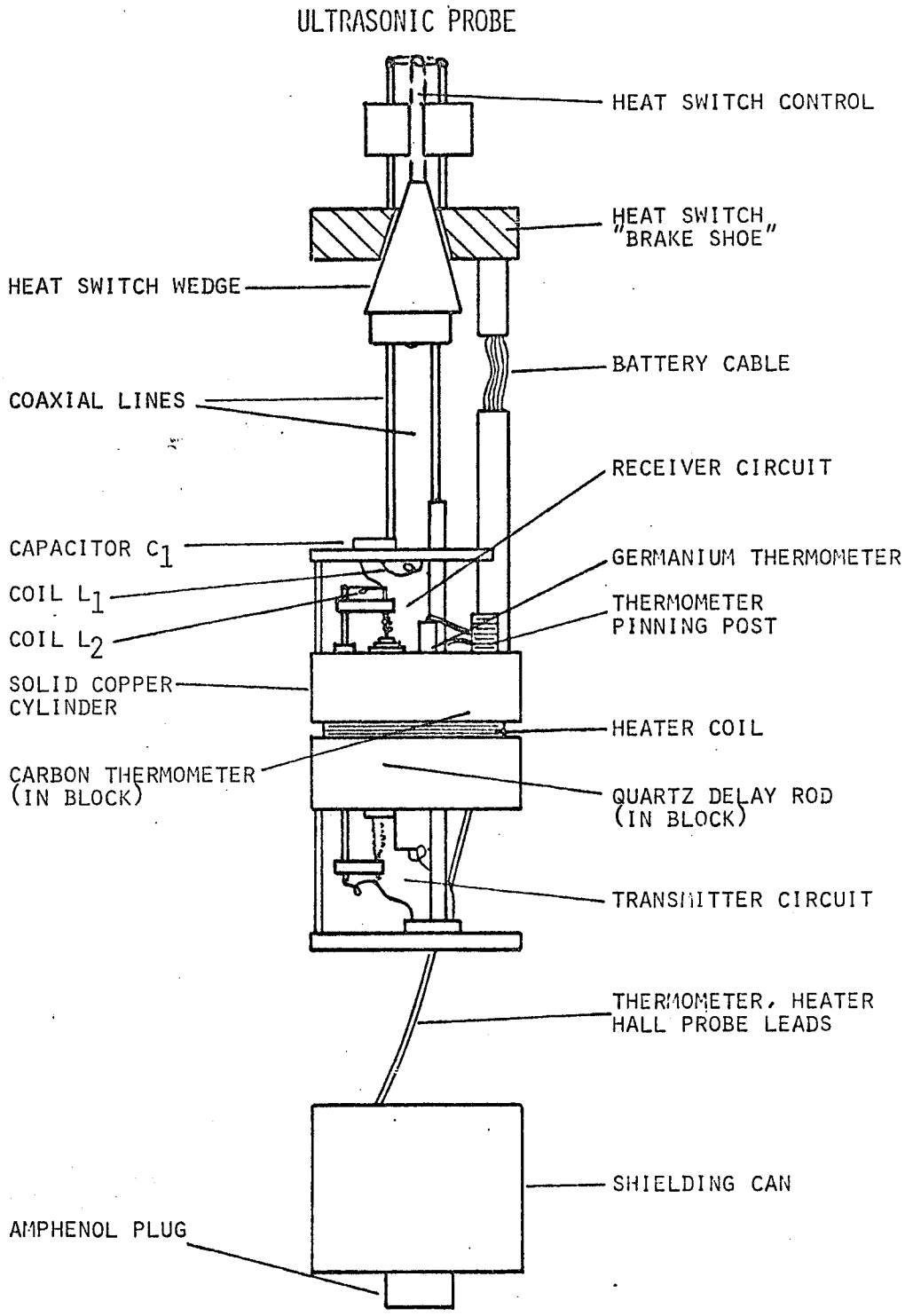
ULTRASONIC PROBE
HEAT SWITCH CONTROL
HEAT SWITCH "BRAKE SHOE"
HEAT SWITCH WEDGE
BATTERY CABLE
COAXIAL LINES
RECEIVER CIRCUIT
CAPACITOR C_1
GERMANIUM THERMOMETER
COIL L_1
THERMOMETER PINNING POST
COIL L_2
SOLID COPPER CYLINDER
HEATER COIL
CARBON THERMOMETER (IN BLOCK)
QUARTZ DELAY ROD (IN BLOCK)
TRANSMITTER CIRCUIT
THERMOMETER, HEATER HALL PROBE LEADS
SHIELDING CAN
AMPHENOL PLUG

Figure 23

which was immersed in liquid helium. From there they led to a 14 contact Amphenol receptacle into which the ultrasonic probe plugged as it was lowered into the can. The leads for the heater, auxilliary carbon thermometer, and Hall probe for monitoring magnetic fields also followed the same route, positively blocking thermal leakage along such leads.

An auxilliary carbon thermometer was used for driving the chart recorder. Its readings were repeatable within a given helium transfer. Its use allowed accurate monitoring of the temperature during broad temperature sweeps via germanium thermometer without disturbing the offset of the data being plotted on the recorder. Additional pinning of the sample holder copper block to the helium bath was necessary; without it, excess heat leaked down the coaxial ultrasonic leads. (These are silver-plated non-magnetic 10 mm stainless tubes, silver-plated on conducting surfaces.) Also, during use of the heater, a heat "drain" was needed to provide freedom of movement both up and down in temperatures. Hence the heat switch was added above the sample block. (See Fig. 23.) It is a "brake shoe" type device. Turning a control rod pulled a wedge between two half cylinder "brake shoes," forcing them against the wall of the vacuum can. The cylinders were flexibly connected to the sample holder block by battery cable which was silver-soldered at both ends.

The most important parts of the probe were its tuned transmitting and receiving transducer circuits. The theory behind such circuits is outlined by Mason.[49] Kamm and Bohm have described a somewhat simpler tuning circuitry for an ultrasonic probe,[50] which suggested to us the development of this probe. The basic objective is impedance matching and resonant tuning in the immediate vicinity of the transducers. Unless this is done at ultrasonic frequencies over 100 MHz, most of the transmitted signal is reflected back by the high impedance transducer. Analogously, and much more importantly, the

feeble signal of the high-impedance receiving transducer couples very weakly to a low impedance receiving line with no matching circuit. One tuning configuration commonly used is given below:

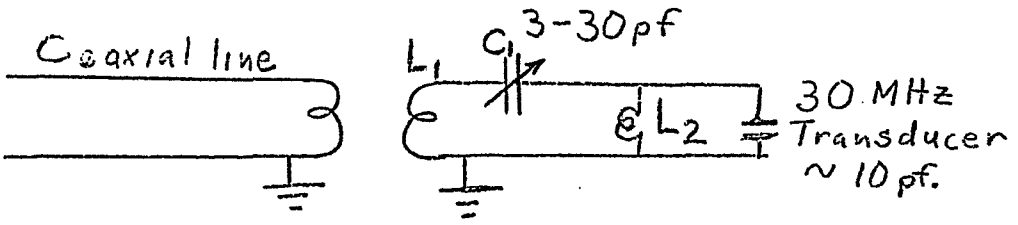

The tunable coil L_2 consisted of one or several loops of silvered copper wire which slid into a set screw clamp arrangement at each end, allowing fine adjustment of inductance. It was adjusted before the experimental run outside the cryostat, the objective being to optimize tuning at one or several frequencies, depending on the experiment to be conducted. Final tuning at each frequency was done at helium temperature by means of capacitor C_1. A calculated circuit construction might seem advisable since "lumped element" descriptions of transducers have been developed. However, ultrasonic frequencies over 100 MHz and below 1 GHz are in a hybrid region. Classical lower frequency tuned circuits are being pushed beyond their normal applicability and yet tuned cavities are still impractical for a large frequency range. In our circuitry every piece of metal was found to have an influence. A "cut and try" method was found to be most successful in a very literal sense. The proper sizes of inductors L_1 and L_2 and the actual usefulness of L_2 were determined this way. The compactness (actually the result of having to fit inside a superconducting magnet) of the tuning areas is also important. The short lead-in wires allow more room for inductor adjustment and, hence, more tuning range.

One measure of the impedance-matching success of this tuning circuitry

was that at peak tuning external stub tuners could not improve the signal. In fact, they were not used because their insertion loss reduced the signal. Most importantly, useful attenuation data were able to be taken with as much as 85 db of attenuation after the Matec #560 transmitter which produces maximum pulses of approximately 50v at 150 MHz. This kind of sensitivity permitted amplitude independent attenuation data to be taken in pure, undeformed lead at frequencies up to 450 MHz.

C. The Attenuation Measurements

The external electronics were arranged as in Fig. 24 for attenuation measurements. This arrangement is the usual form in all but two respects. No stub tuners were needed or even helpful on either the transmitter or receiver side of the ultrasonic probe. This was true because of the internal tuning capability of the probes transducer circuits themselves. Also, a switch was not used before the mixer to protect the I.F. strip from paralysis by leakage of the initial transmitter pulse. In many cases, particularly when the probe tuning was sharp, the leakage pulse was not large enough, compared with the first pulse transmitted through the sample, to cause saturation of the receiver. When this was not true, the local oscillator was pulsed so that, in effect, the receiver was turned off outside of an approximate 5μ sec neighborhood of the first transmitted pulse. The insertion loss of a switch was thus avoided. Transmitter pulses of approximately 1μ sec width were used for our measurements.

Wider pulses could not be used because the ultrasound would undergo several internal reflections within our thin (1 - 2 mm) samples. The emerging signal peaks from the several reflections were as little as 0.9μ sec apart. At low sample attenuation levels, if broad pulses were used or if too

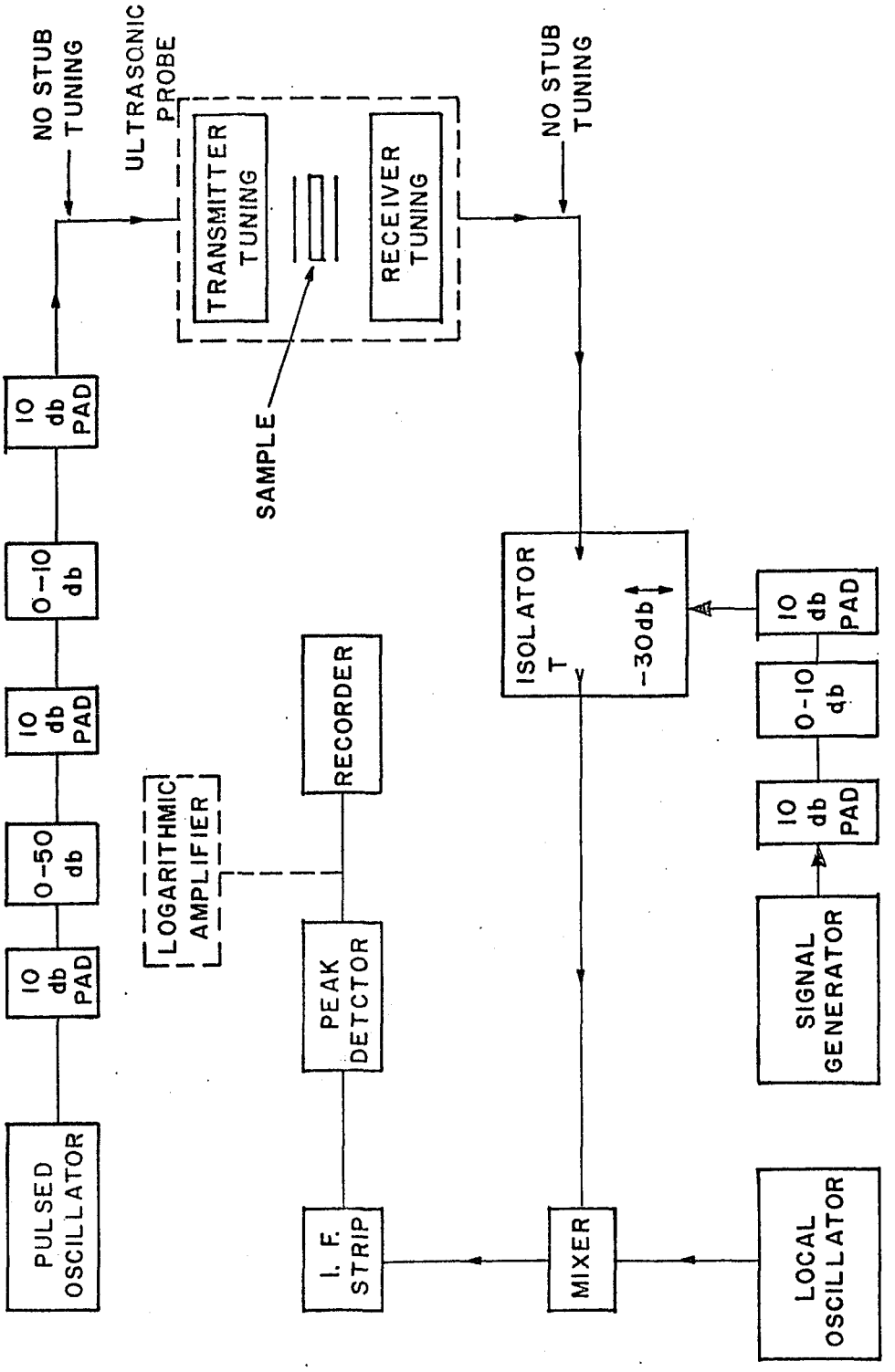
NO STUB TUNING
ULTRASONIC PROBE
TRANSMITTER TUNING
RECEIVER TUNING
NO STUB TUNING
SAMPLE
10 db PAD
0-10 db
10 db PAD
0-50 db
10 db PAD
PULSED OSCILLATOR
LOGARITHMIC AMPLIFIER
RECORDER
PEAK DETCTOR
I. F. STRIP
ISOLATOR T
-30db
MIXER
10 db PAD
0-10 db
10 db PAD
SIGNAL GENERATOR
LOCAL OSCILLATOR

Figure 24

wide a peak detector gate width were used, gross overestimation of attenuation changes would result. Pulse widths less than about 0.75μ sec were not achievable because of the high Q of the transmitting and receiving tuned circuits.

For fine temperature sweeps in the region 6.5 - 7.2°K, estimating from the repeatability of our data, attenuation was measured with $\pm$ 0.1 dB error. For broad sweeps 1.5 - 14°K, estimated error was less than $\pm$ 0.2 dB for the attenuation measurements.

The thermometry was accurate to a degree exceeding our requirements in the lead experiment. Measurements within a given run were easily repeatable within 2 m°K near T_c = 7.2°K for a given experimental run. Measurements would tend to differ from one run to the next because of thermal voltages in the thermometer leads. However, these were easily corrected for by reversing thermometer current. In any event any uncertainties in T were unimportant on the scale of the computed strong coupling features near T_c. The SSW strong coupling calculations with which we compare our data were made only at T/T_c = .95, .978, and .989. One certain conclusion can be made from comparison of our results, other ultrasonic results[38] and thermal conductivity measurements[18] with strong-coupling theory. There is considerable room for improvement in the understanding of strong-coupling theory and dislocation attenuation theory without a need for refining experimental accuracy.

CHAPTER VII

CONCLUSION

The strong-coupling electron-phonon interaction and the very mobile dislocation motion in lead present the ultrasonics experimentalist with a surplus of interesting effects and anomalies. Attempts to ignore either dislocation or strong-coupling attenuation effects have led to unfortunate results. In this work, as far as our knowledge allowed, we have considered fully both kinds of effects. Our initial experimental plan of studying only the strong-coupling properties of lead by using low amplitude and high frequency was inevitably modified by the glaring dislocation attenuation effects. One of these, the intermediate state magnetic field-dependent amplitude effect, stood by itself but was interesting enough to study for its relation to the structure of the intermediate state. The other dislocation attenuation effects we examined bear directly on (interfere directly with) the findings for strong-coupling electronic attenuation.

A "ledge" we have seen at several frequencies in the $\alpha_s(T)$ curve appears to fit an amplitude-independent dislocation attenuation model adapted to the superconducting state from the Granato-Lücke theory.[6,7] Within this model we compute an undamped resonant frequency $f_o \doteq 190$ MHz for dislocation loops in our sample 3. The normal state damping constant, for damping of dislocation loops motion by electrons at $T = 0$ is computed from our data to be $d_o = 1.6 \times 10^{10}$ sec^{-1}. This is in fair agreement with a theoretical computation of $d_o = 2.1 \times 10^{9}$ sec^{-1} by Holstein.[6] Experimentalists have traditionally assumed that temperature dependent dislocation contributions were absent from their data if there was no evidence for amplitude dependent effects. The present work demonstrates that the "amplitude-dependence criterion" is inadequate.

Our findings for the electronic attenuation in an unstrained lead sample agree essentially with those of Fate et al[9] for a strained sample. Using the strong-coupling theory results of Nam[16] and the calculations of Swihart Scalapino and Wada[17], we have computed the theoretical attenuation values $\alpha_{st}(f, T)$ and $\alpha_{nt}(f,T)$ explicitly. The computed attenuation ratio $(\alpha_{st}/\alpha_{nt})(f,T)$ has a temperature dependence which agrees with experimental attenuation measurements to the same quantitative extent that the computed thermal conductivity ratio $K_s/K_n(T)$ of Ambegaokar and Woo agrees with experimental results. In the case of ultrasonic attenuation the dependence on the additional variable, ultrasonic frequency f, is examined. We find the attenuation ratio α_s/α_n at a given temperature T to increase with f as did Fate et al[9]. This is in keeping with the strong-coupling prediction of a reduced effective electron mean-free-path in the superconducting state. Additionally we find that the strong-coupling theory predicts an increase in the ratio of effective mean-free-paths $\bar{\ell}_s/\bar{\ell}_n(f,T)$ with increasing f at a given T. This is confirmed in an examination of our data and that of Fate.[38]

The agreement of the strong-coupling computations with purely normal-state attenuation measurements is less clear. The theory predicts an effective normal state mean-free-path $\bar{\ell}_{nt}$ which decreases with frequency. Fate's normal-state attenuation measurements [38] are fit extremely well with Pippard free electron theory and an assumed constant frequency dependence for the mean-free-path. Our attenuation data, because of dislocation effects, lack a positive determination at the highest frequencies of the zero electronic attenuation level. However, as far as they can be interpreted using only the temperature dependence of α_n above T_c, our data confirm Fate's findings

up to 510 MHz, much higher than his maximum frequency.

In matching the theoretical $\bar{\ell}_{nt}(f,T_c)$ to the experimental mean free path at a single frequency, 90 MHz, we find our free parameter, the zero temperature Fermi velocity, to be $v_{FO} = 1.3 \times 10^8$ cm/sec. Thus the ultrasonic attenuation measurements yield an estimate of the Fermi velocity effective for attenuation of longitudinal waves propagated along the [100] axis of lead.

At our highest frequencies our superconducting state measurements were hampered by an amplitude independent, temperature-dependent attenuation source which, apparently, increases linearly with frequency and appears to be caused by dislocations. This source unfortunately prevented a positive check on the strong-coupling predictions at these high frequencies, one of our primary goals. Recognition of this attenuation source is important in itself, however, if only to prevent more theoretical work aimed at explaining behavior erroneously attributed to electronic attenuation.

REFERENCES

1. J. Bardeen, L. N. Cooper, and J. R. Schrieffer, Phys. Rev. 108, 1175 (1957).
2. H. E. Bömmel, Phys. Rev. 96, 220 (1954).
3. R. E. Love and R. W. Shaw, Rev. Mod. Phys. 36, 260 (1964).
4. R. E. Love, R. W. Shaw, and W. A. Fate, Phys. Rev. 138, A1953, (1965).
5. B. R. Tittman and H. E. Bömmel, Phys. Rev. Letters 14, 296 (1965).
6. B. R. Tittman and H. E. Bömmel, Phys. Rev. 151, 178 (1966).
7. A. Granato and K. Lücke, J. Appl. Phys. 27, 583 (1956).
8. W. P. Mason, Phys. Rev. 143, A229 (1966).
9. W. A. Fate, R. W. Shaw and G. L. Salinger, Phys. Rev. 172, 413 (1968).
10. B. C. Deaton, Phys. Rev. Letters 16, 577 (1966).
11. V. Ambegaokar and J. Woo, Phys. Rev. 139, A1818 (1965).
12. V. Ambegaokar, Phys. Rev. Letters 16, 1047 (1966).
13. W. A. Fate and R. W. Shaw, Phys. Rev. Letters 19, 230 (1967).
14. J. W. F. Woo, Phys. Rev. 155, 429 (1967).
15. J. H. Simmons, NASA T. N. DN-3817 (1967).
16. S. B. Nam, J. Korean Phys. Soc., Vol. 1, No. 1, 1 (1968).
17. J. C. Swihart, D. J. Scalapino, and Y. Wada, Phys. Rev. Letters 14, 106 (1965).
18. J. W. F. Woo, Thesis, Cornell University (1966).
19. L. T. Claiborne and N.G. Einspruch, Phys. Rev. 132, 621 (1963).
20. T. Olsen, L. T. Claiborne and N. G. Einspruch, J. Appl. Phys. 37, 760 (1966).
21. J. S. Koehler, Imperfections in Nearly Perfect Crystals (John Wiley & Sons, Inc., New York, 1952)
22. I. Giaever, H. R. Hart, and K. Megerle, Phys. Rev. 126, 941 (1962).
23. W. P. Mason, J. Accoust. Soc. Am. 27, 643 (1955).
24. A. Granato and K. Lücke, J. Appl. Phys. 27, 789 (1956).

25. L. P. Kadanoff and I. I. Falko, Phys. Rev. 136, A1170 (1964).

26. Y. Nambu, Phys. Rev., 117, 648 (1960).

27. J. R. Schrieffer, Theory of Superconductivity, W. A. Benjamin, Inc. New York, 1964.

28. S. B. Nam, Phys. Rev., 156, 470 (1967).

29. L. P. Kadanoff and G. Baym, Quantum Statistical Mechanics, W. A. Benjamin Inc., New York (1962).

30. A. B. Pippard, Phil. Mag. 43, 1104 (1955).

31. A. A. Abrikosov, L. P. Gofkov and I. E. Dzaloshinski, Methods of Quantum Field Theory in Statistical Physics, translated by R. A. Silverman, Prentice-Hall, Inc., Englewood Cliffs, New Jersey (1963).

32. P. C. Martin and J. Schwinger, Phys. Rev. 115, 1342 (1959).

33. B. N. Brockhouse, T. Arase, G. Cagliotti, K. P. Rao, and A.D.B. Woods, Phys. Rev. 128, 1099 (1962).

34. J. M. Rowell, P. W. Anderson, and D. E. Thomas Phys. Rev. Letters 10, 334 (1963).

35. Anderson and Gold, Phys. Rev.139, A1459 (1965).

36. E. I. Blount, Phys. Rev. 114, 418 (1958).

37. B. Mühlschlegel, Z. Phys. 155, 313 (1959).

38. W. A. Fate, Phys. Rev. 172, 402 (1968).

39. R. W. Morse, Prog. Cryogenics 1, 220 (1959).

40. The existance of a new set of calculations was reported by J. C. Swihart in a private communication. These appeared too late for our use.

41. J. A. Osborn, Phys. Rev. 67, 351 (1945).

42. H. Traüble and U. Essmann, Phys. Stat. Sol. 18, 813 (1966).

43. U. Essmann (Private communication).

44. H. G. Van Bueren, Imperfections in Crystals, North Holland Publishing Co., Amsterdam (1960)

45. N. V. Sarma and J. R. Moon, Phil. Mag. 17, 501 (1968).

46. N. V. Sarma, Phil. Mag. 17, 1233 (1968).

47. U. Essmann and H. Traüble, Phys. Lett. 24A, 526 (1967).

48. W. F. Druyvesteyn and D. J. VanOoijen, Phys. Lett. 2, 328 (1962).

49. W. P. Mason, Physical Accoustics: Principles and Methods, Academic Press, New York (1964).

50. G. N. Kamm and H. V. Bohm, Rev. Sci. Inst., 957 (1963).

51. J. R. Leibowitz, R. L. Sebastian, E. M. Alexander, and R. E. Reed, Bull. Am. Phys. Soc. (April 1970).

VITA

Name: Richard L. Sebastian

Permanent Address: 3320 Woodburn Village Drive
Annandale, Virginia

Degree and Date to be conferred: Ph.D., 1970

Date of Birth: June 22, 1942

Place of Birth: Hutchinson, Kansas

Secondary Education: Eisenhower High School, Yakima, Washington

Collegiate Institutions Attended:	Dates	Degree	Date of Degree
Princeton University	1960-1964	A.B.	1964
University of Maryland	1964-1970	Ph.D.	1970

Major: Solid State Physics

Minors: General Physics, Elementary Particles

Positions Held: Ensco Incroporated, Springfield, Virginia
Staff Scientist 1969 -

University of Maryland, College Park, Maryland
Research Assistant 1966-1969
Teaching Assistant 1964-1966